TURUN YLIOPISTON JULKAISUJA
ANNALES UNIVERSITATIS TURKUENSIS

SARJA - SER. D OSA - TOM. 945

MEDICA - ODONTOLOGICA

THE USE OF RADIOSTEREOMETRIC ANALYSIS IN FRACTURES OF THE DISTAL RADIUS

From Phantom Models to Clinical Application

by

Rami Madanat

TURUN YLIOPISTO
UNIVERSITY OF TURKU
Turku 2011

From the Orthopaedic Research Unit, Department of Orthopaedic Surgery and Traumatology, Turku, Finland, and the National Graduate School of Muskuloskeletal Disorders and Biomaterials

Supervised by:
Professor Hannu T. Aro
Department of Orthopaedic Surgery and Traumatology
University of Turku
Turku, Finland

Reviewed by:
Professor Juhana Leppilahti
Department of Orthopaedic and Trauma Surgery
Oulu University Hospital
Oulu, Finland

and

Docent Jari Salo
Department of Orthopaedics and Traumatology
Helsinki University Hospital
Helsinki, Finland

Dissertation opponent:
Professor Søren Overgaard
Department of Orthopaedic Surgery and Traumatology
Odense University Hospital
Odense, Denmark

ISBN 978-951-29-4515-3 (PRINT)
ISBN 978-951-29-4516-0 (PDF)
ISSN 0355-9483
Painosalama Oy – Turku, Finland 2011

To my Family

Cover: computer-simulated 3-D model of a distal radius fracture with implanted RSA markers fixed with a locked volar plate.

ABSTRACT

Rami Madanat

**The use of radiostereometric analysis in fractures of the distal radius:
From phantom models to clinical application**

Orthopaedic Research Unit, Department of Orthopaedic Surgery and Traumatology, University of Turku, Turku, Finland.
Annales Universitatis Turkuensis, Medica-Odontologica, 2011, Turku, Finland.

Radiostereometric analysis (RSA) is a highly accurate method for the measurement of *in vivo* micromotion of orthopaedic implants. Validation of the RSA method is a prerequisite for performing clinical RSA studies. Only a limited number of studies have utilised the RSA method in the evaluation of migration and inducible micromotion during fracture healing. Volar plate fixation of distal radial fractures has increased in popularity. There is still very little prospective randomised evidence supporting the use of these implants over other treatments. The aim of this study was to investigate the precision, accuracy, and feasibility of using RSA in the evaluation of healing in distal radius fractures treated with a volar fixed-angle plate.

A physical phantom model was used to validate the RSA method for simple distal radius fractures. A computer simulation model was then used to validate the RSA method for more complex interfragmentary motion in intra-articular fractures. A separate pre-clinical investigation was performed in order to evaluate the possibility of using novel resorbable markers for RSA. Based on the validation studies, a prospective RSA cohort study of fifteen patients with plated AO type-C distal radius fractures with a 1-year follow-up was performed.

RSA was shown to be highly accurate and precise in the measurement of fracture micromotion using both physical and computer simulated models of distal radius fractures. Resorbable RSA markers demonstrated potential for use in RSA. The RSA method was found to have a high clinical precision. The fractures underwent significant translational and rotational migration during the first two weeks after surgery, but not thereafter. Maximal grip caused significant translational and rotational interfragmentary micromotion. This inducible micromotion was detectable up to eighteen weeks, even after the achievement of radiographic union.

The application of RSA in the measurement of fracture fragment migration and inducible interfragmentary micromotion in AO type-C distal radius fractures is feasible but technically demanding. RSA may be a unique tool in defining the progress of fracture union.

Keywords: radiostereometric analysis, distal radius, migration, inducible micromotion, fracture healing

TIIVISTELMÄ

Rami Madanat

Radiostereometrisen analyysin käyttö värttinäluun alaosan murtumissa: Fantom-malleista kliinisiin sovelluksiin

Ortopedian tutkimusyksikkö, Ortopedian ja traumatologian klinikka,
Turun yliopisto, Turku
Annales Universitatis Turkuensis, Medica-Odontologica, 2011, Turku

Radiostereometrinen analyysi (RSA) on tarkka menetelmä *in vivo* mikroliikkeen mittaamiseen ortopedisissa implanteissa. RSA-menetelmän validointi on tehtävä ennen kliinisen tutkimuksen aloittamista. On vain vähän tutkimuksia, jotka ovat hyödyntäneet RSA-menetelmää luun paranemisen aikana tapahtuvan migraation tai dynaamisen mikroliikkeen mittaamisessa. Volaarinen levytys on tullut suosituksi distaalisten radiusmurtumien operatiivisessa hoidossa. Satunnaistettuja kliinisiä tutkimuksia tarvitaan vertailemaan levytyksellä hoidettujen potilaiden hoitotuloksia muihin hoitomuotoihin. Tämän tutkimuksen tarkoituksena oli selvittää RSA-menetelmän tarkkuus, toistettavuus ja käyttökelpoisuus distaalisten radiusmurtumien paranemisen seurannassa.

RSA-menetelmä validoitiin ensin käyttäen yksinkertaista radiusmurtuman fantom-mallia. Tämän jälkeen tietokonesimulaatiomallin avulla validoitiin RSA-menetelmän käyttö intra-artikulaarisissa murtumissa. Erillisessä prekliinisessä tutkimuksessa arvioitiin biohajoavien merkkikuulien soveltuvuutta RSA:ssa. Menetelmän validoinnin jälkeen suoritettiin prospektiivinen viidentoista potilaan kliininen RSA-tutkimus, jossa AO C-tyypin värttinäluun alaosan murtumat korjattiin volaarisella lukkolevyllä.

RSA-menetelmä osoittautui sekä fyysisellä että tietokonesimuloiduilla mallinnuksella tarkaksi ja toistettavaksi radiusmurtuman mikroliikkeen arvioinnissa. Biohajoavat röntgenpositiiviset merkkikuulat osoittautuivat käyttökelpoisiksi RSA-menetelmän suhteen. RSA menetelmällä oli hyvä kliininen toistettavuus. Lukkolevyillä fiksoiduissa distaalisissa radiusmurtumissa tapahtui ensimmäisen kahden viikon aikana tilastollisesti merkittävä translaatio ja rotaatiomigraatio. Kahden viikon jälkeen murtuma stabiloitui eikä merkittävää liikettä enää tämän jälkeen tapahtunut. Dynaamisessa RSA-analyysissä maksimaalinen käden puristus aiheutti merkittävän mikroliikkeen murtumafragmenttien välillä 18 viikkoon asti siitä huolimatta, että murtumat olivat siihen mennessä radiologisesti luutuneet.

RSA:n soveltaminen murtumafragmentin migraation ja dynaamisen mikroliikkeen arvioinnissa värttinäluun alaosan murtumissa on kannattavaa, mutta teknisesti vaativaa. RSA on ainutlaatuinen työkalu murtuman luutumisen arvioinnissa.

Avainsanat: radiostereometrinen analyysi, värttinäluun alaosan murtumat, migraatio, dynaaminen mikroliike, murtuman paraneminen

TABLE OF CONTENTS

ABSTRACT v
TIIVISTELMÄ vi
ABBREVIATIONS x
LIST OF ORIGINAL PUBLICATIONS xi
1. INTRODUCTION 1
2. REVIEW OF THE LITERATURE 2
2.1 FRACTURE HEALING AND MICROMOTION 2
2.2 ANATOMY OF THE WRIST 3
2.3 FRACTURES OF THE DISTAL RADIUS 4
2.3.1 Aetiology and incidence 4
2.3.2 Classification 5
2.3.3 Radiographic Evaluation and Prediction of Instability 5
2.3.4 Treatment 6
2.3.4.1 Closed reduction and casting 6
2.3.4.2 Closed reduction and percutaneous pinning 6
2.3.4.3 External fixation 7
2.3.4.4 Open reduction and internal fixation (ORIF) 7
2.3.4.5 Fragment-specific fixation 10
2.3.4.6 Arthroscopic treatment 10
2.3.4.7 Intramedullary nailing 10
2.3.4.8 Treatment of ulnar-sided wrist injuries 10
2.3.4.9 Bone grafting and bone graft substitutes 11
2.3.5 Rehabilitation 11
2.3.6 Factors affecting outcome 11
2.3.7 Outcome measures 12
2.3.7.1 Objective parameters 13
2.3.7.2 Subjective parameters 14
2.3.8 Complications 14
2.4 RADIOSTEREOMETRIC ANALYSIS (RSA) 15
2.4.1 History 15
2.4.2 Basic principles 15
2.4.3 Implantation of markers 15
2.4.4 Radiographic examination 16
2.4.5 Marking and analysis of radiographs 17
2.4.6 Calculation of micromotion 17
2.4.7 The accuracy and precision of RSA 18
2.4.8 RSA standardization guidelines 18
2.4.9 Model based RSA (MBRSA) 19

2.4.10 Dynamic RSA and inducible micromotion 19
2.5 MONITORING OF HEALING USING RSA 25
2.5.1 Distal radius fractures 25
2.5.2 Femoral neck fractures 25
2.5.3 Trochanteric fractures 26
2.5.4 Tibial plateau fractures 26
2.5.5 Ankle fractures 28
2.5.6 Vertebral fusion 28
2.5.7 Osteotomies 29
3. AIMS OF THE PRESENT STUDY 30
4. MATERIALS AND METHODS 31
4.1 MATERIALS (Studies II-V) 31
4.1.1 Creating physical phantom models 31
4.1.2 Creating a computer simulation model 32
4.1.3 Manufacturing of bioactive glass implants 34
4.2 ANIMALS (Study IV) 35
4.2.1 Experimental animals and anaesthesia 35
4.2.2 Animal model and study protocol 36
4.3 PATIENTS (Study V) 36
4.3.1 Patient selection 36
4.3.2 Operative technique 37
4.3.3 Postoperative aftercare of patients 38
4.3.4 Patient follow-up 38
4.4 ANALYTICAL METHODS (Studies II-V) 39
4.4.1 Radiostereometric analysis (RSA) (Studies II-V) 39
4.4.1.1 RSA accuracy and precision using physical phantom models 40
4.4.1.2 RSA simulation using a computer model 42
4.4.1.3 Clinical RSA examinations 44
4.4.2 Conventional radiography 44
4.4.3 X-ray diffraction 45
4.4.4 UV-visible spectroscopy 45
4.4.5 BEI-SEM/EDXA 45
4.4.6 Micro-CT 46
4.4.7 pQCT 46
4.4.8 Mechanical testing 46
4.4.9 Histology 47
4.4.10 Range of motion measurements 47
4.4.11 Strength measurements 47
4.4.12 Subjective outcome measurements 48
4.5 STATISTICS 48

5. RESULTS 49
5.1 RSA ACCURACY AND PRECISION USING A PHYSICAL PHANTOM MODEL (Study II) 49
5.2 RSA COMPUTER SIMULATION FOR FRACTURES OF THE DISTAL RADIUS (Study III) 51
5.3 EVALUATION OF RESORBABLE MARKERS FOR RSA (Study IV) 52
5.3.1 In vitro characterisation of implant reactivity 52
5.3.2 In vivo characterisation of implants 52
5.3.3 Radiostereometric analysis 55
5.4 RSA IN TYPE-C DISTAL RADIUS FRACTURES TREATED WITH A LOCKED VOLAR PLATE (Study V) 55
5.4.1 Precision 55
5.4.2 Clinical Outcomes 56
5.4.3 Radiographic Outcomes 59
5.4.4 RSA Results 60
6. DISCUSSION 64
6.1 MONITORING OF FRACTURE HEALING USING RSA 64
6.2 PHYSICAL AND COMPUTER SIMULATION PHANTOM MODELS OF RSA USE IN DISTAL RADIUS FRACTURES 64
6.3 RESORBABLE MARKERS FOR RSA 66
6.4 FRACTURE MIGRATION AND INDUCIBLE MICROMOTION IN PLATED DISTAL RADIUS FRACTURES 67
6.5 LIMITATIONS AND STRENGTHS OF THE STUDY 69
6.6 FUTURE ASPECTS 71
7. CONCLUSIONS 74
ACKNOWLEDGEMENTS 75
REFERENCES 77
ORIGINAL PUBLICATIONS 88

ABBREVIATIONS

ACDF	anterior cervical discectomy and fusion
AO	arbeitsgemeinschaft für osteosynthesefragen
BEI-SEM	backscattered electron imaging of scanning electron microscopy
CN	condition number
CT	computed tomography
DASH	disabilities of the arm, shoulder and hand
DLRSA	differentially loaded radiostereometric analysis
DRUJ	distal radioulnar joint
EDXA	energy dispersive X-ray analysis
FE	finite element
HCO	hemicallotasis osteotomy
HTO	high tibial osteotomy
MBRSA	model-based radiostereometric analysis
ME	mean error of rigid body fitting
MRI	magnetic resonance imaging
MTPM	maximum total point motion
ORIF	open reduction and internal fixation
OTA	orthopaedic trauma association
pQCT	peripheral quantitative computed tomography
PRWE	patient-rated wrist evaluation
ROM	range of motion
RSA	radiostereometric analysis
SBF	simulated body fluid
TFCC	triangular fibrocartilage complex
THA/THR	total hip arthroplasty/replacement
TKA/TKR	total knee arthroplasty/replacement
UKR	unicompartmental knee replacement
VAS	visual analogue scale

LIST OF ORIGINAL PUBLICATIONS

This thesis is based on the following original publications, which will be referred to in the text by their respective Roman numerals:

I. Madanat R, Moritz N, Larsson S, Aro HT. RSA applications in monitoring of fracture healing in clinical trials. *Scandinavian Journal of Surgery* 2006; 95(2):119-127.

II. Madanat R, Mäkinen TJ, Moritz N, Mattila KT, Aro HT. Accuracy and precision of radiostereometric analysis in the measurement of three-dimensional micromotion in a fracture model of the distal radius. *Journal of Orthopaedic Research* 2005; 23(2):481-488.

III. Madanat R, Moritz N, Aro HT. Three-dimensional computer simulation of radiostereometric analysis (RSA) in distal radius fractures. *Journal of Biomechanics* 2007; 40(8):1855-1861.

IV. Madanat R, Moritz N, Vedel E, Svedström E, Aro HT. Radio-opaque bioactive glass markers for radiostereometric analysis. *Acta Biomaterialia* 2009; 5(9):3497-3505.

V. Madanat R, Strandberg N, Moritz N, Mattila K, Vahlberg T, Aro HT. Radiostereometric analysis in measurements of migration and inducible micromotion in OTA type-C distal radius fractures treated with a volar plate. Submitted.

1. INTRODUCTION

Radiostereometric analysis (RSA) has been developed and used in orthopaedic research for over thirty years in the measurement of micromotion. The RSA method is still the most accurate method for the measurement of *in vivo* micromotion of bone fragments or orthopaedic implants. There are currently more than 480 publications that have utilised or evaluated RSA in micromotion measurements. One of the main focuses of RSA studies has been the evaluation of the micromotion of total joint replacement components following arthroplasty. Only less than 5% of all RSA studies have utilised the RSA method in the evaluation of micromotion during the fracture healing process.

The validation of the RSA method is a prerequisite for performing clinical RSA studies. This is essential for determining accuracy and precision levels as well as potential technical limitations. Phantom models can be used to validate RSA. The accuracy of RSA is determined by comparing micromotion results to those determined by another method that has a better resolution than RSA. Validation of precision is performed using double examination or multiple repeated measurements.

The treatment of unstable distal radius fractures has been greatly influenced by the emergence of volar fixed-angle implants during the past decade. Reflecting the growing popularity of the fixation method, a large number of different plate designs are now available. Surprisingly, there is very little prospective randomised evidence supporting the use of these implants over other treatment modalities. Furthermore, there is very scarce data to guide the orthopaedic surgeon in selecting one volar fixed-angle implant over another. One of the obstacles in performing such trials is the lack of validated methods for the quantitative assessment of fracture union.

RSA is an objective measurement method that can be used in the comparison of different fracture treatment modalities in clinical trials. Although RSA is a powerful tool, it has several limitations when applied to small bone fragments in combination with radio-opaque fixation devices.

This doctoral thesis was initiated to investigate the precision, accuracy and feasibility of using RSA in the evaluation of healing in distal radius fractures. The RSA method is validated by using a physical distal radius fracture phantom model. Validation of RSA for more complex fractures is then performed by using a computer simulation model. A separate pre-clinical investigation of novel resorbable RSA markers is also performed. Finally, RSA is applied in a prospective cohort study to evaluate the quantity of fracture migration and inducible micromotion that occurs when complex distal radius fractures are stabilized with a volar locking plate.

2. REVIEW OF THE LITERATURE

2.1 FRACTURE HEALING AND MICROMOTION

Fracture healing is conventionally divided into three main phases (Wood 2008). The first phase is an inflammatory phase in which a haematoma is formed. This initiates the cascade of cellular events that enable fracture healing. The second phase is a reparative phase that usually begins 4-5 days after the injury. This phase is characterized by the invasion of pluripotential mesenchymal cells and formation of a soft fracture callus. Blood vessel proliferation in this phase helps the routing of appropriate cells to the fracture site, as well as contributes to the formation of granulation tissue. The fracture callus is replaced by woven bone and the mineralisation process strengthens the newly formed bone. The remodelling stage is the final stage of healing and may last for months or years. It is characterized by the substitution of woven bone by lamellar bone, as well as restoration of the medullary canal. The bone is restored to normal, or nearly normal morphology and mechanical strength. Each of these phases overlaps with the end of the preceding phase forming a continuous healing process.

Fracture healing has long been recognized to be sensitive to mechanical loading, in a manner that can have either beneficial or detrimental consequences (Aro and Chao 1993, Claes et al. 1995, Gardner and Mishra 2003, Goodship et al. 2009). A suitable level of loading can enhance the healing process (Chao et al. 1989, Augat et al. 2005), whereas excessive loading can disturb healing (Goodship et al 1993, Augat et al. 1996). The type of fracture stabilization and loading conditions during the healing period will influence micromotion at the fracture site. This in turn impacts the mechanical signals to the bone, thereby affecting the quality and progression of repair (Goodship and Kenwright 1985, Kenwright et al. 1991, Goodship et al. 2009).

The method of fracture treatment is crucial in determining fracture stability. Stability determines the quantity of strain at the fracture site, and strain influences which type of healing will occur (Egol et al. 2004). Strain is a measure of the deformation of a body as a result of loading and is equal to the change in fracture gap divided by the original fracture gap (Egol et al. 2004). Primary bone healing (endosteal) takes place when strain is below 2%, and secondary bone healing (enchondral) occurs when the strain level is between 2% and 10% (Egol et al. 2004). Strain levels greater than 10% prevent bone formation (Egol et al. 2004). The absolute stability required for primary bone healing is achieved with rigid fixation, such as that provided by compression plating (Egol et al. 2004). Secondary bone healing is characterized by callus formation and occurs when relative stability is achieved through stabilization methods such as casts, splints, locked plates and external fixators (Egol et al. 2004).

The application of cyclic compressive displacements can enhance fracture healing through increased callus formation and faster ossification (Goodship and Kenwright 1985, Claes et al. 1995). Furthermore, the application of successive tensile displacements has been shown to promote bone formation as demonstrated by distraction osteogenesis (Morgan et al. 2008). The complexity, as well as potency, of

using mechanical loading to stimulate healing has been acknowledged, and a better understanding of the effects of mechanical factors on bone healing is needed (Morgan et al. 2008).

The assessment of the time to fracture union is complex, because the methods for quantitatively monitoring fracture union have not been fully established (Goldhahn et al. 2008). Clinical union takes place when the increasing stiffness and strength brought about by the mineralisation process make the fracture site stable and pain free (Wood 2008). Radiographic assessment of fracture healing has conventionally been performed using repeated radiographic evaluations, especially around the expected time of fracture union (Goldhahn et al. 2008). The use of computed tomography may improve the ability to assess fracture union (Goldhahn et al. 2008). Radiographic evaluation of fracture union involves the assessment of the disappearance of fracture lines, determination of size and shape of callus, as well as identification of cortical bridging (Bhandari et al. 2002). This radiographic scoring has relied on objective evaluation by an investigator (Goldhahn et al. 2008).

The measurement of applied loads and fracture displacements also remains a major challenge. External fixators instrumented with strain gauges or displacement transducers have been shown to provide reasonably good estimates of fracture callus displacement, but possibly underestimate actual displacements (Morgan et al. 2008).

2.2 ANATOMY OF THE WRIST

The distal part of the radius is the anatomic basis of the wrist joint (Wulf et al. 2007). The wrist joint includes both the radiocarpal and distal radioulnar joints. The metaphysis of the distal radius starts approximately 2 to 3 cm proximal to the radiocarpal joint and is primarily composed of cancellous bone **(Fig. 1)**. The volar surface of the distal radius is concave, whereas the dorsal surface is convex and irregular. The articular surface of the distal radius is triangular in shape, with the apex of the triangle at the radial styloid **(Fig. 1)**. The base of the triangle forms the sigmoid notch. The distal radius articulates with the ulnar head in the sigmoid notch forming the distal radioulnar joint (DRUJ). The radiocarpal articular surface is divided into two concave facets for articulation with the scaphoid and lunate **(Fig. 1)**. The radiocarpal surface has approximately 10 to 14 degrees of volar inclination and 22 degrees of radial inclination (Wulf et al. 2007).

The extensor tendons are located in six compartments on the dorsal surface of the distal radius with Lister's tubercle acting as a fulcrum for the tendon of the extensor pollicis longus. The radiocarpal ligaments are attached to the distal part of the radius on the volar side. More proximally on the volar side the bone is covered by the pronator quadratus muscle, which attaches to the radial side of the bone. The triangular fibrocartilage, which is important for the stability of the DRUJ arises from the lunate facet and attaches to the base of the ulnar styloid.

The geometry of the distal radius determines the functional range of motion of the wrist joint. Flexion and ulnar deviation are larger than extension and radial deviation. Supination and pronation of the forearm result in a functional change in radius length (Wulf et al. 2007). In a neutral position, the radiocarpal joint receives 80% to 85% of the load transmitted from the hand to the arm (Palmer and Werner 1984). The proportion of force transmission may be altered with changes in ulnar variance or in the dorsal tilt of the radius (Short et al. 1987).

The three-column model is a structural concept of the distal radius, which consists of a medial, an intermediate, and a lateral column (Rikli and Regazzoni 1996). The lateral column acts as an osseous buttress for the carpus and is an attachment point for intracapsular ligaments; the intermediate column functions in primary load transmission; and the medial column serves as an axis for forearm and wrist rotation, as well as secondary load transmission.

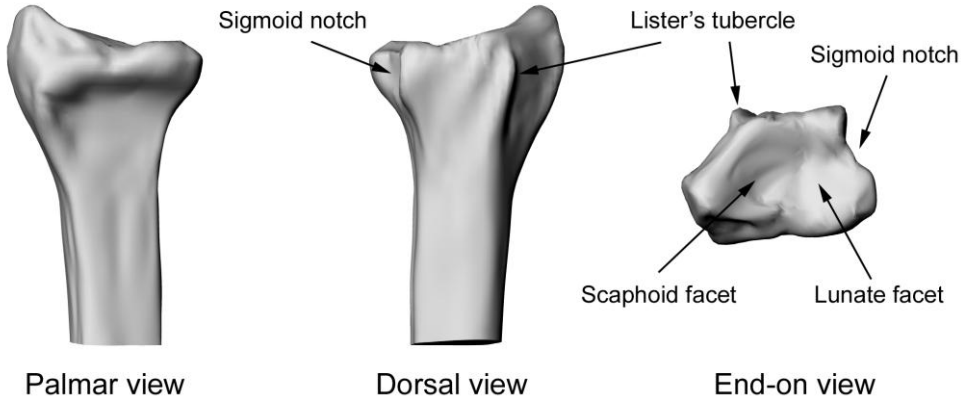

Figure 1. Anatomy of the distal radius.

2.3 FRACTURES OF THE DISTAL RADIUS

2.3.1 Aetiology and incidence

Abraham Colles first described distal radius fractures in the 1814 volume of the Edinburgh Medical Surgical Journal (Colles 1814). Colles' descriptions were based on clinical examinations since radiography was not yet invented then.

Distal radius fractures are the most common fractures treated at emergency departments, comprising more than 20% of all fractures (Grewal et al. 2005). These fractures are also the most common upper-limb fracture in individuals over 65 years, with 15% of Caucasian women suffering a distal radius fracture after the age of 50 (Cummings et al. 1989). Distal radius fractures typically present in a bimodal distribution with two distinct groups: children and the elderly (Alffram and Bauer

1962). The incidence of distal radius fractures also increases with the average age of the population (Wulf et al. 2007). Annual incidences of distal forearm fractures in Finland are 36.5/10 000 of the population, totalling more than 19,000 fractures per year (Kaukonen 1985, Vasenius 2008).

The incidence of distal radius fractures increases in the winter months due to icy weather conditions (Court-Brown et al. 2006). Most of these fractures occur in a low-energy injury such as a same level fall on the dorsiflexed wrist. Distal radius fractures are often associated with postmenopausal osteopenia or osteoporosis (Court-Brown et al. 2006). Younger individuals are more likely to sustain a higher energy injury associated with greater comminution (Court-Brown et al. 2006).

2.3.2 Classification

Distal radius fractures have more classification systems than any other fracture (Ilyas and Jupiter 2007). Some of these classifications are the Gartland and Werley (1951), Lidström (1959), Older and colleagues (1965), Frykman (1967), Thomas (1957), Melone (1984), Jenkins (1989), McMurtry and Jupiter (1990), Universal (1990), Mayo Clinic (1992), and Fernandez (1993). The classification most commonly used today is the OTA (AO) classification of the distal radius (Müller et al. 1987, Court-Brown et al. 2006). This is not a predictive classification and is based on fracture morphology.

The OTA (AO) type A fracture is extra-articular, type B is partial articular, and type C is a complete articular fracture with the articular surface detached from the diaphysis. Differentiation between subgroups of each type is dependent on anatomy, complexity and comminution of the fracture. Although this is not the most convenient classification when considering treatment options, it is very valuable in clinical research (Ilyas and Jupiter 2007).

2.3.3 Radiographic Evaluation and Prediction of Instability

Anteroposterior (AP) and lateral radiographs of the distal radius and ulna and the entire forearm should be obtained if the patient has pain, swelling or deformity in the proximal region of the forearm or elbow (Boyer 2007). Additional oblique anatomic tilt radiographs may be obtained to assess the articular surface more accurately (Boyer et al. 2004). Computed tomography (CT) scans are useful in the assessment of distal radius fractures and can evaluate the articular gap and step displacements better than plain radiographs (Cole et al. 1997). Furthermore, Katz et al. (2001) demonstrated that information obtained from CT scans often altered their treatment plans. The use of CT scans is especially useful in evaluating intra-articular fractures with significant comminution (Wulf et al. 2007). Magnetic resonance imaging (MRI) may be indicated especially in the subacute and chronic stages following the fracture if there is a suspicion of occult fracture, triangular fibrocartilage complex or ligament injury (Boyer 2007).

Lafontaine et al. (1989) identified various risk factors for secondary displacement following initial reduction. These included a dorsal tilt greater than 20 degrees,

comminution, intra-articular involvement, an associated fracture of the ulna, and age older than 60 years (Lafontaine et al. 1989). When three or more of these factors where present, the likelihood of secondary displacement was high (Lafontaine et al 1989). A study by Mackenney et al. (2006) showed that patient age, metaphyseal comminution, and ulnar variance were the most consistent predictors of radiographic outcome. In this study, however, dorsal angulation was not found to be significant in the prediction of radiographic outcome when controlled for comminution. The degree of expected fracture stability will influence treatment decisions (Wulf et al. 2007).

2.3.4 Treatment

Many available options exist for the treatment of distal radius fractures. Regardless of the large number of clinical trials evaluating different treatment methods, there are only a few level I randomised studies and there is still no clear evidence to favour any one of these treatment methods over the others (Handoll and Madhok 2003, Lichtman et al. 2010). There is moderate evidence to support operative fixation over cast fixation for fractures with post-reduction radial shortening > 3 mm, dorsal tilt > 10 degrees, or intra-articular displacement or step-off > 2 mm (Lichtman et al. 2010). In addition to fracture pattern, stability, and associated injuries, patient factors should always be taken into account when considering treatment options (Ilyas and Jupiter 2007).

The use of a national or regional treatment protocol for distal radius fractures may facilitate decision-making and improve fracture outcome. Liporace et al. (2009) suggested a treatment algorithm for distal radius fractures based on factors such as displacement, bone quality, ability to achieve reduction with ligamentotaxis, and surgeon preference. Abramo et al. (2008) similarly published an evaluation of the treatment protocol used at the Lund University Hospital since 1998. The Lund treatment protocol is sufficiently simple for routine clinical use and has performed well in practice.

2.3.4.1 Closed reduction and casting

Closed treatment of distal radius fractures is suitable for nondisplaced or displaced fractures that are reducible and stable (Wulf et al. 2007). Nondisplaced distal radius fractures need to be protected for 3 to 6 weeks using splinting, casting, or a combination of the two methods (Wulf et al. 2007). There is moderate evidence to support the use of rigid immobilization rather than removable splints in the non-operative treatment of displaced distal radius fractures (Lichtman et al. 2010).

2.3.4.2 Closed reduction and percutaneous pinning

This fixation method is suitable for extra-articular fractures and fractures without intra-articular instability or metaphyseal comminution (Greatting and Bishop 1993, Gofton et al. 2007). Several techniques have been described with the two most common being the trans-styloid and Kapandji techniques (Kapandji 1976, Munson and Gainor 1981, Benoist and Freeland 1995, Lenoble et al. 1995).

2.3.4.3 External fixation

External fixation has been used extensively and continues to have an important role in the treatment of distal radius fractures (Kaukonen et al. 1989, Haddad et al. 2000, Wulf et al. 2007). It can be used as a bridging or nonbridging technique. The bridging technique utilizes the concept of ligamentotaxis in the achievement and maintenance of fracture fragment reduction, whereas nonbridging relies on direct fracture stabilization (Slutsky 2007).

Indications for definitive external fixation include: unstable extra-articular distal radius fractures, two-part and selected 3-part intra-articular fractures without displacement, and combined internal and external fixation (Slutsky 2007). External fixation is also indicated in the temporary management of severe open fractures, as well as in the management of distal radius fractures in polytrauma patients (Slutsky 2007).

Contraindications for the sole use of bridging external fixation include: ulnar translocation due to an unstable distal radioulnar joint, intra-articular volar shear fractures, disrupted volar carpal ligaments/radiocarpal dislocations, and fractures with significant metaphyseal comminution (Slutsky 2007).

Augmentation of external fixation with K-wire fixation can expand the indications for external fixation to more complex fractures (Slutsky 2007). Nonbridging external fixation is suitable for extra-articular fractures with sufficient space for pin placement in the distal fragment. The results of nonbridging fixation are comparable to those of bridging external fixation (Lichtman et al. 2010).

2.3.4.4 Open reduction and internal fixation (ORIF)

Dorsal plating

Surgical exposure through a dorsal approach allows for easy access and good visualization of the fracture site. The stabilization of a dorsally displaced fracture using a dorsal plate can provide a biomechanical advantage, but the surgical procedure becomes significantly more difficult in comminuted fractures (Wulf et al. 2007, Vasenius 2008).

The high incidence of extensor tendon-related complications, such as tenosynovitis and ruptures (Axelrod and McMurtry 1990, Hove et al. 1997), has made this method less popular. It is noteworthy, however, that these complications have been reduced with modern low-profile plates (Kamath et al. 2006).

Fixed angle volar plating

Volar fixed-angle plating is becoming the preferred method of fixation of unstable and intra-articular distal radius fractures. Furthermore, many fractures that were previously treated with external fixation and pinning are now treated with these plates (Wulf et al. 2007). Using a volar surgical approach to the distal radius has several advantages (Henry MH et al. 2001, Orbay and Touhami 2006, Downing and Karantana 2008).

There is more space for the plate and the flexor tendons are located further from the bone with the interposition of the pronator quadratus muscle (Downing and Karantana 2008). Reduction of the fracture is often easier from the volar side since it is usually less comminuted and blood supply is less likely to be disturbed (Downing and Karantana 2008). Visualization of the fracture can be further improved by using the extended flexor carpi radialis approach (Orbay 2005).

The advantages of angular stable fixation include: 1) mechanical fracture bridging through a load-bearing construct; 2) locking head screws are not dependent on bone thread for purchase; and 3) locking screws reduce the chance of fixation failure due to screw loosening (Chen and Jupiter 2007). The stability of fixed-angle volar plates has benefits such as the early return of hand function, diminished frequency and duration of occupational therapy, potentially less overall pain, decreased risk of secondary displacement, and potentially less follow-up radiographs (Chen and Jupiter 2007).

Contraindications to volar plating include severely comminuted fractures, and fractures in children with skeletally immature bone (Orbay and Touhami 2006). The most common complications of volar plating are flexor and extensor tendon irritation or rupture due to incorrect plate positioning and dorsal past-pointing of screws, respectively (Downing and Karantana 2008).

The design of fixed-angle volar plates has been influenced by the volar anatomy of the radius and more specifically the ‘watershed line’ (Downing and Karantana 2008). A volar plate should not be placed beyond this line in order to prevent injury to flexor tendons. Currently, there are more than 30 different designs of volar locking plates, some have fixed-angle locking screws and others have polyaxial screw fixation that enables some variation of the screw insertion angle prior to locking.

Plates are available with one or more rows of distal locking screws or pegs (Downing and Karantana 2008). In a biomechanical study, locking screws have been shown to be superior to locking pegs in providing stability for AO type-C3 intra-articular distal radial fractures (Martineau et al. 2008). Biomechanical studies have also shown that the most distal screws need to be placed just beneath the subchondral bone in order to provide maximal stability and benefit from this fixation method (Drobetz et al. 2006). Biomechanical studies have also demonstrated that the various locking plates available on the market may have differing abilities to withstand fracture loading (Liporace et al. 2006, Willis et al. 2006). However, only limited clinical research exists to guide the orthopaedic surgeon in choosing a specific implant, and unfortunately this decision is often only based on factors such as surgeon preference, cost and marketing (Downing and Karantana 2008).

Several uncontrolled case series of distal radius fractures treated with volar locking plates have reported good to excellent clinical outcomes (Orbay and Fernandez 2002, Chung et al. 2006, Rozental and Blazer 2006). Similarly, several clinical studies suggest that volar plate fixation of distal radius fractures in elderly patients with osteoporosis result in good or excellent outcomes (Chung et al. 2008, Mudgal and

Jupiter 2008). There are, however only a few prospective randomised studies comparing volar locking plate fixation to other treatment modalities **(Table 1A and 1B)**. The current studies suggest that one of the main benefits of volar plate fixation over external fixation or closed reduction and percutaneous fixation is faster recovery in the early postoperative period **(Table 1A)**. This would imply an important socio-economic impact if the finding correlates with an earlier return to work. These benefits still need to be examined in the light of the costs of these modern fixed-angle plates.

Table 1A. Summary of relevant prospective randomised studies comparing volar plating to other operative treatment modalities for unstable distal radius fractures.

Reference	Treatments compared	N	Conclusions
Egol et al. 2008	Bridging external fixation and supplementary K-wire fixation (n=38) vs. volar locked plating (n=39).	77	Volar locked plating group had better ROM in the early postoperative period but no clinically significant differences at 1 year. No significant differences in radiological measurements.
Wei et al. 2009	External fixation (n=22) vs. locked radial column plate (n=12) vs. volar locked plate (n=12).	46	Locked volar plate group had better DASH scores at 3 months but no significant differences at 6 months or 1 year. Better maintenance of radial inclination and radial length in radial column plate group at 1 year.
Rozental et al. 2009	Closed reduction and percutaneous fixation (n=21) vs. volar locked plating (n=21).	42	Volar locked plating group had better range of motion, strength and lower DASH scores during the early postoperative period (6 and 9 weeks) but not at 1 year. No significant differences in radiological measurements.

Table 1B. Follow-up protocol and measured variables in relevant prospective randomised studies comparing volar plating to other operative treatment modalities for unstable distal radius fractures.

Reference	Follow-up visits (weeks)	Measured clinical variables						Measured radiological variables			
		Grip strength	Pinch strength	ROM	DASH	Pain	Digital motion	Volar tilt	Radial inclination	Radial length	Ulnar variance
Egol et al. 2008	2,6,12,25,52	X		X	X	X		X	X	X	X
Wei et al. 2009	2,6,12,25,52	X	X	X	X	X		X	X	X	X
Rozental et al. 2009	1,6,9,12,52	X	X	X	X		X	X	X	X	

2.3.4.5 Fragment-specific fixation

Fragment specific fixation is a method of internal fixation that uses a series of screws, k-wires, and small low-profile plates. The method enables internal fixation of a wide variety of fracture patterns (Konrath and Bahler 2002). In a biomechanical study evaluating intra articular distal radius fractures, the method has been shown to provide greater stiffness in four of six motion axes under cyclical loading when compared with external fixation (Dodds et al. 2002). Clinical trials have shown good to excellent results using this fixation method (Konrath and Bahler 2002, Martinez et al. 2004, Schnall et al. 2006).

2.3.4.6 Arthroscopic treatment

Wrist arthroscopy can provide a direct view of the articular surface and aid in the anatomic reduction of intra-articular fractures. The method has been found to help with identifying and treating concomitant injuries such as scapholunate ligament tears, lunotriquetral ligament tears or triangular fibrocartilage complex tears (Shih et al. 2001).

In a randomised prospective study comparing the fluoroscopically and arthroscopically assisted reduction of intra-articular fractures, it was shown that arthroscopy improved outcomes (Varitimidis et al. 2008). On the other hand, arthroscopically assisted reduction has been shown to have similar success in detecting articular stepoff as plain radiographs and fluoroscopy, but is better at detecting articular gapping (Edwards et al. 2001). Furthermore, arthroscopically assisted reduction has been shown to lead to additional re-reduction when performed after initial fluoroscopic reduction in more complex intra-articular fractures (Augé et al. 2000).

2.3.4.7 Intramedullary nailing

Intramedullary nailing as a treatment modality for distal radius fractures has only been used in a small number of published clinical studies. Ilyas and Thoder (2008) used an intramedullary nail in a series of ten patients with either extra-articular or simple intra-articular distal radial fractures. They found that this method resulted in good functional outcome, but a high incidence of complications. Gradl et al. (2009) proposed that intramedullary nailing could be used in extra-articular fractures of the distal radius, as well as intra-articular fractures without displacement and with a sagittal fracture line. Contraindications were flexion fractures, intra-articular fractures with displacement of the articular surface or a frontal fracture line (Gradl et al. 2009).

2.3.4.8 Treatment of ulnar-sided wrist injuries

Injuries to the ulnar aspect of the wrist can be associated with distal radius fractures (Lindau et al. 1997). Injuries such as ulnar styloid fractures, distal radius fractures extending to the DRUJ, or a TFCC tear can sometimes destabilize the DRUJ (Wulf et al. 2007).

Assessment of DRUJ stability is best performed and addressed following fixation of the radius (Wulf et al. 2007). The assessment of distal radioulnar instability has traditionally been performed by stressing the ulna dorsally and volarly (Sammer et al. 2009). Recognition of the stabilizing importance of the distal oblique band of the interosseous membrane has suggested that this test may not be accurate enough for the detection of true dynamic instability (Jupiter 2009). Compression of the ulna to the radius after plate fixation, followed by rotation of the hand and wrist, should be performed. If this test produces a palpable ¨click" then true instability is likely (Jupiter 2009). Studies have shown that patients with associated DRUJ instability have poorer outcomes when identified at the conclusion of treatment (Roysam 1993, Lindau et al. 2000). However, there are no randomised clinical studies that have evaluated whether early operative intervention is necessary (Lichtman et al. 2010).

2.3.4.9 Bone grafting and bone graft substitutes

Autologous bone graft has long been considered the gold standard for bone loss in the treatment of fractures. Problems associated with harvesting autologous bone graft, such as increased operative time, blood loss, and donor site morbidity, have led to the development of several alternatives such as demineralised bone matrix and calcium phosphate cements to name a few (Ladd and Pliam 2001). Bone graft or bone graft substitutes are used to fill the fracture void and in creating a structural support, and are used to augment internal or external fixation. The increased use of fixed angle plates has reduced the need for additional structural support since the screw-plate construct itself bridges the fracture site in a load-bearing manner (Orbay and Fernandez 2004).

2.3.5 Rehabilitation

The rehabilitation protocol following a distal radius fracture is dependent on the type of fracture and on the treatment modality. Rehabilitation of soft tissues in the form of oedema management and tendon gliding exercises is important. Furthermore, an understanding of fracture site forces and the stages of fracture healing is critical in guiding rehabilitation. Cadaver studies have shown that for every 10 N of grip force, 26 N is transmitted through the distal radius metaphysis (Putnam et al. 2000). Since the average male grip force is 463 N, then 1203 N of force could be applied to the distal radius during power gripping (Mathiowetz et al. 1985). To prevent a failure of fixation, the grip forces during rehabilitation should not exceed 159 N and 140 N for plates and external fixators in the first 4 weeks respectively (Frykman et al. 1993, Gesensway et al. 1995). Displaced comminuted fractures require a slower pace of fracture site loading during rehabilitation (Slutsky and Herman 2005). Gripping and grip strengthening exercises should be delayed until there is some fracture site healing (Slutsky and Herman 2005).

2.3.6 Factors affecting outcome

The question of whether anatomical restoration of the distal radius is necessary for the achievement of good long-term functional outcome has been the primary research question in many clinical studies. Biomechanical studies have demonstrated that radial

shortening disturbs the kinematics of the DRUJ and distortion of the TFCC (Adams 1993). Axial shortening has also been shown to correlate with a poor functional outcome (Aro and Koivunen 1991). Furthermore, decreases in the radial inclination increase load in the lunate fossa (Pogue et al. 1990). Angulations of more than 20 degrees in palmar or dorsal directions cause higher load concentrations in the distal radius (Pogue et al. 1990). Dorsal carpal instability may be associated with dorsal angulation due to changes in carpal kinematics (Park et al. 2002).

The load changes in the distal radius associated with malposition are expected to accelerate degenerative changes in the long run (Ilyas and Jupiter 2007). Similarly, even small step-offs in articular congruity are associated with late radiocarpal arthrosis (Knirk and Jupiter 1986, Geissler and Fernandez 1991, Kopylov et al. 1993). The study by Knirk and Jupiter, published in 1986, was a landmark study that is still considered one of the most important papers on the management of intra-articular distal radial fractures. Although the article has been criticized for having some methodological flaws, the finding that accurate articular restoration is the most critical factor in preventing arthrosis in young patients is still valid today (Haus and Jupiter 2009).

Overgaard and Solgaard (1989) found that the occurrence of arthrosis 7 years after a distal radius fracture correlated with the initial fracture displacement. A study by Catalano et al. (1997) also demonstrated a strong association between residual articular displacement and arthrosis, but the presence of radiological arthrosis did not correlate with functional or subjective outcomes. Currently, the guidelines for acceptable closed reduction are: radial inclination $\geq$ 15 degrees, radial length $\leq$ 5 mm shortening, dorsal tilt < 15 degrees, volar tilt < 20 degrees, and articular incongruity < 2 mm (Graham 1997, Nana et al. 2005, Ilyas and Jupiter 2007).

Factors unrelated to anatomical malalignment have also been shown to affect outcome following a distal radius fracture. Lower education levels, third-party compensation claims, and the presence of other medical comorbidities seem to be associated with poorer outcomes (MacDermid et al. 2002, Grewal et al. 2007). Objective features of complex regional pain syndrome (CRPS) have been found in up to 62% of patients with an unsatisfactory result at ten years after a Colles' fracture (Warwick et al. 1993). Interestingly, there is moderate evidence to support the use of Vitamin C in the prevention of CRPS or disproportionate pain following these fractures (Zollinger et al. 1999, Zollinger et al. 2007, Lichtman et al. 2010).

2.3.7 Outcome measures

The outcome following a fracture of the distal radius can be measured and reported using both subjective and objective parameters. During the last ten years, the importance of the patient's self-reported outcomes has been recognized and several questionnaires have been created for this purpose (Chen and Jupiter 2007).

2.3.7.1 Objective parameters

Radiographic evaluation

Conventional radiographic evaluation of distal radius fractures is performed from AP and lateral radiographs of the wrist (van der Linden and Ericson 1981). The most commonly measured parameters are radial height, radial inclination, volar tilt, and ulnar variance. Additional measurements can include articular gap and step-off. Newer radiographic parameters, such as teardrop angle and anteroposterior distance, may also have clinical significance (Medoff 2005). The evaluation of arthrosis can also be performed from plain radiographs and can be graded according to classifications such as that presented by Knirk and Jupiter (1986). The limitations of evaluations made from plain radiographs have been acknowledged, and computerized tomography appears to be a more reliable method in the evaluation of articular incongruities (Cole at al. 1997).

Strength measurements

The commonly reported strength measurements in clinical studies of distal radius fractures are grip strength and pinch grip strength. These measurements are performed using dynamometers and are preferably repeated three times with a short resting interval in between in order to minimize the effects of cumulative fatigue. The three results are then averaged to obtain a more accurate value. The strength measurements are presented in kilograms and also commonly as a percentage of the value of the uninjured contralateral side since this ratio has been shown to be more sensitive in detecting clinical changes (MacDermid et al. 2000). Some studies have accounted for hand dominance in grip strength measurements by adjusting the values to reflect 10% greater strength of the dominant hand (Hegeman et al. 2005). Grip strength evaluations have shown that this 10% rule is valid for right-handed persons only, whereas for left-handed persons, grip strength should be considered equal in both hands (Petersen et al. 1989).

Range of motion measurements

The commonly evaluated range of motion (ROM) measurements, following a distal radius fracture are: wrist flexion, extension, radial and ulnar deviation, as well as supination and pronation (Wei et al. 2009). ROM measurements are usually carried out using a standard goniometer, and results are presented in degrees, as well as a percentage relative to the value of the unaffected limb. Additionally, measurement of digital motion to palm has also been reported in some studies and can be measured as the distance of the finger pad from the distal palmar crease (Rozental et al. 2009).

Functional evaluation

The Jebsen-Taylor Hand Function Test (JTT) was created to provide quantitative measurements of standardized tasks for the assessment of hand function (Jebsen et al. 1969). The test involves several tasks, which are timed and can be compared with established normative values. A recent study found poor correlation between changes

in JTT and patient-reported outcomes using the Michigan Hand Outcomes Questionnaire (MHQ) (Sears and Chung 2010). Another functional outcome measure is the Gartland and Werley score, which is an objective evaluation of wrist function based on the range of motion (Gartland and Werley 1951).

2.3.7.2 Subjective parameters

Several types of questionnaires have been used to evaluate subjective outcomes following a fracture of the distal radius. The most commonly used validated questionnaires are the Short-Form-36 (SF-36), the Disabilities of the Arm, Shoulder and Hand (DASH), and the Patient-Rated Wrist Evaluation (PRWE) (Amadio et al. 1996, Changulani et al. 2008). The PRWE questionnaire has been shown to be more responsive than the DASH or the SF-36 questionnaires in the assessment of recovery following a distal radius fracture (MacDermid et al. 2000). Other subjective outcomes include the Michigan Hand Outcomes Questionnaire (MHQ) and the Musculoskeletal Function Assessment (MFA) (Engelberg et al. 1996, Chung et al. 1998).

2.3.8 Complications

The reported complication rates of distal radius fractures vary from 6%-80% (Turner et al. 2007). These complications may be due to the fracture or its treatment. Inadequate treatment of forearm fractures is one of the most common reasons for malpractice compensation in Finland with nearly 100 compensated patients per year (Vasenius 2008). Furthermore, malunion of the distal radius was found in most of the patients who received malpractice compensation during 1997-1999 (Vasenius 2008).

Turner et al. (2007) divide distal radius fracture complications chronologically into 3 groups: immediate, early (less than 6 weeks), and late (greater than 6 weeks). Immediate complications include nerve injury, open injury, skin injury during manipulation, compartment syndrome, and missed associated injuries. Early complications include cast issues, loss of reduction, infection, neurologic complications, and tendon rupture. Late complications include nerve complications and complex regional pain syndrome, arthrosis, nonunion/delayed union, malunion, and tendon complications.

Early identification and prompt treatment can reduce the long-term effects of these complications (Turner et al. 2007). Potential complications may go unnoticed if not actively suspected. McKay et al. (2001) developed a checklist that grades individual complications and provides an overall score for the complications. Although this checklist is somewhat more suitable for research purposes, shorter versions may be useful in the clinical setting.

2.4 RADIOSTEREOMETRIC ANALYSIS (RSA)

Radiostereometric analysis is a method that enables accurate determination of three-dimensional measurements of object motion from repeated radiographic examinations (Selvik et al. 1983).

2.4.1 History

The basic principles of modern-day radiostereometric analysis were presented by Göran Selvik in 1974 (Selvik 1974). The method was based on previous studies of the metallic implant technique (Björk 1968), x-ray photogrammetry (Hallert 1970), and mathematical principles of rigid-body kinematics (Euler 1775). Selvik constructed a system for performing roentgen stereophotogrammetry, which he later named roentgen stereophotogrammetric analysis (RSA) (Selvik 1974, Kärrholm 1989). The terms radiostereometric analysis, radiostereometry and roentgen stereophotogrammetric analysis are synonymous and can all be abbreviated by RSA (Valstar et al. 2005). Since 1974, the RSA method has seen numerous developments that have facilitated performance and improved accuracy (Kärrholm 1989).

The main topics that have been studied using RSA have included: prosthetic fixation (Ryd 1992), joint kinematics and joint stability (Uvehammer et al. 2000), skeletal growth (Hägglund et al. 1986), fracture stability (Mattson and Larsson 2004), vertebral motion (Pearcy 1985), and spinal fusion (Johnsson et al. 1990).

The increased interest in the use of RSA has led to the development of several types of RSA software and hardware (Kärrholm 1989, Ryd and Toksvig-Larsen 1993, Vrooman et al. 1998, Alfaro-Adrián et al 1999). There are currently three systems that are commercially available for carrying out RSA studies: UmRSA (RSA Biomedical, Umeå, Sweden), WinRSA (Tilly Medical Products, Lund, Sweden), and RSA-CMS (MEDIS Medical Imaging Systems BV, Leiden, the Netherlands).

2.4.2 Basic principles

The RSA technique utilizes dual simultaneous radiographs in association with a calibration cage. The calibration cage contains a number of 1.0 mm tantalum beads that are located in fixed and well-defined positions in the walls of the cage. These markers enable the construction of a three-dimensional reference coordinate system.

A RSA investigation can be divided into four main stages: 1) implantation of tantalum markers into the body segments to be studied, 2) radiographic examination, 3) measurements from radiographs, and 4) mathematical calculations (Kärrholm 1989).

2.4.3 Implantation of markers

Spherical tantalum markers with a diameter of 0.5, 0.8, or 1.0 mm are used to define the body segments to be studied. Tantalum metal has been chosen for this purpose since it has a high atomic number and can easily be identified on radiographs. Tantalum metal is biocompatible (Grundschober et al. 1982, Alberius 1983), and

resistant to corrosion (Burke 1940). The tantalum markers used in RSA are permanently deposited in bone, but have not been associated with any adverse reactions (Kärrholm et al. 1997). However, one case of chronic urticaria from tantalum surgical staples has been reported in the literature (Werman and Rietschel 1981).

The tantalum markers can be inserted using a spring-loaded piston (Aronson et al. 1974). Depending on the insertion site and the quality of bone, pre-drilling or use of a cannula with a beveled tip may be required to facilitate insertion. At least 3 non-collinear markers should be used to mark each rigid body being studied in order to perform a complete kinematic analysis (Selvik 1974). Some implanted tantalum markers may be obscured by metal implants, and some markers may remain loose. These markers often have to be excluded, and therefore it is recommended that 6 or more markers be used to mark each segment whenever possible (Valstar et al. 2005).

2.4.4 Radiographic examination

There are several radiographic set-ups that can be used in RSA. The most common techniques are uniplanar and biplanar. Each of these set-ups uses a special calibration cage. Tantalum markers in the cage walls closest to the film plates are called fiducial markers and are used to identify the coordinate system. The markers in the walls nearest to the radiographic tubes are known as control markers and are used to calculate the positions of the radiographic foci.

In the uniplanar set-up, the film cassettes are placed side-by-side, whereas in the biplanar set-up the film cassettes are positioned at a 90-degree angle to one another **(Fig. 2)**. In the uniplanar set-up, the area to be examined is placed above the calibration cage. The biplanar set-up requires that the area to be examined be placed inside the calibration cage. In both set-ups it is important that the body under examination be aligned with the cage so that movements are recorded in relation to axes with a standardized orientation relative to anatomic landmarks.

Ceiling mounted or mobile X-ray tubes can be used for radiography. The radiation doses used in RSA examinations have proven to be lower than corresponding doses in conventional radiographic examinations (Kärrholm et al. 1982, Kärrholm et al. 1988).

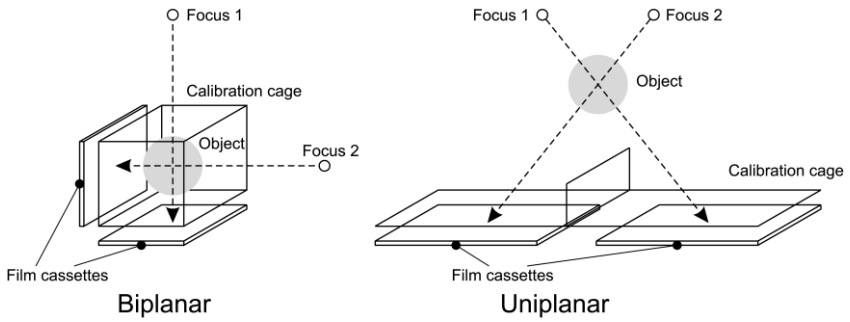

Figure 2. The two commonly used radiographic set-ups for RSA.

2.4.5 Marking and analysis of radiographs

In the past, RSA radiographs were scanned into digital images. Modern-day RSA is performed using digital radiographs, which are imported into the RSA software. There are several software packages available for marking the radiographs and calculating the three-dimensional locations of the tantalum markers in the body segment to be studied. Mathematical models of ideal radiographic images of tantalum markers are used to obtain the best fit to an actual marker image. If two marker images partially overlap or the marker is projected close to a radio-opaque edge of a metallic implant, special algorithms in the software have to be used to avoid distortion.

The stability and distribution of markers within an object have been shown to affect the accuracy of motion calculations (Kärrholm et al. 1989). Two important quality control parameters in RSA examinations are the mean error of rigid body fitting (ME) and the condition number (CN). The former is the mean difference between the relative distances of markers in a rigid body in one examination compared to that in another examination and is an indicator of marker stability (Ryd 1986). The latter is an indicator of marker distribution and demonstrates how well markers are scattered (Söderqvist and Wedin 1993). A low condition number reflects a wide spatial distribution, whereas a high number indicates that markers are placed close to a line.

2.4.6 Calculation of micromotion

The calibration cage in RSA studies is used to define the location and orientations of the global coordinate system. A reference rigid body has to be selected when calculating relative motion. The choice of reference segment is usually based on the clinical question being studied.

There are several ways for calculating and presenting micromotion results. The most common is to present the motion as orthogonal translations and rotations in three axes. Another way is to present the motion as Maximal Total Point Motion (MTPM) and helical axes. For measurements of translation, it is vital to account for the selected point of measurement. This can either be a single marker, or the centre of gravity of a rigid body. Furthermore, the points used should be standardized and utilized during all follow-up occasions. The right-hand co-ordinate system should be used for all calculations of micromotion. In order to compare motion in the left and right extremities it is important to recognize sign changes for X-axis translation as well as for Y-axis and Z-axis rotations **(Fig. 3)**. The total translation and total rotation can also be summarized using the 3-D Pythagorean Theorem ($T^2 = X^2 + Y^2 + Z^2$), provided that the rotations are relatively small (Selvik 1989, Kaptein et al. 2007).

MTPM is the length of the translation vector of the point in a rigid body that undergoes the greatest movement. The use of MTPM to describe the motion of a body may have more clinical significance in some instances, as the biological effect is likely to be greatest at the point of maximal motion (Valstar et al. 2005). An important shortcoming of MTPM is that it is highly dependant on the points of measurement. Furthermore, MTPM is highly sensitive to marker loosening (Valstar et al. 2005).

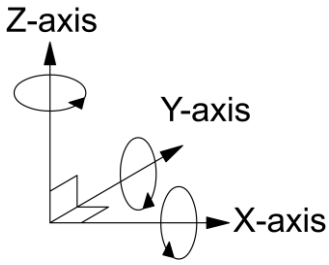

Figure 3. The right hand co-ordinate system used in RSA.

Helical axes can also be used to describe combined translation and rotation but require rotations to be larger than 4 degrees in order to obtain accurate results (Kärrholm et al. 1994). The helical axis is useful for describing joint kinematics but not fracture or implant micromotion.

2.4.7 The accuracy and precision of RSA

Two critical properties of any measurement system are accuracy and precision. Accuracy is defined as the closeness of agreement between a test result and an accepted reference value (ASTM 1990). Precision is defined as the closeness of agreement between repeated independent test results obtained under stipulated conditions (ASTM 1990).

The high accuracy and precision of RSA enable performing randomised clinical trials with small patient populations (Ryd et al. 1995). Validation of specific RSA set-ups are conventionally performed using phantom model studies. The accuracy and precision of RSA have been evaluated in several *in vitro* **(Table 2A)** and clinical studies **(Table 2B)**. The accuracy of RSA is determined by comparing micromotion results to those determined by another method that has a better resolution than RSA, such as micrometers (Ranstam et al. 2000, Ryd et al. 2000). The validation of precision is performed using double examination or multiple repeated measurements. In clinical RSA studies, precision is evaluated for each patient using double examinations within a time interval of 10-15 minutes. The precision provides the basis for power calculations, thereby dictating the number of patients required to obtain significant results.

2.4.8 RSA standardization guidelines

With a growing number of published RSA studies, the need for standardization of these investigations to facilitate the comparison of outcomes from different research groups was acknowledged. The first guidelines for the standardization of radiostereometric analysis of implants were published in 2005 (Valstar et al. 2005). The guidelines include a description of RSA arrangements and accepted minimum requirements for accurate analysis **(Table 3)**. These published guidelines will form the basis of a detailed standardization protocol under the supervision of ISO and the European Standards Working Group on Joint Replacement Implants (CEN/TC

285/WG4). This protocol is aimed at facilitating the inclusion of RSA in a standard protocol for testing implants prior to their release for general use.

2.4.9 Model based RSA (MBRSA)

Model based RSA techniques have been recently developed to avoid the problems related to attaching markers to prostheses. In this technique, the position of the implant is evaluated by matching a virtual projection of a three-dimensional model of the implant to the radiographic projection of the implant (Valstar et al. 2001, Kaptein et al 2003). If the implant is asymmetrical, its projection will appear unique. Thus, the orientation of an implant can be estimated from its projection by determining the corresponding shape in the model of the implant until minimal differences are achieved.

With modern MBRSA it is possible to achieve levels of accuracy comparable to the accuracy of techniques using markers (Kärrholm et al. 2006, Hurschler et al. 2009). The introduction of model based RSA has facilitated the introduction of new implant-related RSA studies, since it does not require technical modifications of the implants. The model-based technique has, however, not yet solved the problem of marking bone, which is a prerequisite in most RSA applications.

2.4.10 Dynamic RSA and inducible micromotion

In addition to being an accurate and precise method for static measurements, RSA has been used to study joint kinematics dynamically. Dynamic RSA has been used to study wrist movements (de Lange et al. 1985), glenohumeral joint kinematics (Bey et al. 2006, Hallström and Kärrholm 2009), ankle and subtalar joint motion (Lundberg 1988, Lundberg et al. 1989), knee joint kinematics (Kärrholm et al. 1988, Brandsson et al. 2002, Saari et al. 2005), as well as joint kinematics following total knee arthroplasty (Li et al. 2006, Russo et al. 2006).

One of the most powerful applications of dynamic RSA is the ability to detect inducible micromotion. These measurements were developed so as to detect the amount of cyclic micromotion by comparing relative positions of implants in different states of loading (Wilson et al. 2009). Dynamic RSA can measure inducible motion at the bone-implant interface following knee and hip arthroplasty (Uvehammer and Kärrholm 2001, Glyn-Jones et al. 2006). Additionally, the method can be used to measure inducible motion at the bone-bone interface in healing fractures (Downing et al. 2008, Chehade et al. 2009). Various methods of loading have been used to induce micromotion of implants or fractures, among these are maximal grip, different types of weight bearing, resisted torque, as well as the use of standard weights. A summary of clinical RSA studies of inducible micro motion is presented in **Tables 4A** and **4B**.

Inducible displacements of tibial components in TKR have been considered to indicate the quality of the prosthetic-bone or cement-bone interfaces (Regnér et al. 2000). There is very little data in the literature regarding the clinical significance of this inducible micromotion. The rotational inducible micromotion measured by RSA was shown to

be significantly higher in 2 out of 16 patients who underwent unicompartmental knee replacement (Bragonzoni et al. 2005). These two patients suffered from inexplicable pain, although RSA migration patterns indicated a stable prosthesis.

Table 2A. The levels of accuracy and precision of the RSA method obtained in various in vitro studies.

Study type, radiographic setup	Reference	Accuracy		Precision	
		Translation (mm)	Rotation (degrees)	Translation (mm)	Rotation (degrees)
Glass model Uniplanar	Kärrholm et al. 1997	0.007 – 0.025[d]	0.02-0.03[d]		
THR model, Uniplanar	Önsten et al. 2001	0.045-0.12[a]		0.024-0.104	
Plexiglass model, Uniplanar	Allen et al. 2004			0.004-0.017	0.01-0.22
THR model, Uniplanar	Mäkinen et al. 2004			0.013-0.123	0.02-0.35
THR model, Uniplanar	von Schewelov et al. 2004	0.19-0.25[b]			
THR model, Uniplanar	Bragdon et al. 2004	0.021-0.050[c]		0.006-0.012	
	Bragdon et al. 2002	0.022-0.086[c]		0.006-0.016	
Distal femur fracture model, Biplanar	Duffy et al. 2006			0.020	0.15
TKR model, Biplanar	Laende et al. 2009	0.018-0.075[a]	0.061-0.153[a]	0.017-0.044	0.014-0.049
Tibial plateau fracture model, Uniplanar	Solomon et al. 2010	0.037[e]	0.123[e]	0.016	0.024

[a] Accuracy calculated as the 95% prediction intervals from regression analyses between the measured and actual displacements.
[b] Accuracy calculated as a sum of bias and repeatability (confidence level 95%).
[c] Accuracy calculated using an analysis of variance (confidence level 95%).
[d] Accuracy calculated as the mean difference between the two measurement methods used, namely radiostereometry and a coordinate measurement machine (standard deviation 40-214 µm and 0.04-0.3°).
[e] Accuracy calculated as root mean square error (RMSE).

Table 2B. The precision levels of the RSA method obtained in relevant clinical studies.

Study type, Radiographic setup	Reference	Precision	
		Translation (mm)	Rotation (degrees)
THR studies, Uniplanar	Kärrholm et al. 1997	0.15-0.60	0.3-2
Cervical spine fusion, Uniplanar	Zoëga et al. 1998	0.27-0.85	1.3-4.2
Proximal tibial osteotomy, Biplanar	Magyar et al. 1999	0.20	0.3
Lumbar spine fusion, Uniplanar	Johnsson et al. 2002	0.41-0.60	0.43-1.89
Femoral neck fractures, Uniplanar	Ragnarsson et al. 1993	0.4-1.0	0.5-1.4
	Mattsson and Larsson 2003	0.31-0.67	0.6-1.16
Trochanteric fractures, Uniplanar	Mattsson and Larsson 2004	0.16-0.64	0.91-1.32
Distal radius fracture, Biplanar	Downing et al. 2008	Migration 0.06-0.13 IM 0.10-0.14	Migration 0.5-0.8 IM 0.6-1.0
Total shoulder arthroplasty, Uniplanar	Rahme et al. 2009	0.10-0.19	0.93-1.29
TKR study, Biplanar	Gao et al. 2009	0.15	0.2-0.37

IM: inducible micormotion

Table 3. Standardized output guidelines for a clinical RSA study (Valstar et al. 2005)

1.	The units for translation should always be millimetres and the units for rotations should be degrees.
2.	The accuracy and precision of the arrangement used should be presented. Measurement interval and window tolerance should be quoted.
3.	Type of calibration cage and use of reference plates should be given.
4.	It should be stated whether fixed or portable X-ray sources were used.
5.	Positioning of subject, calibration cage, X-ray tubes and X-ray cassettes should be standardized or described in detail. Orientation of the global coordinate system should be presented.
6.	Method of image acquisition should be stated.
7.	Software used should be stated, and if appropriate which version.
8.	Size of marker beads used should be given and validation results should be reported for the sizes used in the study.
9.	The method of determining the position of the implant, whether based on attached beads, geometrically or model-based should be stated. If appropriate, reference to any new/novel technique should be given.
10.	The following should be stated: cut-off level for condition number and mean error of rigid body fitting for exclusion of subjects from the study.
11.	Rigid body fixed coordinate frames and angular rotation sequence should be defined.
12.	The precision of the measurements assessed by double examinations of all patients enrolled in the study should be stated.
13.	Migration/motion data should be given in terms of translations and angular rotations. All 6 degrees of freedom should be reported.
14.	The point(s) used to measure translations should be indicated, standardized, and its (their) location on the implant (or in the bone) should always be presented.

There is also very little data regarding the link between inducible micromotion and long-term migration. Uvehammer and Kärrholm (2001), in a study of cemented tibial component migration following total knee replacement, showed that increased inducible micromotion at 1 year was associated with increased migration between 0 and 2 years (Spearman's rho = 0.54, p = 0.03). Similarly, Toksvig-Larssen et al. (1998) noted a relationship between inducible micromotion at 1 year and tibial component migration during the first year (r^2 = 0.20, p = 0.04). The authors also noted a relationship between inducible micromotion at 6 weeks and at 1 year (r^2 = 0.20, p = 0.035). Regnér et al. (2000) also reported a tendency for increased migration of uncemented tibial components at 5 years after TKR in implants, which had demonstrated high inducible displacements caused by an inward torque one year postoperatively.

Table 4 A. Summary of clinical RSA studies examining inducible micromotion in TKA.

Study focus	N*	Method of loading**	Measured inducible micromotion	Reference
Uncemented tibial component with and without metal backing and stem	32	1-Weight bearing 2-Weight bearing on one leg 3-Internally and externally rotating torque	-16 knees at 2 years -Mean inducible motion (MTPM) 0.7 to 1.2 mm for stemmed and 0.8 to 2.1 mm for non-stemmed prostheses -Significantly less inducible motion in stemmed group	Albrektsson et al. 1990
Uncemented tibia component with screw fixation	7	1-Weight bearing on one leg 2- Internally and externally rotating torque 3-Squatting with knee in 60˚ flexion	-At 1 year inducible displacement was detected in 6 patients -Mean inducible displacement (MTPM) 0.5 mm (rotatory and weight bearing) and 0.2 mm (squat)	Ryd et al. 1993
Cemented vs. uncemented tibial components	19	1-Weight bearing standing 2-Internally and externally rotating torque 3-Squatting with knee in 60˚ flexion	-Measurement of inducible motion at 1 to 2 months postoperatively -Inducible displacement (MTPM) 0.3-1.3 mm in 18 patients -No significant difference in inducible motion in the two groups	Ryd and Toksvig-Larsen 1993
Tibial components, with and without a cooled blade	33	1-Weight bearing standing 2-Internally and externally rotating torque 3-Squatting	-Inducible micromotion in all cases at 1 year -Mean inducible displacement (MTPM) 0.4-0.6 mm –Significantly less inducible motion in the cooled blade group in standing and squatting	Toksvig-Larsen et al. 1994
Cemented vs. uncemented tibial components	26	1-Weight bearing on one leg 2-Internally and externally rotating torque 3-Squatting	-Inducible displacement found in all knees at 6 weeks and 1 year with no difference in two groups -6 week MTPM 0.5-0.6 mm -1 year MTPM 0.3-0.7 mm	Toksvig-Larsen et al. 1998
Porous vs. hydroxyapatite-coated (HA) components	51	1-Internally and externally rotating torque	-Inducible displacement measured at 2 and 12 months -2 month MTPM 0.30-0.51 mm -1 year MTPM 0.31-0.36 mm -Tendency towards less inducible displacement in HA-coated prostheses	Regnér et al. 2000
Cemented tibial component	16	1-Film exchanger technique, inducible displacements at 5˚ intervals of extension	-At 1 year, knee extension from 45˚ to 15˚ caused median MTPM of 0.37 to 0.52 mm	Uvehammer and Kärrholm 2001
Trabecular metal vs. cemented tibial component	25	1-Weight bearing on one leg 2-Internally and externally rotating torque 3-Passive stress test (PST) axial load of 30 kg with knee in 90˚ flexion	-At 24 to 48 months -Cemented group MTPM 0.2-0.5 mm -Trabecular group MTPM 0.1-0.2 mm -Significantly less inducible micromotion in trabecular group	Wilson et al. 2009

* Number of knees, ** All inducible motion measurements relative to supine

Table 4B. Summary of clinical RSA studies examining inducible micromotion in other applications.

Study focus	N	Method of loading	Measured inducible micromotion	Reference
Anterior cervical spinal fusions	45	1-Maximal flexion and extension 2-Maximal rotation from right to left	-At 3 and 12 months -10 cases with significant motion at 3 months and 3 cases at 12 months	Zoëga et al. 2003
UKR Cemented tibial component	16	1-Supine 2-Weight bearing 3-Maximal internal and external rotation 4-Squatting 5-Internally and externally rotating torque	-Inducible micromotion in all prostheses at 14 and 26 months -Largest inducible rotations during squatting and rotational stress (0.4˚-0.6˚) -Inducible translation negligible	Bragonzoni et al. 2005
THA Cemented stem	21*	1-Double leg stance 2-Single leg stance	-Mean inducible displacement of head at 3 months 0.08 mm inferiorly and 0.1 mm posteriorly. -At 12 months 0.09 mm inferiorly and 0.12 mm posteriorly	Glyn-Jones et al. 2006
Plated distal radius fracture	9	1-Resting 2-Maximal voluntary grip	-Maximum inducible motion at 2 weeks -0.3 mm axial compression, 0.3 mm dorsal compression, 2.5˚ dorsiflexion. -No longer detectable at 26 weeks	Downing et al. 2008
Distal femoral fracture treated with a locking plate	6	1-Loading limb with 1-3 kg (preload) 2-Loading in increments of 20 kg up to 60 kg 3-loading limb with 1-3 kg (postload)	-At 6, 12, 18, and 26 weeks -Inducible micromotion increased as load was increased -The inducible micromotion progressively decreased in 5 of the patients reaching 0.01-1.05 mm and 0.2-1.2˚ for individual axes	Chehade et al. 2009
Anterior cervical discectomy and fusion	16	1-Maximal physiologic flexion 2-Maximal physiologic extension	-At 12 months -Average sagittal ROM 1.3 ± 1.4° -The inducible micromotion correlated with radiological measurements in the detection of pseudoarthrosis	Park et al. 2009

* Number of hips

2.5 MONITORING OF HEALING USING RSA

A computerized literature search was performed using MEDLINE to identify all citations concerning fractures, osteotomies, or vertebral fusion and radiostereometric analysis published from January 1970 through December 2009. The aim was to identify how RSA had been used to study the healing of bone in these various clinical settings. A second goal was to identify the magnitude of micromotion that had been detected in these studies during the healing period. The results of this literature search are presented in **tables 5**, **6** and **7**. The results of these studies are discussed below.

2.5.1 Distal radius fractures

In a randomised study, Kopylov et al. (2001) used RSA to compare distal radius fracture healing in 23 osteoporotic patients. The study compared the use of dorsal splint immobilization associated with the use of a self-setting hydroxyapatite, Norian SRS, to external fixation. By examining the micromotion in the fracture system, the study revealed that 5 weeks of immobilization is sufficient for healing with external fixation in the age group studied. The study also suggested that the immobilization time might be reduced to 2 weeks for fractures treated with Norian SRS, but additional hardware is needed to ensure the stability of the fracture system. The study showed that micromotion along the longitudinal axis during the immobilization period varied from 1.5 to 2.6 mm.

Downing et al. (2008) used RSA to assess inducible fracture micromotion in 9 patients with plated distal radius fractures. 4 patients had extra-articular fractures (types A2 and A3) and 5 had intra-articular fractures (types C1 and C2). The fractures were all treated with a volar locked plate with a small surface area. RSA examinations were performed at day 1, then at 2, 6, 26, and 52 weeks. Inducible micromotion presented as axial and dorsal compression in combination with dorsiflexion. The median inducible motion reached a maximum at 2 weeks and consisted of 0.3 mm axial compression, 0.3 mm dorsal compression, and 2.5 degrees dorsiflexion. Inducible motion was shown to cease by 26 weeks, indicating a union of all fractures by this point.

2.5.2 Femoral neck fractures

Ragnarsson and co-workers used RSA as a tool in several studies of femoral neck fractures (Ragnarsson et al. 1989, 1992, 1993, Ragnarsson and Kärrholm 1992). In one study (Ragnarsson et al. 1989), the spontaneous compression of femoral neck fractures was recorded between the operation and mobilization of the patients, with the finding of an average movement of 3.7 mm in displaced fractures, corresponding to about one third of the total fracture movements during the first postoperative month. In another study, the connection between instability and femoral head vitality in fractures of the femoral neck were examined (Ragnarsson et al. 1993). It was observed that absence of micromotion six months after fracture implied uncomplicated healing, whereas fracture stabilization at 9 to 12 months postfracture was associated with femoral head necrosis or delayed union in four of six cases.

Mattsson and Larsson (2003) used RSA to examine the stability of internally fixed femoral neck fractures augmented with resorbable cement. The study found that augmentation with calcium phosphate cement improved the stability of internally fixed femoral neck fractures during the first six weeks after surgery. The improvement in stability was found to be less pronounced at six weeks compared with at one week.

2.5.3 Trochanteric fractures

RSA has also been used to determine whether augmentation with resorbable calcium-phosphate cement could improve fracture stability in unstable trochanteric fractures as previously shown in biomechanical studies (Mattsson and Larsson 2004). The study compared fracture fixation with either a sliding screw device alone or the same device combined with calcium-phosphate cement for augmentation. Augmentation with calcium-phosphate cement was shown to improve fracture stability. The improvement was most pronounced for lateral and distal migration, as well as varus angulation of the head and neck fragment. The results showed that translation of the femoral head and neck fragment in the distal direction varied from 6-12 mm at 6 months follow-up.

2.5.4 Tibial plateau fractures

RSA has been used to study the stability of the elevated fragment in tibial plateau fractures (Ryd and Toksvig-Larsen 1994). Five cases of fractures of the lateral tibial condyle of the split depression type were treated by elevating the depressed fragment, bone grafting and internal fixation. During the procedure, tantalum markers were inserted into the depressed fragment and the tibial metaphysis. Plaster cast immobilization was used postoperatively for one month, and weight bearing was not allowed for three months. The results showed that in three cases, a depression of the elevated fragment, at the most 2.8 mm, recurred during the first postoperative month. This was not considered to be significant and suggested a more aggressive postoperative mobilization scheme.

Larsson et al. (2004) studied the use of calcium phosphate cement in the augmentation of tibial plateau fractures. The results of the study were presented at the Orthopaedic Trauma Association annual meeting in 2004. Conventional metal fixation was used to fix the fracture following elevation of the articular fragment. The subchondral void was filled with either injectable calcium-phosphate cement (Norian SRS, Synthes) or conventional iliac bone graft according to randomisation. Radiostereometry was used to study the stability during healing. The results showed that injectable calcium-phosphate cement provided a more stable fixation of the elevated articular fragment when compared with conventional bone graft; albeit cement augmented patients were allowed earlier weight bearing.

Table 5. Summary of clinical studies using RSA in the evaluation of healing fractures.

Study focus	N	Reference
Early weight bearing of malleolar fractures	46	Ahl et al. 1986
Early weight bearing of displaced ankle fractures	53	Ahl et al. 1987
Stability of internally fixed femoral neck fractures	16	Ragnarsson et al. 1989
Accuracy of measurements of femoral neck fractures	60	Ragnarsson et al. 1992
Factors influencing postoperative movement in femoral neck fractures	46	Ragnarsson and Kärrholm 1992
Instability and femoral head vitality in fractures of the femoral neck	16	Ragnarsson et al. 1993
Biodegradable fixation of ankle fractures	32	Ahl et al. 1994
Comparison of Norian SRS and external fixation in distal radius fracture treatment	23	Kopylov et al. 2001
Stability of internally fixed femoral neck fractures augmented with resorbable cement	40	Mattsson and Larsson 2003
Unstable trochanteric fractures augmented with calcium phosphate cement	26	Mattsson and Larsson 2004
Augmentation of tibial plateau fractures with calcium phosphate cement	24	Larsson et al. 2004
Assessment of inducible fracture micromotion in distal radial fractures	9	Downing et al. 2008
Monitoring of fracture stiffness in plated fractures of the distal femur using differential loads	6	Chehade et al. 2009

Table 6. Summary of clinical studies using RSA in the evaluation of vertebral fusions.

Study focus	N	Reference
Kinematic analysis of posterolateral fusion in the lumbosacral spine	3	Olsson et al. 1976
Mobility in the lumbosacral spine after fusion	12	Olsson et al. 1977
Postoperative kinematics in structural scoliosis	3	Olsson et al. 1977
Mobility of the lower lumbar spine after posterolateral fusion	11	Johnsson et al. 1990
Posterolateral lumbar fusion using facet joint fixation with biodegradable rods	11	Johnsson et al. 1997
One-level cervical spine fusion with or without plate fixation	27	Zoëga et al. 1998
Two-level cervical spine fusion with or without plate fixation	18	Zoëga et al. 1998
Comparison of BMP-7 and autograft bone in noninstrumented posterolateral lumbar fusion	20	Johnsson et al. 2002
Mobility provocation in anterior cervical spine fusions	45	Zoëga et al. 2003
One-level cervical fusion with or without plate fixation	37	Nabhan et al. 2007
Cervical range of motion after anterior cervical discectomy and fusion	16	Park et al. 2009

2.5.5 Ankle fractures

Ahl et al. (1994) compared the use of polyglycolic acid screws to the use of rods in the fixation of 32 selected displaced supination-eversion ankle fractures. RSA was used to study the movements in the ankle mortise during fracture healing. RSA showed that a better stability was achieved by using screws. After 6 months however, the clinical results did not differ. The results were also compared to those obtained using a nondegradable osteosynthesis technique. RSA showed better fracture stability with nondegradable fixation. Once again however, the clinical results did not differ.

In randomised studies, Ahl and co-workers (Ahl et al. 1986, 1987) observed that early weight bearing did not compromise the stability of malleolar fractures treated with open reduction and internal fixation using pins, wires, and staples. The studies also showed that at 18 months of fracture follow-up, supination injuries proved to be more stable than pronation ankle fractures (Ahl 1988).

2.5.6 Vertebral fusion

RSA has been used to study the loss of correction after the Harrington fusion of structural scoliosis (Olsson et al. 1977). In posterolateral fusions (Olsson et al. 1976), it was observed that vertebral motions did not decrease until 5-6 months after successful operations. This suggested that solid fusion is not necessary for pain relief (Olsson et al. 1976, 1977, Johnsson et al. 1990). Johnsson et al. (2002) also used RSA to compare osteogenic protein-1 (BMP-7) and autogenous bone graft in lumbar fusion. The osteogenic protein-1 did not yield better stabilizing bony fusion than an autograft.

In a study carried out by Zoëga et al. (1998), randomisation of 27 consecutive patients undergoing one-level cervical disc surgery (ACDF) with or without anterior plate fixation was carried out. The patients were studied with radiostereometry and clinically with visual analogue scores (VAS) for arm and neck pain. The use of an anterior plate appeared to prevent rotational deformation, without changing the clinical outcome or fusion rate. Nabhan et al. (2007) performed a similar study comparing one-level cervical fusion conducted using a stand-alone cage or a cage and plate fixation. The study did not demonstrate any differences in RSA measured micromotion between the groups at one, six or twelve weeks, as well as after six months, one and two years postoperatively. Similarly, no differences were detected in pain as measured using VAS (Nabhan et al. 2007).

Another randomised study examined whether the addition of a cervical spine locking plate in two-level disc fusions improved the postoperative stability and healing rate in 18 patients (Zoëga et al. 1998). The study found that the mean RSA measured compression was larger in patients operated without a plate. Also, these patients had more arm pain at one year. The addition of the plate did not, however, increase the healing rate or promote more rapid fusion.

Recently, Park et al. (2009) carried out a study to evaluate whether RSA measured sagittal range of motion (ROM) after ACDF correlated with radiographic findings.

They enrolled 16 patients who underwent multi-level ACDF, and cervical plates were utilized in each case. The study showed that RSA could detect a significant difference in segmental motion between segments that demonstrated radiographic signs of fusion and those with evidence of pseudoarthrosis (Park et al. 2009).

2.5.7 Osteotomies

Tjörnstrand et al. (1981) measured the correction obtained after high tibial osteotomy (HTO) for knee osteoarthritis by means of RSA, and found a postoperative loss of correction of up to 3-4°. Comparison with conventional radiography showed a sufficient accuracy of the latter when angular deviations were measured in the frontal plane. Another similar study by Pape et al. (2005) examined fixation stability following HTO. The study revealed that osteotomies in which larger wedge sizes were used (>8°) resulted in a 1.3-mm increase in lateral displacement of the distal tibial segment within 3 weeks following surgery. The study also showed that most of the displacement took place in the first three weeks following surgery and ranged from 2.6 mm to 3.2 mm in the cranial direction.

RSA has been used to compare HTO and open-wedge osteotomy by hemicallotasis (HCO) in the treatment of medial gonarthrosis (Magyar et al. 1999). In the HTO group, the RSA measurements were carried out at the time of plaster removal, 1 month later and 1 year after surgery, whereas in the HCO group, the measurements were performed at the time of the removal of the external fixator, 1 month later and at 1 year after surgery. After the removal of fixation RSA measured osseous correction, it demonstrated increased medial/lateral and distal translation of the proximal segment following HTO when compared with HCO. Furthermore, the tibial plateau showed more rotation around the longitudinal axis of the tibia after HTO. The study had a clear limitation since the time of plaster removal and external fixator removal were not standardised, but depended on when the osteotomy was considered stable. Additionally, the study did not examine whether the differences in migration between the groups had a clinical significance.

Hansson et al. (1978) used RSA to evaluate the changes of the acetabular position after innominate osteotomy for hip dysplasia. The study showed rotations of up to 32° and mainly craniodorsal translations of the acetabulum.

Table 7. Summary of clinical studies using RSA in the evaluation of osteotomies.

Study focus	N	Reference
Innominate osteotomy	1	Hansson et al. 1978
High tibial osteotomy in gonarthrosis	3	Tjörnstrand et al. 1981
Changes in osseous correction after proximal tibial osteotomy	33	Magyar et al. 1999
Fixation stability following high tibial osteotomy	15	Pape et al. 2005

3. AIMS OF THE PRESENT STUDY

This study was initiated to investigate the feasibility of using radiostereometric analysis (RSA) in the monitoring of healing in comminuted fractures of the distal radius. The present investigation had the following aims:

1. To validate RSA for the measurement of migration in distal radius fractures using a physical phantom model.

2. To validate RSA for the measurement of complex migration in intra-articular distal radius fractures using a computer simulation model.

3. To determine if resorbable markers can be used for accurate radiostereometric analysis.

4. To evaluate if RSA can be applied in the follow-up of healing in plated AO type-C distal radius fractures and to determine whether RSA can detect migration, inducible interfragmentary micromotion and fracture union during the healing period.

4. MATERIALS AND METHODS

4.1 MATERIALS (Studies II-V)

4.1.1 Creating physical phantom models

A physical plastic sawbone model of the left radius was used in **Study II** (model 1027, Sawbones Europe AB, Sweden). An extra-articular Colles' fracture (AO type 23-A2) was created by performing an osteotomy through the distal metaphysis of the radius. The proximal part of the radius was rigidly fixed to a plexiglass base plate with the volar surface facing downwards. Ten tantalum markers of a diameter of 0.8 mm were implanted, five placed proximally and five distally to the fracture site. Markers were inserted into pre-drilled holes using a spring-loaded piston (RSA Biomedical, Umeå, Sweden) and distributed in a pattern that could be used in a clinical insertion through a limited approach. The insertion holes were sealed with liquid adhesive to ensure no marker movement within the bone.

In the first part of **Study II,** the distal fragment of the radius was rigidly attached to a high precision x,y,z translation stage (M-460A-xyz, Newport, Irvine, CA, USA) via a plastic holder connected to a high precision rotation stage (M-UTR80, Newport, Irvine, CA, USA). The translation stage was instrumented with three Vernier micrometers (model SM 13, Newport, Irvine, CA, USA). According to the manufacturer, the system is accurate to 1 µm for translation with an angular deviation of less than 0.009° and accurate to 1/60° for rotation with a wobble of ± 0.003°. The translation stage was fixed to the same plexiglass base plate as the proximal part of the radius **(Fig. 4A).** The distal fragment was then aligned with the proximal radius as before the fracture, but with a clearance of at least 1 mm from it in the longitudinal axis. This experimental set-up allowed translation movements in three axes and rotation about the longitudinal axis.

In the second part of **Study II,** the distal part of the radius was rigidly attached to the high precision rotation stage (M-UTR80, Newport, Irvine, CA, USA) via a plastic holder. The rotation stage was fixed directly to the same plexiglass base plate as the proximal part of the radius **(Fig. 4B)**. The distal fragment was then aligned again with the proximal radius as before the fracture, but with a clearance of at least 4 mm from it in the longitudinal axis. This experimental set-up allowed rotation only about the transverse axis but no translation.

In **Study IV,** a fresh-frozen porcine cadaver forearm was thawed. The soft tissues were excised and saved for later use. An experimental two-part extra-articular fracture of the distal radius was created. A total of ten novel resorbable RSA markers were implanted into the bone with five placed proximal and five distal to the osteotomy site. The markers were inserted into bone holes made by a dental drill. In order to ensure the stability of the markers, the insertion holes were sealed using bone wax. The proximal end of the radius was rigidly fixed to a plexiglass base plate **(Fig. 4C).** The distal fragment was rigidly attached to a high precision x,y,z translation stage (M-460A-xyz,

Newport, Irvine, CA, USA) via a plastic holder connected to a high precision rotation stage (M-UTR80, Newport, Irvine, CA, USA). The translation stage was instrumented with three Vernier micrometers (model SM 13, Newport, Irvine, CA, USA). This experimental set-up allowed translation movements in three axes and rotation about the longitudinal axis. The soft tissue envelope initially removed from the limb was suspended around the bone on a specially designed frame to simulate the conditions of *in vivo* RSA imaging of a wrist fracture.

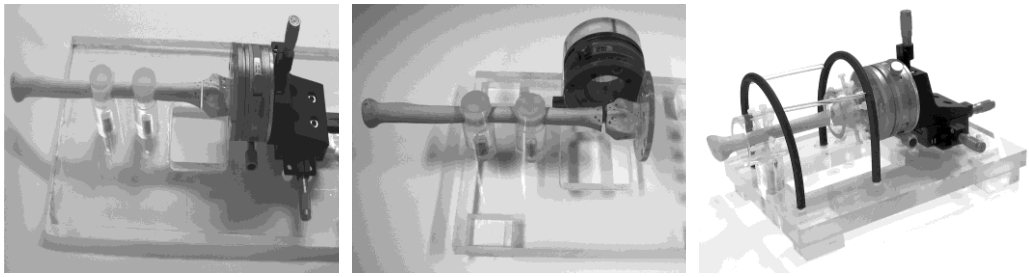

A B C

Figure 4. The physical phantom models used in Studies II (A and B) and IV (C) for testing the accuracy and precision of RSA (figures from Studies II and IV).

4.1.2 Creating a computer simulation model

In **Study III**, A physical plastic sawbone model of the left radius (model 1027, Sawbones Europe AB, Sweden) was used to create a three-dimensional computer simulation model of the radius. The model was digitised using a pQCT device (Stratec XCT Research M, Norland Stratec Medizintechnik GmbH, Birkenfeld, Germany). The radius was imaged perpendicular to its longitudinal axis. Two groups of cross-sectional CT slices were created **(Fig. 5A)**. The CT slices from the distal part of the radius were obtained at 1 mm intervals and those from the diaphysial area at 2 mm intervals from each other. The voxel size was 0.1 mm x 0.1 mm x 0.5 mm. The data from the pQCT slices was exported in ASCII format and converted to an 8-bit bitmap image format.

The bitmap images were then imported into a CAD program (Rhinoceros, Robert McNeel & Associates, Seattle, USA). The outlines of each of the images were traced in two dimensions and then moved in the third dimension in the modelling space in the order in which the slices were obtained by pQCT. Thus, an array of two-dimensional curves separated from each other by 1 mm and 2 mm was created. Based on these curves, a three-dimensional geometrical model of the bone was made **(Fig. 5A)**. For further use in the ray-tracing scene the 3D geometry was converted into a triangular mesh and presented according to the syntax of POV-Ray SDL.

In order to mimic the spherical tantalum markers used for marking bone fragments for radiostereometric analysis, simulated markers were inserted into the model of the radius. In the CAD program, points representing the positions of the bone markers

were first selected. These points were offset by 0.4 mm from the surface of the 3D model of the radius. The coordinates of these points were used in the ray-tracing scene to position spheres with a radius of 0.4 mm. A total of ten spherical markers were placed into the model with five placed proximally and five distally to the fracture site using the SPHERE function of the POV-Ray program (Persistence of Vision Raytracer Pty. Ltd., version 3.5). The spheres had spatial arrangements similar to those in **Study II**.

Experimental extra-articular (two-fragment, AO type A2) and intra-articular (three-fragment, AO type C1) fracture model was created by digitally osteotomising the distal metaphysis of the 3-D model of the radius in the POV-Ray program **(Figs. 5B and 5C)**.

Figure 5. Creation of the three-dimensional computer model of the distal radius (A) and the two fracture patterns used (figures from Study III).

A three-dimensional model of the RSA calibration cage (Cage type 10, RSA Biomedical, Umeå, Sweden) was created by measuring the cage dimensions, and then scanning each of the four walls with a flatbed scanner (UMAX PowerLook 2100 XL, UMAX, Taiwan) to determine the exact locations of reference markers. This information was coded using the POV-Ray SDL. In the ray-tracing scene, the reference markers of the RSA calibration cage were simulated by spheres with a radius of 0.4 mm. The spheres were assembled into four two-dimensional arrays, each representing their physical arrangement on each face of the RSA-cage. The arrays were positioned in the three-dimensional virtual space with the same orientation and relations as in the physical RSA cage **(Figs. 6A and 6B)**. This object, consisting of the four arrays of spheres, was used as the 3D model of the RSA calibration cage.

The 3D model of the radius was placed into the simulated model of the calibration cage with the volar surface facing downwards, such that the axis of the camera crossed the longitudinal axis of the bone at the osteotomy site **(Fig. 6C)**. The position of the proximal radius was fixed during simulation, while rotational and translational movements were applied to the distal fracture fragment.

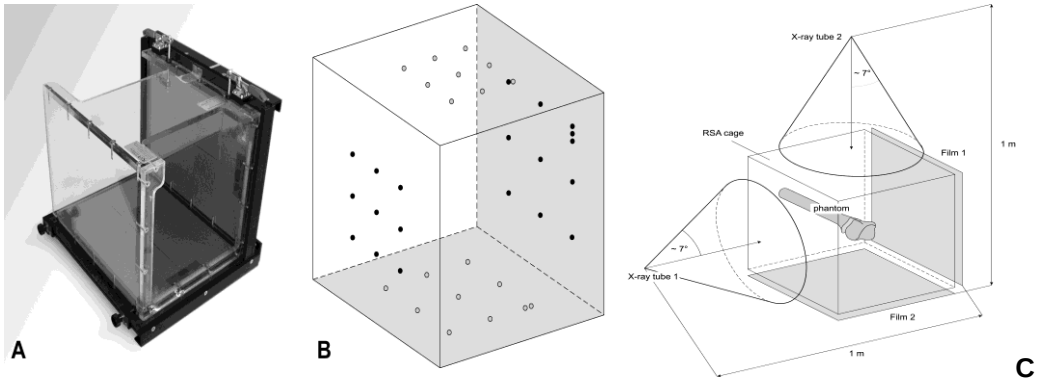

Figure 6. Diagram showing how a simulation model of the RSA calibration cage (Cage type 10, RSA Biomedical, Umeå, Sweden) was created. The RSA cage type 10 (A) and the simulation model (B) composed of spheres assembled into four two-dimensional arrays, each representing the physical arrangement of tantalum markers on each face of the RSA-cage. (C) Schematic of the set-up. The simulated x-ray tube in the ray-tracing scene was positioned 1 m from the image plane. The shaded rectangles represent the two image planes simulating radiographic film cassettes (figures from study III).

4.1.3 Manufacturing of bioactive glass implants

The composition of the bioactive glass selected for **Study IV** (coded 1-06, Åbo Akademi University, Turku, Finland), was 50.0 wt% SiO_2, 4.0 wt% P_2O_5, 0.2 wt% B_2O_3, 5.9 wt% Na_2O, 12.0 wt% K_2O, 22.6 wt% CaO, 5.3 wt% MgO (Vedel 2008). This composition was chosen since it is known to have good bioactivity, as well as a wide working range, enabling the manufacture of various morphologies (Vedel 2008). Native glass 1-06 is inadequately visible on plain X-rays. Two radio-opaque glasses were created by adding $BaSO_4$ to the basic glass composition.

Study IV compared the following four glasses: (1) bioactive glass 1-06 with 2.5 weight % of $BaSO_4$, (2) bioactive glass 1-06 with 10 weight % of $BaSO_4$, (3) bioactive glass 1-06 without any additives, and (4) nearly inert glass (flat glass). In this study, these four glasses were coded as glass 1-06, 1-06B2.5, 1-06B10 and FG, respectively.

Truncated glass cones with a height of 7 mm, base Ø 3 mm, tip Ø 1.9 mm and a tip angle of 9° were manufactured for *in vitro* and in *vivo* studies. As a first step to produce bioactive glass 1-06, Ph.Eur. analytical reagent grade of $CaCO_3$, Na_2CO_3, $CaHPO_4{\cdot}2H_2O$, H_3BO_3, K_2CO_3, MgO, as well as commercial quartz sand (Belgian Sand 99.8% purity) were mixed and used for the glass batches **(Table 8)**. These batches (giving 300 g of glass) were melted in a platinum crucible for 3 hours at 1,360 ºC in an electrical laboratory furnace. The melt was first cast into a plate using a pre-heated graphite mould, annealed at 520°C for 1 hour, allowed to cool to room temperature in an annealing furnace and crushed. In the next manufacturing step, the crush was either used as such to produce generic glass 1-06, or mixed with 2.5 and 10 weight % of Ph.Eur. analytical reagent grade $BaSO_4$ to produce the two novel radio-opaque glasses.

The crush was re-melted at 1,360 ºC for 3 hours, and, to produce conically-shaped implants, the melts were cast into pre-heated graphite moulds, annealed at 520°C for 1 hour, and allowed to cool to room temperature in an annealing furnace. In this way, all the glasses used in the study were subjected to the same melting and annealing procedure. Based on plain X-ray examinations, *in vitro*, and *in vivo* results, glass 1-06B10 was selected as the material for creating RSA markers. RSA markers of spherical shape (diameter of approximately 1.5 mm) were manually manufactured.

Table 8. Raw materials used to prepare the glasses used in the study (table from Study IV).

Product name	Provider	Lot number	Assay
Calcium carbonate $CaCO_3$	Yliopiston apteekki Analyyttinen laboratorio Finland	62607	98.7%
Sodium carbonate Na_2CO_3	Sigma-Aldrich Co.	6224A	100.0%
Calcium phosphate dibasic dehydrate $CaHPO_4 \cdot 2H_2O$	Sigma-Aldrich Co.	51440	100.4%
Boric acid H_3BO_3	Merck KGaA	A696960 603	100.0%
Potassium carbonate K_2CO_3	Sigma-Aldrich Co.	51820	99.6%
Magnesium oxide MgO	Yliopiston apteekki Analyyttinen laboratorio Finland	62283	99.4%
Barium sulphate $BaSO_4$	Sigma-Aldrich Co.	04512AD	99%
Belgian sand Mam1	SRC-Sibelco NV		99.8%

4.2 ANIMALS (Study IV)

4.2.1 Experimental animals and anaesthesia

In **Study IV,** an *in vivo* examination of the bone bonding properties of two $BaSO_4$-containing glass compositions (1-06B2.5 and 1-06B10) was carried out. Ten three-month-old female Sprague Dawley rats (Harlan Netherlands), weighing 225 to 250g, were anaesthetised with a subcutaneous administration of medetomidine (Domitor®, Orion Pharma, Espoo, Finland) and fentanyl citrate (Fentanyl®, B.Braun Melsungen AG, Melsungen, Germany).

The surgery was performed under strict sterile conditions in a veterinary operating room, and standard surgical techniques were employed. The skin preparation involved careful shaving and disinfection with 20% chlorhexidine (Klorhexol®) and surgical

draping. Postoperatively, the animals were administrated atipamezole (Antisedan®, Orion Pharma, Espoo, Finland) and naloxone (Narcanti®, Bristol-Myers Squibb S.p.A., Anagni, Italy) to reverse the anaesthesia, followed by carprofen (Rimadyl®, Pfizer Oy, Espoo, Finland) as pain medication.

The animals were allowed to move without any restriction and were inspected daily. Eight weeks after surgery the animals were sacrificed using CO_2. The Ethical Committee for Animal Experiments of the University of Turku and the Provincial State office of Western Finland approved the study protocols. The experiments were carried out in accordance with the guidelines of the local Animal Welfare Committee.

4.2.2 Animal model and study protocol

Using an anterolateral approach, two unicortical holes were drilled in the anterior cortex of the right femur with a high-speed dental drill under saline irrigation. The employed drill bit (Frialit 5/0, Friedrichsfeld GmbH, Mannheim, Germany) had the same geometric shape as the conical glass implants (Hench and Andersson 1999). Two $BaSO_4$-containg glass cones of the same composition were implanted in each animal. The implants were pressed-fit into the holes with the tip pointing into the medullary cavity. The analysis included ten implants of glass 1-06B2.5 and ten implants of glass 1-06B10. Eight implants made of bioactive glass 1-06 and eight implants made of FG, tested using the identical implantation protocol in a large-scale screening study of bioactive glasses (unpublished data), served as the controls.

4.3 PATIENTS (Study V)

4.3.1 Patient selection

Study V was a prospective clinical trial at the University Hospital in Turku, Finland during the period 2007-2009. Adult skeletally mature patients (age ≥ 20 years and ≤ 70 years) with an acute intra-articular AO type-C1 (simple intra-articular), C2 (simple intra-articular with a multifragmentary metaphysis) or C3 (multifragmentary with involvement of the intra-articular cortex) distal radial fracture were considered for inclusion into the study. One attempt at closed reduction was performed, and patients with an unacceptable reduction were recruited into the study. Unacceptable reduction was defined as a dorsal angulation of more than 10°, or volar angulation of more than 25°, and/or ulnar variance of more than 2 mm, and/or articular step of more than 2 mm. Patients with pathological fractures and those with a history of drug or alcohol abuse, as well as those with open fractures were excluded. Patients with other fractures of the ipsilateral upper extremity (except ulnar styloid fractures) or the contralateral upper extremity were excluded from the study. Previous fracture of the injured wrist was also a criterion for exclusion.

A prospective cohort of fifteen eligible patients was recruited in **Study V (Table 9)**. The study group included eleven female patients and four male patients with a mean age of fifty-five years (range, thirty-nine to sixty-seven years). Five fractures involved the dominant side. Five patients had a concomitant fracture of the base of the ulnar

styloid. Among the fifteen patients, eight fractures were the result of low-energy trauma and seven were the result of high-energy trauma. Fractures were classified according to the AO classification system (Müller et al. 1987). The study was approved by the Ethical Committee of the Hospital District of Southwest Finland and was in accordance with the Declaration of Helsinki ethical principles for medical research involving human subjects. All subjects signed the informed consent document prior to participation into the study.

Table 9. Demographic characteristics of the fifteen consecutive patients (table from Study V).

Number*	Sex	Age *(yr)*	AO Fracture Classification	Fracture Side	Fracture of Dominant Hand
1	Male	45	C3	Left	No
2	Female	63	C3	Right	Yes
3	Female	55	C3	Right	Yes
4	Female	63	C1	Right	Yes
5	Male	44	C3	Left	No
6	Female	59	C3	Left	No
7	Female	67	C3	Left	No
8	Female	56	C3	Left	No
9	Female	39	C3	Right	No
10	Female	63	C3	Left	No
11	Male	55	C1	Left	No
12	Female	42	C3	Left	No
13	Female	46	C2	Left	Yes
14	Female	59	C3	Left	No
15	Male	67	C2	Right	Yes

*Intracortical RSA marker insertion was used for patients 1 to 5, combined intracortical and fracture site RSA marker insertion was used for patients 6 to 15.

4.3.2 Operative technique

All surgical procedures in **Study V** were performed within three days following the fracture by one orthopaedic surgeon. All patients received prophylactic antibiotics. Surgical exposure of the fracture site was performed through a volar approach under tourniquet control. An Acu-Loc (Acumed Ltd, Hampshire, UK) volar locking plate was used as the method of internal fixation in all patients. Tantalum markers with a diameter of 0.8 mm were used. For the first five consecutive patients, markers were inserted intracortically into predrilled holes using a spring-loaded piston (RSA Biomedical, Umeå, Sweden). Four markers were placed proximally to the fracture site and five markers were placed distally. The distal markers were placed into the largest fracture fragment and additional markers were inserted into the smaller fragments where possible. In this group of patients, both proximal and distal markers were placed after fracture reduction and plate fixation. The plate was fixed with two to three screws proximally and a combination of seven to nine locking screws and pegs distally.

During the analysis of immediate post-operative radiographs of these first five patients, it was observed that marker visibility was limited and markers were not spread well in the dorsovolar direction. The marker insertion technique was therefore modified and the number of markers inserted was also increased for the following ten patients. In these patients, tantalum markers were first inserted through the fracture site into the endosteal surface of the main fracture fragments. The insertion was done atraumatically using the spring-loaded piston without further tissue dissection. After this, the fracture was reduced and fixed using the plate. Finally, additional intracortical markers were inserted proximally and distally into the fracture site. A total of four to five markers were placed proximally and five to eight markers distally.

The quality of fracture reduction was assessed intra-operatively under fluoroscopy. The stability of the distal radio-ulnar joint (DRUJ) in both pronation and supination was tested after plate fixation. Five patients had concomitant displaced ulnar styloid fractures that required tension-band fixation.

4.3.3 Postoperative aftercare of patients

After the plate fixation and wound closure, a dorsal plaster splint was used to immobilize the wrist. Two weeks after surgery the plaster splint and sutures were removed and the wrist was placed in a removable volar splint. Volar splint immobilization was continued until six weeks postoperatively. All patients received supervised physiotherapy, including early finger and elbow mobilization instructions as well as wrist range-of-motion exercises at the time of the plaster splint removal. Active and passive finger motion was encouraged early in the postoperative period. Passive motion of the wrist and grip strengthening exercises were started at six weeks.

4.3.4 Patient follow-up

The patients in **Study V** were assessed in the early postoperative period and at two, six, twelve, eighteen, and fifty-two weeks and there were no drop-outs. Clinical assessment was performed at all follow-up visits. Additionally, an assigned physiotherapist received training on the functional assessment protocol and was responsible for functional measurements during the follow-up.

4.4 ANALYTICAL METHODS (Studies II-V)

The following *in vivo*, *ex vivo* and *in vitro* methods were used **(Table 10).**

Table 10. Applied analytical methods in Studies **II-V.**

Method	Study II	Study III	Study IV	Study V
RSA	X	X	X	X
Conventional radiography			X	X
Computer simulation of RSA		X		
BEI-SEM/EDXA			X	
X-ray diffraction			X	
UV-visible spectroscopy			X	
Micro-CT			X	
pQCT		X		
Mechanical testing			X	
Histology			X	
Range of motion measurements				X
Strength measurements				X
Pain and subjective outcome measurements				X

4.4.1 Radiostereometric analysis (RSA) (Studies II-V)

Radiostereometric analysis was performed in **Studies II-V**. In **Studies II** and **IV,** the plexiglass base plate with the fracture model was placed inside a biplanar calibration cage (Cage type 10, RSA Biomedical, Umeå, Sweden) **(Fig. 6A)**. The base plate was visually aligned to the RSA cage. The calibration cage had tantalum markers with known positions embedded in the walls overlying two radiographic film cassettes, which were held into a built-in cassette holder for standard size film. Digital film plates (ADCC MD 10, Agfa-Gevaert AG/CAWO, Schrobenhausen, Germany) of a standard size (24 x 30 cm) were used. Two portable radiographic tubes (Siemens Mobilett Plus and Siemens Mobilett, Siemens-Elema AB, Solna, Sweden), were mounted so that the beams crossed at an angle of approximately 90° **(Fig. 6C)**. The distance of each radiographic tube from the film was set to 100 cm and the radiographic tubes were operated simultaneously at 60 kV and 8 mAs. In **Study V,** each patient's forearm was placed inside the same calibration cage as above, but on an armrest with the arm in pronation **(Fig. 7)**. In **Study V,** orthogonal radiographs were obtained using one ceiling mounted (Philips Optimus 50, Philips Medical Systems DMC GmbH, Hamburg, Germany) and one mobile (Siemens Mobilett Plus, Siemens-Elema AB, Solna, Sweden), X-ray tube. The same RSA and radiographic equipment was used throughout each of the studies. In **Study III**, RSA simulation was performed so as to create simulated RSA radiographs.

4.4.1.1 RSA accuracy and precision using physical phantom models

In **Study II**, first, one double examination was performed with the distal fragment in zero rotation and translation **(Fig. 4A)**. This was done in order to obtain baseline values to which other movements would be compared. Isolated translation along each of the three axes **(Fig. 8)** was examined, during which no rotation was permitted. Four different series were obtained, consisting of proximal and distal displacements along the longitudinal axis, medial displacement along the transverse axis and anterior displacement along the sagittal axis. For three of these directions (distal, medial and anterior) a film pair was exposed at the following displacements: 25 µm, 50 µm, 100 µm, 500 µm, 1 mm, 2 mm, and 5 mm. For proximal displacement along the longitudinal axis a film pair was exposed at the following displacements: 25 µm, 50 µm, 100 µm, 500 µm, and 900 µm. Motion in this direction was limited by the width of the fracture site. A total of 27 film pairs were obtained.

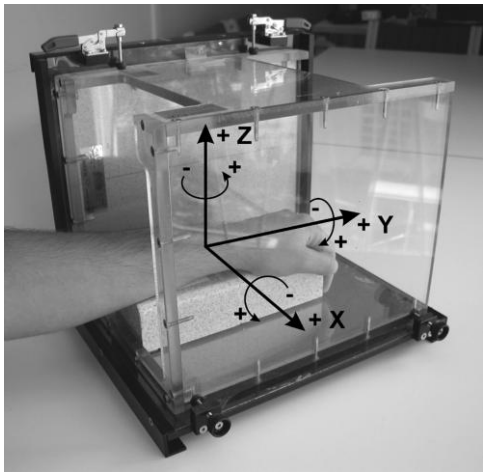

Figure 7. Photograph showing a patient's left forearm in the RSA calibration cage. The coordinate system with three orthogonal axes is also demonstrated. The directions of positive and negative translation as well as rotation are marked for each axis (figure from Study V).

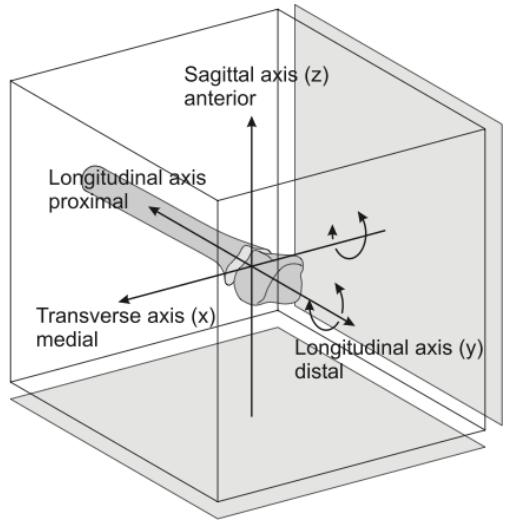

Figure 8. Schematic diagram showing the different axes examined (figure from Study II).

Eight double examinations were then performed in order to determine the accuracy of the rotation of the distal fragment along the longitudinal axis. The distal fragment was rotated using a high precision rotation stage while allowing no translation to take place. The fragment was rotated both clockwise and anti-clockwise to the following angles: 1/6º, 1/2º, 1º, and 2º. A simultaneous film pair was exposed for each incremental rotation. A total of 8 film pairs were obtained.

In order to determine the precision of translation measurements, the model was exposed once at zero, and thereafter five times after a single 200 µm displacement

along each of the three axes (distal displacement along the longitudinal axis, medial and lateral displacement along the transverse axis and anterior displacement along the sagittal axis). In order to determine the precision of rotation along the longitudinal axis, the model was exposed five times after a clockwise rotation of 1/2º. Thus, a total of 26 film pairs were obtained.

In the second part of **Study II**, first, one double examination was performed with the distal fragment in zero rotational displacement. In order to determine the accuracy of measuring the rotation about the transverse axis, the distal fragment was then rotated both clockwise and anti-clockwise to the following angles: 1/6º, 1/2 º, 1º, 2º, 5º, and 10º **(Fig. 4B)**. A simultaneous film pair was exposed for each incremental rotation. For the precision part of the study, the model was exposed once at zero and thereafter five times after a single clockwise rotation of 1/2 º. A total of 19 film pairs were obtained for this part of the study.

The model in **Study II** was also used to evaluate optimum bead number and configuration for radiostereometry **(Fig. 9)**. Three separate calculations of the displacement of the distal fragment were performed using different numbers of markers in the distal fragment. In addition, displacements were calculated for two separate combinations of three markers in the distal fragment. The spatial configuration of the markers in each bone segment was evaluated using the condition number. Four simple patterns of marker placement for both experiments were used. The first alternative used all five markers in the distal fragment **(Fig. 9A)**, the second used four markers **(Fig. 9B)** and the third **(Fig. 9C)** and fourth **(Fig. 9D)** used three markers. The corresponding condition numbers were 215, 220, 273, and 758, respectively.

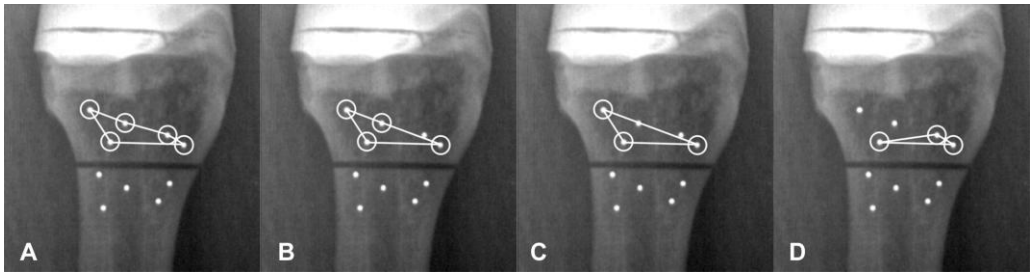

Figure 9. Anteroposterior radiographs showing the four different marker configurations used to define the distal rigid body segment (figure from Study II).

A total of 80 film pairs were obtained in **Study II**. The film plates were digitised to high quality films. The radiographs were scanned with a flatbed scanner (UMAX PowerLook 2100 XL, UMAX, Taiwan) equipped with a transparency adapter.

In **Study IV**, first, one double examination was performed with the distal fragment in zero rotation and translation **(Fig. 4C)**. This was done in order to obtain baseline

readings. Isolated translation along the longitudinal axis was examined, during which no rotation was permitted. Two series were obtained, consisting of proximal and distal displacements along the longitudinal axis. For each of these directions a film pair was exposed at the following displacements: 25 µm, 50 µm, 100 µm, 500 µm, 1 mm and 2 mm. A total of 13 film pairs were obtained.

Eight double examinations were then performed in order to determine the accuracy of the rotation of the distal fragment along the longitudinal axis. The distal fragment was rotated using a high precision rotation stage while allowing no translation to take place. The fragment was rotated both clockwise and anti-clockwise to the following angles: 1/6º, 1/2º, 1º, and 2º. A simultaneous film pair was exposed for each incremental rotation.

To determine the precision of translation measurements, the fracture model was exposed once at zero and thereafter five times after a single distal 200 µm displacement along the longitudinal axis. To determine the precision of rotation along the longitudinal axis, the model was exposed five times after a clockwise rotation of 1/2º. Thus, a total of 11 film pairs were obtained.

In **Study IV,** the digital radiographs were imported directly into the RSA software. Marking of the scanned images in all the studies (**II-V**) were performed with UmRSA Digital Measure 1.0 software (RSA Biomedical, Umeå, Sweden). The RSA determination of the migration of the distal fragment of the radius relative to the proximal part was performed by using the "segment motion" method of the UmRSA 4.1.0.10 software (RSA Biomedical, Umeå, Sweden).

4.4.1.2 RSA simulation using a computer model

In **Study III**, X-ray images were simulated using a ray-tracing computer software application (POV-Ray, Persistence of Vision Raytracer Pty. Ltd, version 3.5) running on a personal computer. The ray-tracing scene was coded using POV-Ray Scene Description Language (SDL). The units used in coding were millimetres. A left-hand coordinate system was used in the ray-tracing scene. For RSA measurements, all the movements were converted to the right-hand RSA coordinate system. All the movements were presented in the RSA coordinate system **(Fig. 8)**.

The ray-tracing scene consisted of the following objects: camera, light source, 3D model of the RSA cage, and 3D model of the radius with bone markers. The images calculated by ray-tracing were used to simulate the two radiographs produced on film plates. The size of a ray-traced image was 2857 x 2143 pixels to equal a radiograph scanned with 300 dots per inch (dpi) resolution using a flatbed scanner.

To create perspective distortions on the images similar to those produced by the X-ray imaging, the simulated camera in the ray-tracing scene was positioned 1000 mm from the image plane. Thus, to get an image equivalent to a RSA radiograph the angle of the camera was set to 13.69 degrees **(Fig. 6C)**. In order to simulate the first radiograph, the

camera was pointed to the centre of the 3D model of the RSA cage. The light source was positioned at the same points as the camera. To achieve the simulation of the second radiograph the camera and the light source were positioned perpendicular to the first arrangement **(Fig. 6C)**.

In the first part of **Study III,** an extra-articular computer simulation model of a distal radius fracture was used **(Fig. 5B)**. First, one double examination was performed with the distal fragment in zero rotation and translation. This was done in order to obtain baseline values to which other movements would be compared. Isolated translation of the distal fragment along each of the three axes was examined, during which no rotation was permitted. Six different series were obtained, consisting of proximal and distal displacements along the longitudinal axis, medial and lateral displacements along the transverse axis, as well as anterior and posterior displacements along the sagittal axis **(Fig. 8)**. For all these directions simulated radiographs were created for the following displacements: 25 µm, 50 µm, 100 µm, 500 µm, 1 mm, and 2 mm.

Three series of double examinations were then performed in order to determine the accuracy of the rotation of the distal fragment along each of the three axes. The distal fragment was rotated relative to the proximal radius while allowing no translation of the distal fragment to take place. The fragment was rotated both clockwise and anti-clockwise to the following angles: 1/6º, 1/2º, 1º, and 2º. A simultaneous film pair was exposed for each incremental rotation.

All the values representing translational and rotational movements of the distal fragment were saved in a separate text file. Each line in the file consisted of a set of three translational and three rotational values, which were used to create one set of images. A batch file was used to run through all the sets of values and create the respective images. A total of 61 pairs of simulated radiographs were obtained.

In the second part of **Study III,** the same 3D model of the radius was used. The fixed proximal fragment grouped with the bone markers was retained the same as in the first experiment. The distal fragment was further osteotomised into two separate fragments to simulate a simple articular fracture (three-fragment, AO/ASIF type C1) **(Fig. 5C)**. The position of the larger laterally located distal fragment was also fixed. Five bone markers represented by spheres with a radius of 0.4 mm were applied to the smaller distal fragment. A clinically relevant spatial arrangement of bone markers was used. The movement of the smaller distal fragment was simulated using the technique from the first experiment. In addition to examining translation and rotation individually for each axis, a series of complex movements were also examined. Combined translation in all three axes was carried out while allowing no rotation to take place. For all six directions of translation, a film pair was exposed at the following simultaneous displacements in three axes: 25 µm, 50 µm, 100 µm, 500 µm, 1 mm, and 2 mm. Following this, a similar examination was carried out for simultaneous rotation in all three axes for both clockwise and anti-clockwise directions for the following angles: 1/6º, 1/2º, 1º, and 2º. A total of 81 pairs of simulated radiographs were obtained.

For RSA measurements, all the images created in POV-Ray were saved in 8-bit non-compressed tagged image file format (TIFF). The resolution of the images was set to 300 dpi. The pairs of images were placed in separate subdirectories on the hard drive of a PC. Thereafter, the measuring procedure was exactly the same as used for the analysis of conventional digitised radiographs.

4.4.1.3 Clinical RSA examinations

In **Study V**, baseline RSA assessment was performed in the immediate postoperative period and the RSA imaging was repeated during each follow-up visit at two, six, twelve, eighteen, and fifty-two weeks in order to determine the migration of the distal fracture fragment. In order to test the possibility to quantify inducible fracture micromotion by means of RSA, the patients were also asked to squeeze a rubber ball with maximum voluntary strength during the imaging. This additional RSA imaging was performed at each follow-up visit starting at six weeks. Inducible micromotion measurements were performed for ten patients at the six-week follow-up, for twelve patients at the twelve and eighteen week follow-ups, and for fifteen patients at the fifty-two week follow-up.

Digital standard size (24x30 cm) film plates (ADCC MD 10, Agfa-Gevaert AG/CAWO, Schrobenhausen, Germany) were used and the images were digitally imported into the measurement software. The images had gray-scale and spatial resolutions of 16 bit and 2320x2920 pixels, respectively. UmRSA Digital Measure and UmRSA Analysis version 6.0 software (RSA Biomedical AB, Sweden) were used to mark the digital images and to measure marker positions. Fracture migration in terms of translation and rotation in three orthogonal axes (X-, Y-, and Z-axis) were then determined **(Fig. 7)**. To summarize the data for analysis, the total translation and total rotation using the 3-D Pythagorean Theorem were also calculated (Kaptein et al. 2007).

At each visit, RSA imaging was repeated after repositioning with and without rubber ball squeezing in order to determine the precision of the set-ups. Based on these examinations, the 95% confidence limits (CI) were calculated for translations and rotations along each of the orthogonal axes, as well as for total translation and rotation.

4.4.2 Conventional radiography

In **Study IV**, plain X-rays of glass cones made from glass 1-06B2.5 and glass 1-06B10 were first obtained. Based on plain X-ray examinations, *in vitro,* and *in vivo* results, glass 1-06B10 was selected as the material for creating RSA markers.

In **Study V**, anteroposterior (AP) and lateral digital radiographs of the patients' wrists were obtained in the immediate postoperative period and during the follow-up visits at two, six, twelve, eighteen, and fifty-two weeks. Measurements of volar tilt, radial inclination, radial length, ulnar variance, and articular step were performed using digital measurement software (Kodak, WebAccess 4.0) by two trained clinical

investigators. The assessment of radiographic union was performed by an independent skeletal radiologist and the reading was confirmed by the two clinical investigators. Fracture union was defined by the absence of local tenderness at the fracture site combined with radiographic evidence of bone trabeculae spanning the fracture lines.

4.4.3 X-ray diffraction

The surfaces of the glass implants in **Study IV** were initially examined by X-ray diffraction (XRD, Philips PW-series) for possible structural changes such as crystallization of the glass due to the addition of $BaSO_4$.

4.4.4 UV-visible spectroscopy

In **Study IV,** specimens of three bioactive glass compositions were immersed in SBF. The specimens had the same morphology as the implants. The ratio of the surface area of the materials to the volume of the SBF (SA/V ratio) was 0.4 cm^{-1}. The concentrations of soluble calcium (Ca), phosphorus (P), and silicon (Si) were monitored at 4, 8, 24, 96, and 168 hours. For each of the bioactive glass compositions, three parallel specimens were immersed in SBF, and three samples of SBF were taken for analysis at each time point. The SBF samples were analysed by UV-visible spectroscopy (UV-visible spectrophotometer, Shimadzu UV-1601, Shimadzu Corporation). In the ion concentration measurements, average values of the three SBF samples taken for each of the three parallel glass specimens were calculated, and then an average value for the three specimens was calculated.

4.4.5 BEI-SEM/EDXA

Oxide compositions of the glasses used in **Study IV** were determined using an energy dispersive X-ray analyser **(Table 11)**.

Table 11. Oxide compositions of the glasses used in the study measured by SEM-EDXA (table from Study IV).

Compound (wt %)	Glass			
	1-06	1-06B2.5	1-06B10	FG
SiO_2	51.2	52.2	49.4	73.5
P_2O_5	4.5	4.4	4.4	0.3
B_2O_3	0.2	0.2	0.2	0.0
Na_2O	6.1	6.0	5.5	14.3
K_2O	11.8	11.0	9.4	0.0
CaO	20.9	19.2	19.1	7.7
MgO	5.5	4.8	5.1	3.5
TiO_2	not measured	not measured	not measured	0.2
$BaSO_4$	0.0	1.8	6.9	not measured

Following 168 hours of immersion in SBF, the glass implants were removed, dried in a controlled environment, coated with carbon and analysed with a scanning electron microscope equipped with an energy dispersive X-ray analyser (SEM: JEOL JSM-5500, EDXA: Princeton Gamma Tech Prism 2000) to study the morphology of the apatite layer. The specimens were then embedded in plastic, cut in two halves perpendicular to the long axis of the implant (approximately in the middle of the height of the cone), coated with carbon and analysed with SEM-EDXA in a cross-section to study the thickness of the reaction layers. The thickness of the reaction layers was measured at four random locations on each implant.

4.4.6 Micro-CT

Immediately after harvesting, micro-computed tomography (Skyscan 1072 micro-CT, Skyscan n.v. Aartselaar, Belgium) was performed on all the femur specimens in **Study IV**. Each femur was placed in a plastic container, which was then filled with saline solution, sealed and mounted on the specimen holder for imaging. Each one of the implants was imaged separately with a step angle of 0.675 degrees within a full angle of 180 degrees. The source voltage was 91 kV, the source current was 110 µA, and no filters were used. In image acquisition, a single 16-bit greyscale shadow projection image was obtained for each step angle, and no frame averaging was used.

The parameters were chosen as a compromise between the imaging quality and the acquisition time. All imaging and reconstruction parameters were kept identical for each of the implants imaged. For each implant the acquired shadow projection images were reconstructed into an array of cross-sectional 8-bit greyscale images using NRecon software (version v.1.4.3, Skyscan n.v. Aartselaar, Belgium). Automatic post-alignment and beam hardening correction were used in the reconstruction. The resulting spatial resolution of the cross-sectional images was 7.33 µm per voxel. These images were then used to study bone-implant interfaces.

4.4.7 pQCT

In **Study III**, a physical plastic sawbone model of the left radius (model 1027, Sawbones Europe AB, Sweden) was used to create a three-dimensional computer simulation model of the radius. The model was digitised using a pQCT device (Stratec XCT Research M, Norland Stratec Medizintechnik GmbH, Birkenfeld, Germany).

4.4.8 Mechanical testing

Continuing directly after micro-CT imaging in **Study IV**, the posterior cortex of the femurs with implants was ground away by a dental drill in order to expose the intramedullary tips of the conical implants. The anterior cortex was carefully cleaned off any surrounding new bone. Push-out testing was performed using a universal mechanical testing device for small specimens (Avalon Technologies, Rochester, MI, USA) (Hench et al. 1999, Zhao et al. 2008). The femur specimens were mounted on a custom-made gyroscopic jig in order to achieve a better alignment of the long axis of an implant with the direction of the applied force. The implants were pushed out of the

bone at a constant cross-head speed of 0.825 mm/min. The push-out force was registered by a load cell (SM-50, Interface Inc. Scottsdale, Arizona USA) and acquired under computer control with a sampling rate of 20 Hz. The software for data acquisition was written under Visual Designer 3.0 (Intelligent Instrumentation, Tucson, Arizona, USA). The data acquired by the computer was further processed (Origin, OriginLab Corp., Northampton, USA) to calculate ultimate push-out load, apparent sheer stiffness (the relation between the applied load and the displacement of the implant) and energy to failure absorbed during the test.

4.4.9 Histology

After the mechanical testing of the implants in **Study IV**, the femur specimens with two mechanically tested implants left in situ were embedded in isobornylmethacrylate (Technovit 1200 VLC, Kulzer, Algol, Germany). The implants were sectioned along the sagittal axis and then stained with the van Gieson method and examined by light microscopy.

4.4.10 Range of motion measurements

The patients in **Study V** were assessed in the early postoperative period and at two, six, twelve, eighteen, and fifty-two weeks. Clinical assessment was performed at all the follow-up intervals. The range of motion (ROM) and grip strength measurements were performed at six weeks and at all remaining follow-up visits. Range of motion measurements included radioulnar and radiocarpal joint ROM measurements (flexion, extension, pronation and supination, as well as radial and ulnar deviation), measured by goniometry and compared to the opposite limb. Metacarpophalangeal joint ROM was determined by measuring the distance of the forefinger and the middle finger from the distal palmar crease during flexion (cm), and by measuring the deficit in extension (degrees). Thumb opposition and abduction were measured by determining the distance from the fifth metacarpophalangeal joint and abduction angle from the second digit, respectively.

4.4.11 Strength measurements

In **Study V,** grip strength (with the handle set in the second position) and precision grip strength (pinch grip) in kilograms, were measured by hand held dynamometers (Jamar Hydraulic Hand Dynamometer and Jamar Hydraulic Pinch Gauge, NexGen Ergonomics Inc. Quebec, Canada) and compared to the opposite limb. Pronation and supination strength were also measured using a dynamometer (Baseline Hydraulic Wrist Dynamometer, Fabrication Enterprises Inc. White Plains, New York) in a custom designed set-up. The dynamometer was calibrated using a set of standard weights for the measurement of maximum torque, expressed as Newton meters (Nm).

For each patient, pronation and supination strength was measured using two different handles (vertical cylindrical and doorknob) (Timm et al. 1993). During these measurements, the physiotherapist carefully monitored that the patient did not use muscle substitution by using their upper body or shoulder to compensate for weakness

in the wrist. All strength measurements (grip, pinch grip, pronation and supination) were performed three times at each visit with a short resting interval in between measurements. The mean of the three strength measurements was then determined. The range of motion and strength measurements were also calculated as percentages of the values of the uninjured contralateral side since these ratios have been shown to be more sensitive for detecting clinical changes (MacDermid et al. 2000).

4.4.12 Subjective outcome measurements

Pain and subjective functional outcome were evaluated for each patient in **Study V** at each visit using a 10-point visual analogue scale (VAS) and the Patient-Rated Wrist Evaluation questionnaire (PRWE). The anchors for the visual analogue scale were 0 = "no pain" and 10 = "worst pain I ever felt".

4.5 STATISTICS

Statistical analysis for **Studies II**, **III**, and **IV** was performed using SigmaStat 3.5 software (SPSS Inc., Chicago, IL) and for **Study V** using the SAS system for Windows version 9.2 (SAS Institute Inc., Cary, NC, USA). Linear regression analysis was used in order to relate the displacements as measured with RSA to the actual displacements measured with micrometers (**Studies II** and **IV**) or with computer software (**Study III**). Accuracy was presented as the 95% prediction interval (Önsten et al. 2001). This interval is obtained by first determining the lower and upper bounds for the prediction interval for each observation and then calculating the mean of the intervals for each observation.

In **Studies II**, **IV**, and **V,** precision was calculated as the standard deviation of repeated measurements. In **Study V,** the precision data obtained using CN limits of 300 and 1,000 were compared. The linear mixed model method was used since each patient had multiple observations. The equality of variances analysis was performed using Levene's test.

After testing normality, the non-parametric Wilcoxon Signed Rank test was used to determine significant changes in clinical and radiographic parameters over the follow-up period (**Study V**). The Wilcoxon Signed Rank test was also applied to evaluate whether the RSA measured migration or inducible micromotion was significant (**Study V**). In comparing the results of the push-out testing of the glass compositions in **Study IV,** Kruskal-Wallis one way analysis of variance was performed followed by multiple comparisons using Mann-Whitney rank sum tests. P-values lower than 0.05 were considered statistically significant.

5. RESULTS

5.1 RSA ACCURACY AND PRECISION USING A PHYSICAL PHANTOM MODEL (Study II)

The implanted markers could all be visualized in both pairs of radiographs in all film pairs. ME values varied from 3 µm to 13 µm for the proximal part of the radius and from 1 µm to 13 µm for the distal fragment.

The prediction interval of the RSA measurements for accuracy of translation varied from ± 6 µm to ± 29 µm ($R^2 \geq 0.99$, $P<0.001$, **Table 12**), and the corresponding values for rotation varied from ± 0.073° to ± 0.187° ($R^2 \geq 0.99$, $P<0.001$, **Table 13**). The precision of 200 µm translations varied from 2 µm to 6 µm **(Table 12)** and the precision of 1/2 º rotations varied from 0.025º to 0.096º **(Table 13)**.

Table 12. The accuracy and precision of translation measurements using a physical phantom model (table from Study II).

Axis (direction) of displacement	Number of markers in the distal fragment (condition number)	Accuracy[a] 95% prediction interval (µm)	Precision Standard deviation of a 200 µm displacement (µm)[b]
Longitudinal (distal)	5 (215)	± 24	6
	4 (220)	± 23	6
	3 (273)	± 21	6
	3 (758)	± 25	6
Longitudinal (proximal)	5 (215)	± 29	nd
	4 (220)	± 27	nd
	3 (273)	± 24	nd
	3 (758)	± 28	nd
Transverse (medial)	5 (215)	± 7	2
	4 (220)	± 6	2
	3 (273)	± 8	3
	3 (758)	± 11	3
Sagittal (anterior)	5 (215)	± 14	6
	4 (220)	± 12	6
	3 (273)	± 13	5
	3 (758)	± 13	6

[a] For each linear regression equation $R^2 \geq 0.99$ and $p < 0.001$.
[b] nd: not determined

The accuracy of translation was found to be similar throughout the range of examined values for all axes examined. The transverse axis had the highest accuracy and precision. The number of markers and their distribution was found to have minimal impact on translation accuracy in both the longitudinal and sagittal axes. However, decreasing the condition number of three markers or increasing the number of markers from three to five was found to increase accuracy in the transverse axis 1.4 to 1.6 – fold, respectively. The number and distribution of markers was found to have a minimal impact on the precision of translation.

For rotation measurements, the transverse axis was found to have a higher accuracy but demonstrated a trend for lower precision than the longitudinal axis. It was found that there was a trend for higher accuracy close to the zero position for both axes examined. The number of markers and their distribution had an impact on both the accuracy and precision of the transverse axis, while the effect was less pronounced in the longitudinal axis. Increasing the number of markers from three to five led to a 2.1-fold increase in accuracy and a 3-fold increase in precision in the transverse axis. The corresponding increase of accuracy and precision in the longitudinal axis were 1.1-fold and 1.6-fold, respectively. Decreasing the condition number of the three markers from 754/758 to 272/273 led to 1.5-fold increase in both accuracy and precision for the transverse axis, but only led to a negligible change in the precision of the longitudinal axis.

Table 13. The accuracy and precision of rotation measurements using a physical phantom model (table from Study II).

Axis (direction) of rotation	Number of markers in the distal fragment (condition number)	Accuracy[a,b] 95% prediction interval (degrees)	Precision[c] Standard deviation of a 0.5º rotation (degrees)
Longitudinal	5 (215)	± 0.175	0.025
	4 (220)	± 0.155	0.035
	3 (273)	± 0.166	0.042
	3 (758)	± 0.187	0.040
Transverse	5 (214)	± 0.073	0.032
	4 (219)	± 0.076	0.032
	3 (272)	± 0.098	0.065
	3 (754)	± 0.150	0.096

[a] Accuracy calculated for both clockwise and anti-clockwise rotation.
[b] For each linear regression equation $R^2 \geq 0.99$ and $p < 0.001$.
[c] Precision calculated for clockwise rotation.

5.2 RSA COMPUTER SIMULATION FOR FRACTURES OF THE DISTAL RADIUS (Study III)

The quality of simulated radiographs in **Study III** was very high. All the markers, both in the proximal radius and in the distal fragment, could be visualized in both pairs of radiographs in all film pairs. The ME values in these experiments varied from 1 µm to 8 µm for the proximal fragment of the radius. The corresponding ranges for the distal fragment were from 1 µm to 2 µm and from 1 µm to 13 µm in the first and second experiments, respectively. The condition number of the markers in the proximal part of the radius was 142 in both experiments, whereas the condition number of the markers in the distal part was found to be 179 and 109 in the first and second experiments, respectively.

The prediction interval of the RSA measurements for accuracy of translation in one axis varied from ± 1 µm to ± 2 µm ($R^2 \geq 0.99$, $P<0.001$, **Table 14**) for the two-part fracture and from ± 3 µm to ± 4 ($R^2 \geq 0.99$, $P<0.001$, **Table 15**) for the three-part fracture. The corresponding values for rotation varied from ± 0.009º to ± 0.015º and from ± 0.009º to ± 0.031º ($R^2 \geq 0.99$, $P<0.001$, **Tables 14 and 15**) for two- and three-part fractures, respectively. The accuracy of translation and rotation for complex movements in the three-part fracture model was found to vary from ± 5 µm to ± 6 µm and from ± 0.017º to ± 0.120º, respectively ($R^2 \geq 0.99$, $P<0.001$, **Table 15**).

For simple measurements of translation in one axis, it was found that accuracy was similar for all three axes examined in both experiments. For complex translation measurements the accuracy was found to decrease 1.3 to 2-fold depending on the axis examined. For all measurements of rotation, the accuracy was found to be highest in the sagittal axis followed by the longitudinal and transverse axes, respectively. For complex rotation, the accuracy was found to decrease 1.9 to 3.9-fold according to the axis examined. For the range of examined values of translation and rotation, it was found that there was a trend for higher accuracy close to the zero position for all axes examined.

Table 14. Comparison of accuracy of translation and rotation for the different axes in a two-part distal radius fracture computer model (table from Study III).

Axis (direction) of displacement	Accuracy of translation/rotation[a] 95% prediction interval	
	Translation (µm)	Rotation in one axis (degrees)
Transverse	± 1	± 0.015
Longitudinal	± 2	± 0.012
Sagittal	± 1	± 0.009

[a] For each linear regression equation $R^2 \geq 0.99$ and $p < 0.001$.

Table 15. Comparison of accuracy of translation and rotation for the different axes stratified according to whether the movement took place in one axis or in all three axes simultaneously in a three-part distal radius fracture computer model (table from Study III).

Axis (direction) of displacement	Accuracy of translation/rotation[a] 95% prediction interval			
	Translation in one axis (µm)	Translation in three axes (µm)	Rotation in one axis (degrees)	Rotation in three axes (degrees)
Transverse	± 3	± 5	± 0.031	± 0.120
Longitudinal	± 3	± 6	± 0.015	± 0.046
Sagittal	± 4	± 5	± 0.009	± 0.017

[a] For each linear regression equation $R^2 \geq 0.99$ and $p < 0.001$.

5.3 EVALUATION OF RESORBABLE MARKERS FOR RSA (Study IV)

5.3.1 In vitro characterisation of implant reactivity

In **Study IV**, X-ray diffraction examination of the specimens showed no signs of crystallization of the bioactive glasses. In *in vitro* immersion testing **(Fig. 10)**, the Si concentration of the SBF solution increased most rapidly in the bioactive glass implants with 10% $BaSO_4$ as a sign of the enhanced release of Si ions **(Fig. 10A)**. All the implants showed a release of Ca ions from the glass bulk during the first 96 hours **(Fig. 10B)**, while only the SBFs of the implants with 10% $BaSO_4$ had maintained a high Ca concentration at 168 hours, probably due to a slower formation of the hydroxyapatite layer. Reflecting the low (4%) phosphate content of the glasses, no changes in the P concentration of the SBFs were observed during the first 96 hours **(Fig. 10C)**. Thereafter, the P concentration started to decrease as a part of the formation of the CaP layer on the glass surface, while the change seemed to be again slowest in the SBFs of the glass implants, with 10% $BaSO_4$. Scanning electron microscopy analysis revealed thick silica-rich and CaP layers on all three bioactive glasses **(Fig. 10D)**. The mean thickness of the CaP layer was highest in glass 1-06 and was slightly reduced for both glasses containing $BaSO_4$.

5.3.2 In vivo characterisation of implants

Eight weeks after implantation *in vivo*, micro-CT imaging revealed the formation of distinct layers on the surface of bioactive glass implants of glass 1-06 **(Fig. 11A)**, glass 1-06B2.5 **(Fig. 11B)** and glass 1-06B10 **(Fig. 11C)**, but not on the surface of FG **(Fig. 11D)**. The imaging also showed areas of direct bone-implant contacts for all three types of bioactive glass implants. In push-out testing, the failure loads **(Fig. 12A)** and stiffness values **(Fig. 12B)** of the bioactive glass 1-06 implants tended to be higher than those of glass implants 1-06B2.5 or 1-06B10.

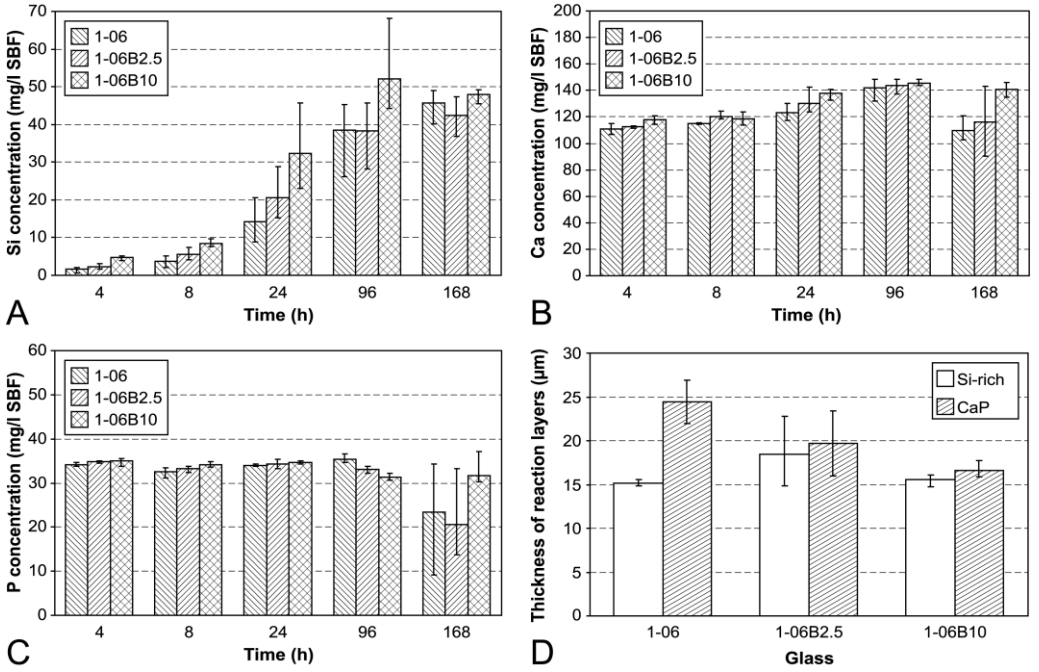

Figure 10. Ionic concentrations of Si (A), Ca (B), and P (C) in SBF as functions of immersion time for the different glass compositions. Thickness of the reaction layers (Si-rich and CaP) was determined by electron microscope scanning (D). The data is presented as means with bars indicating minimum and maximum values measured (figure from Study IV).

The results of **Study IV** indicated statistically significant differences between glasses 1-06 and FG, both in push-out load (p=0.006) and apparent shear stiffness (p=0.006). No statistically significant differences were found between glasses 1-06B2.5 and 1-06B10. Also, no statistically significant differences were found when glasses 1-06B2.5 and 1-06B10 were compared with 1-06. When the push-out load data for glasses 1-06B2.5 and 1-06B10 were compared with FG, a statistically significant difference was found for 1-06B2.5 (p=0.012). When the apparent shear stiffness data for glasses 1-06B2.5 and 1-06B10 were compared with FG, again a statistically significant difference was found for 1-06B2.5 (p=0.018).

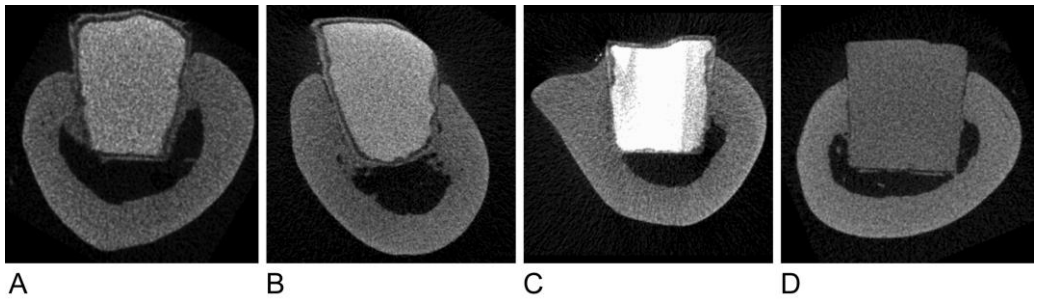

Figure 11. Micro-CT images of glass implants eight weeks after *in vivo* implantation. The imaging revealed the formation of distinct layers on the surface of bioactive glass implants as well as areas of direct bone-implant contacts for glass 1-06 (A), glass 1-06B2.5 (B) and glass 1-06B10 (C), but not on the surface of FG (D) (figure from Study IV).

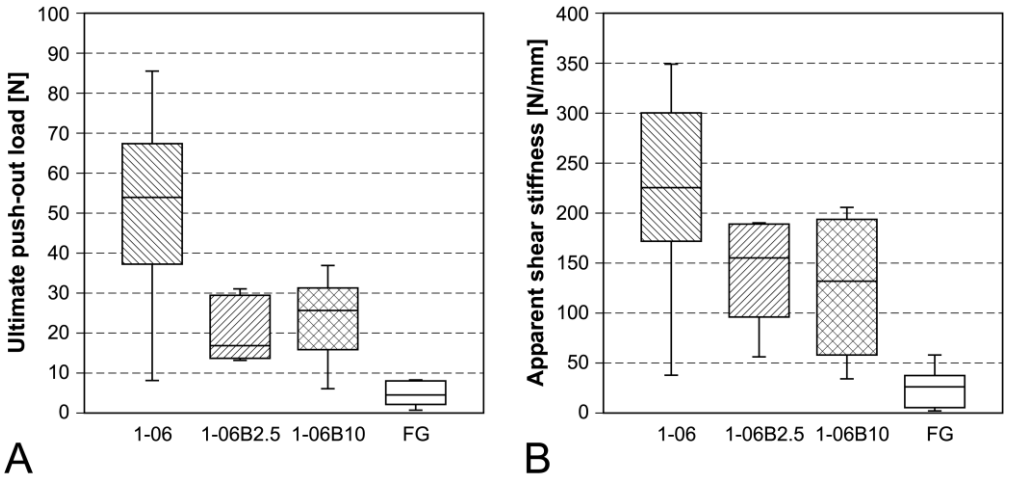

Figure 12. Results of the push-out testing (median, 25 percentile, 75 percentile, maximum value and minimum value) (figure from study IV).

In histological analysis, a narrow rim of new bone was found to surround the surface of all bioactive glass implants with or without $BaSO_4$ **(Fig. 13A-C)**. There were, however, trabeculae of new bone even around the ends of FG implants in the intramedullary canal **(Fig. 13D)**. As a sign of bone incorporation, push-out testing had caused failures through the implant substance of the bioactive glass implants **(Fig. 13A-C)**, whereas FG implants showed failure through the implant-tissue interface. There seemed to be a direct contact in bone-implant interface of the bioactive glass implants. In contrast, the FG implants showed a thin layer of fibrous tissue between the cortical bone and the implant bulk.

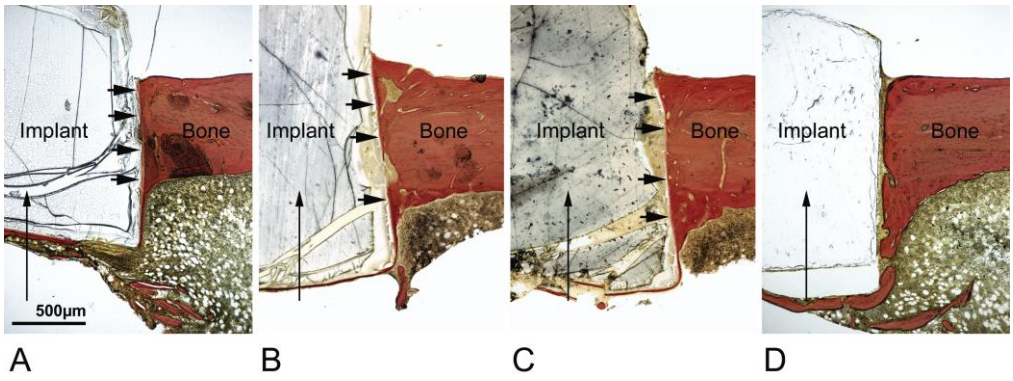

Figure 13. Hard-tissue histology of unicortical glass implants at eight weeks (van Gieson staining): bioactive glass 1-06 (A), bioactive glass 1-06B2.5 (B), bioactive glass 1-06B10 (C), and FG (D). As a sign of incorporation, push-out testing had caused failures through the implant substance of all the bioactive glass implants. FG implants showed failure through implant-tissue interface (D). Bone is stained red and the intramedullary canal is at the bottom of the figures. The implants were placed in the bone with the tip facing the intramedullary canal, which is not evident due to histological sectioning. Horizontal arrows indicate new bone attached to the surface of the implants. Vertical arrows indicate the direction of force applied in the push-out test (figure from Study IV).

5.3.3 Radiostereometric analysis

All the markers implanted into both the proximal radius and the distal fragment could be visualized in both pairs of radiographs from all film pairs. The mean error of rigid body fitting (ME), was applied as an internal control for effects of marker asymmetry since markers were fixed in place. The ME value reflected how well the RSA software located the centre of specific markers from consecutive radiographs. The ME values varied from 6 µm to 139 µm for both the proximal and distal parts of the radius.

The prediction interval of the RSA measurements for accuracy of translation in the longitudinal axis was ± 51 µm ($R^2 \geq 0.99$, $P<0.001$, **Table 16**) and the corresponding value for rotation was ± 0.87 degrees ($R^2 = 0.94$, $P<0.001$, **Table 16**). The precision of 200 µm translations was found to be 9 µm and the precision of 1/2 º rotations was found to be 0.18º.

Table 16. The accuracy and precision of translation and rotation measurements in the longitudinal axis (table from Study IV).

Type of motion	Accuracy[a] 95% prediction interval	Precision[d] Standard deviation of a 200 µm translation or 0.5º rotation
Translation	± 51 µm [b]	9 µm
Rotation	± 0.87° [c]	0.18°

[a] Accuracy calculated for both clockwise and anti-clockwise rotation as well as proximal and distal motion along the longitudinal axis.
[b] For each linear regression equation $R^2 \geq 0.99$ and $p < 0.001$.
[c] For each linear regression equation $R^2 = 0.94$ and $p < 0.001$.
[d] Precision calculated for distal translation and clockwise rotation.

5.4 RSA IN TYPE-C DISTAL RADIUS FRACTURES TREATED WITH A LOCKED VOLAR PLATE (Study V)

5.4.1 Precision

The condition number (CN) values obtained in this study were generally quite high, reflecting the difficulty of achieving a good visible marker scatter. Precision values were therefore determined using two different CN limits so as to evaluate the effect of marker distribution on precision, and hence determine an appropriate CN limit for the study.

Decreasing the CN limit was found to reduce the number of usable data points **(Table 17)**; on the other hand, larger CN values may reduce precision. The precision data obtained using CN limits of 300 and 1,000 were therefore compared. The linear mixed

model method was used since each patient had multiple observations. The equality of variances analysis was performed using Levene's test. The results showed no statistically significant difference in the precision of measurements obtained using CN 300 and CN 1000 **(Table 17)**. This was found to be true for both migration (rotation $p = 0.36$, translation $p = 0.54$) and inducible micromotion (rotation $p = 0.64$, translation $p = 0.37$). Similarly, Levene's test demonstrated no difference in variances of both groups for migration (rotation $p = 0.80$, translation $p = 0.31$) or inducible micromotion (rotation $p = 0.70$, translation $p = 0.87$). Based on this analysis, the CN value of 1,000 with more usable data was chosen as the cut-off point and corresponding levels of precision were used. Confidence limits were calculated separately for migration and for inducible micromotion, thereby providing limits beyond which the motion of each type was considered significant **(Table 17)**.

5.4.2 Clinical Outcomes

All fractures healed uneventfully. One patient had a superficial wound infection that resolved with a course of antibiotics. One patient reported paresthesia in the proximal part of the scar, another patient reported mild paresthesia over part of the median nerve innervation area, and a third patient reported mild paresthesia on the ulnar side of the wrist. Paresthesia symptoms resolved without intervention by eighteen weeks.

All clinical parameters showed a significant improvement from six to fifty-two weeks ($p < 0.02$). The average level of pain as measured by the visual analogue scale (0-10) was low at all follow-up intervals, reaching an average of 0.7 at the fifty-two week follow-up **(Table 18)**. The subjective outcome as measured with the PRWE score also showed a significant time-related improvement ($p < 0.005$), reaching an average of 5.3 at fifty-two weeks **(Table 18)**.

All patients demonstrated full finger flexion and extension as well as thumb adduction and abduction by eighteen weeks. The mean range of wrist motion improved up to fifty-two weeks ($p < 0.005$), with mean ROM values of the fractured wrist reaching over 70 %, 80%, and 90 % of the unaffected side at the twelve, eighteen, and fifty-two week follow-ups, respectively **(Table 19)**.

Grip and pinch strength as well as pronation and supination strength measurements showed a significant increase from six to fifty-two weeks ($p < 0.02$). These strength parameters increased sharply up to twelve weeks, after which there was a more gradual increase up to the fifty-two week follow-up **(Tables 20 and 21)**. Grip and pinch strengths reached over 80% of the strength of the unaffected side by eighteen weeks. The return of pronation and supination strengths was even faster and they were greater using the vertical cylindrical handle than using the doorknob handle **(Table 21)**.

Table 17. Precision of RSA measurements (table from Study V).

	N	Repeated Measurements	Rotation (Degrees)*				Translation (mm)*			
			X-axis	Y-axis	Z-axis	**Total**	X-axis	Y-axis	Z-axis	**Total**
Migration										
CN ≤ 300	11	37	0.81	1.02	0.63	**1.45**	0.11	0.08	0.13	**0.19**
CN ≤ 1000	14	52	0.94	0.94	0.70	**1.51**	0.10	0.08	0.17	**0.21**
All CN values	15	66	1.52	1.63	0.99	**2.44**	0.13	0.12	0.23	**0.29**
Inducible Micromotion										
CN ≤ 300	9	19	0.90	0.29	0.45	**1.04**	0.07	0.04	0.07	**0.10**
CN ≤ 1000	12	22	0.86	0.29	0.44	**1.01**	0.06	0.04	0.07	**0.10**
All CN values	13	27	1.49	1.10	0.43	**1.90**	0.25	0.19	0.40	**0.50**

* The values are given as the 95% confidence interval with total values calculated using the 3-D Pythagorean theorem.

Table 18. Clinical scores of patients in Study V.

	6 Weeks*	12 Weeks*	18 Weeks*	52 Weeks*
Pain score *(points)*[1]	1.1 ± 1.0	0.5 ± 1.1	0.8 ± 1.3	0.7 ± 1.3
PRWE score *(points)*[2]	22.0 ± 10.6	11.5 ± 9.3	10.6 ± 10.0	5.3 ± 6.1

* The values are given as the mean and the standard deviation.
[1] Pain was assessed using a 10-point visual analogue scale.
[2] The PRWE questionnaire is scored on a 100-point scale, with lower scores being better.

Table 19. Range of motion measurements in Study V.

	6 Weeks		12 Weeks		18 Weeks		52 Weeks	
	%*	Degrees	%*	Degrees	%*	Degrees	%*	Degrees
Flexion	63 ± 20	39.7	78 ± 19	49.7	84 ± 24	52.1	94 ± 24	59.0
Extension	46 ± 22	30.3	75 ± 15	49.7	82 ± 13	54.3	93 ± 11	61.7
Pronation	74 ± 22	64.3	86 ± 22	75.0	89 ± 18	77.9	95 ± 9	83.3
Supination	62 ± 24	54.3	87 ± 18	76.3	86 ± 19	75.4	95 ± 15	83.3
Radial deviation	57 ± 25	16.0	72 ± 28	19.7	91 ± 31	24.3	92 ± 27	25.3
Ulnar deviation	57 ± 24	23.3	72 ± 26	29.3	80 ± 25	32.5	98 ± 27	40.3

* The values represent the percentage of the value on the uninjured side and are given as the mean and standard deviation.

Table 20. Strength measurements in Study V.

	6 Weeks		12 Weeks		18 Weeks		52 Weeks	
	%*	kg	%*	Kg	%*	kg	%*	kg
Grip strength	42 ± 22	13.3	76 ± 21	22.7	85 ± 20	25.2	100 ± 22	31.4
Pinch strength	59 ± 26	3.1	76 ± 25	3.8	88 ± 23	4.4	89 ± 35	4.3

* The values represent the percentage of the value on the uninjured side and are given as the mean and standard deviation.

Table 21. Maximum torque measurements in Study V.

	6 Weeks		12 Weeks		18 Weeks		52 Weeks	
	%*	Nm	%*	Nm	%*	Nm	%*	Nm
Pronation								
Doorknob handle	54 ± 28	1.2	95 ± 32	2.0	96 ± 35	1.9	100 ± 35	2.3
Cylindrical handle	50 ± 23	2.5	83 ± 26	4.0	87 ± 28	3.9	94 ± 28	4.3
Supination								
Doorknob handle	50 ± 23	1.2	96 ± 28	2.0	100 ± 43	2.2	100 ± 34	2.6
Cylindrical handle	46 ± 20	2.3	78 ± 16	4.0	91 ± 19	4.6	100 ± 19	5.3

* The values represent the percentage of the value on the uninjured side and are given as the mean and standard deviation.

5.4.3 Radiographic Outcomes

Adequate reductions were obtained in all cases at the time of surgery. One patient showed radiographic signs of union at six weeks, ten patients at twelve weeks, and four patients at eighteen weeks. Dorsal malangulation developed in one patient. Two patients had a minor (< 2 mm) residual articular step-off. At fifty-two weeks, the mean volar tilt and radial inclination were 5.4º and 21.5º, respectively, and the mean radial length and ulnar variance were 9.6 mm and 1.4 mm, respectively, **(Table 22)**. There were no significant time-related changes in the measured radiographic parameters except for ulnar variance, which was increased compared with the immediate postoperative value ($p < 0.03$ at six weeks).

Table 22. Radiographic outcomes (table from Study V).

Radiographic Outcomes	6 Weeks*	12 Weeks*	18 Weeks*	52 Weeks*
Volar tilt *(deg)*	5.3 ± 5.9	5.8 ± 6.1	5.5 ± 5.9	5.4 ± 6.9
Radial inclination *(deg)*	21.6 ± 4.2	21.5 ± 3.1	22.1 ± 3.0	21.5 ± 3.2
Radial length *(mm)*	9.6 ± 2.1	9.2 ± 2.0	9.8 ± 2.0	9.6 ± 2.0
Ulnar variance *(mm)*	1.1 ± 1.7	1.5 ± 1.8	1.4 ± 1.9	1.4 ± 1.9
Articular step-off *(mm)*	0.2 ± 0.4	0.2 ± 0.4	0.1 ± 0.4	0.1 ± 0.4

* The values are given as the mean and the standard deviation.

5.4.4 RSA Results

The stability and visibility of RSA markers was influenced by the marker insertion technique **(Table 23)**. The proportion of unstable markers (extra-osseous markers and markers with high ME values on repeated RSA images) was higher when the combined intracortical and fracture site insertion technique was used. No extra-osseous markers were observed with the intracortical insertion technique, whereas a total of nine extra-osseous markers were visible when the combined intracortical and fracture site insertion technique was applied **(Fig. 14)**.

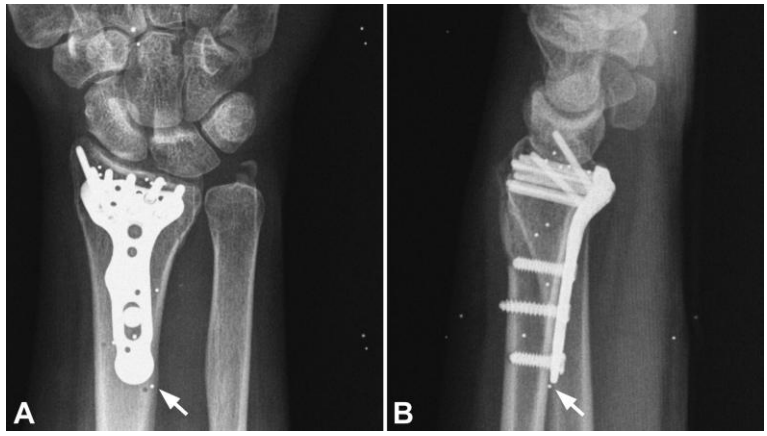

Figure 14. AP (A) and lateral (B) RSA radiographs of 39-year-old female patient at six weeks. Proximal and distal RSA markers are visible. A single extra-osseous marker is visible proximally marked by a white arrow. Some of the calibration cage markers are also visible in the background (figure from Study V).

Table 23. Visibility of RSA markers (table from Study V).

Insertion Location	Number of Inserted Markers/Patient*	Number of Visible Markers/Patient*	Unstable Markers/Total number of markers
Intracortical marker insertion			
Proximal to fracture site	3.8 ± 0.4	3.8 ± 0.13	1/19
Distal to fracture site	5.0 ± 0.0	3.4 ± 0.18	1/25
Combined intracortical and fracture site marker insertion			
Proximal to fracture site	4.5 ± 0.7	4.4 ± 0.07	5/43
Distal to fracture site	6.4 ± 1.0	4.8 ± 0.22	14/64

* The values are given as the mean and standard deviation.

Migration and inducible interfragmentary micromotion were determined for three axes of translation and rotation adjusting for the side. The overall migration of the distal fracture fragment was described using total rotation and translation. The precision (as 95% confidence interval) was 0.21 mm and 1.51° for total migration and 0.10 mm and

1.01º for total inducible micromotion **(Table 17)**. Measured with total translation and rotation, fractures showed significant translation and rotation by two weeks ($p=0.004$ for both) compared with the immediate postoperative RSA images **(Table 24)**. There was no significant further migration. After two weeks there was, however, a trend for a continuing translation mainly in the Y-axis (i.e. axial shortening) and a trend for an increase of total rotation mainly in the X-axis (i.e. dorsal angulation) **(Table 24)**. Looking at translational and rotational migration together, the movement of the distal fragment was generally into the directions that mimicked the initial deformity (dorsal angulation, axial shortening, dorsal shift, and supination). Maximal grip caused significant ($p<0.03$) interfragmentary micromotion in the form of total translation and rotation **(Table 25)**. This inducible micromotion was detectable from six weeks up to eighteen weeks, but not at fifty-two weeks. The measurements of inducible micromotion for individual axes were below the precision threshold of the method.

Table 24. Migration measured by RSA (table from Study V).

	Precision[1]	2 Weeks	6 Weeks	12 Weeks	18 Weeks	52 Weeks
Translation (mm)[2]						
X-axis	±0.10	-0.25 (-1.46 to 0.97)	-0.08 (-0.53 to 0.37)	-0.03 (-0.35 to 0.29)	-0.11 (-0.46 to 0.24)	-0.11 (-0.93 to 0.72)
Y-axis	±0.08	-0.09 (-0.47 to 0.28)	-0.29 (-0.96 to 0.38)	-0.17 (-0.33 to -0.01)	-0.54 (-2.28 to 1.21)	-0.30 (-0.66 to 0.07)
Z-axis	±0.17	0.22 (-0.44 to 0.88)	0.20 (-0.40 to 0.79)	0.22 (-0.02 to 0.45)	0.16 (-0.50 to 0.81)	0.62 (-0.84 to 2.07)
Total	**±0.21**	**0.50* (-0.72 to 1.73)**	**0.54* (-0.03 to 1.11)**	**0.33 (0.06 to 0.60)**	**0.78* (-0.79 to 2.34)**	**0.98 (-0.01 to 1.98)**
Rotation (Degrees)[2]						
X-axis	±0.94	1.27 (-3.81 to 6.35)	3.39 (-5.14 to 11.92)	3.59 (-6.86 to 14.04)	2.41 (-4.36 to 9.18)	3.56 (-10.33 to 17.45)
Y-axis	±0.94	1.02 (-1.12 to 3.16)	0.31 (-2.41 to 3.03)	0.55 (-1.67 to 2.76)	-0.96 (-8.25 to 6.32)	-0.56 (-5.54 to 4.42)
Z-axis	±0.70	0.22 (-1.63 to 2.06)	0.66 (-4.67 to 5.99)	1.75 (-1.36 to 4.86)	2.33 (-4.55 to 9.21)	2.08 (-2.18 to 6.34)
Total	**±1.51**	**2.65* (-1.90 to 7.20)**	**5.34* (-1.47 to 12.16)**	**4.98 (-4.62 to 14.59)**	**5.36* (-3.31 to 14.03)**	**6.49 (-4.47 to 17.46)**

[1] Precision values given as the 95% confidence interval.

[2] Values are given as the mean and 95% confidence interval in parentheses, with total values calculated using the 3-D Pythagorean theorem.

* Significant measurements of total migration that exceeded the precision threshold ($p < 0.03$).

Table 25. Inducible micromotion measured by RSA (table from Study V).

	Precision[1]	6 Weeks	12 Weeks	18 Weeks	52 Weeks
Translation (mm)[2]					
X-axis	±0.06	0.02 (-0.13 to 0.16)	-0.02 (-0.18 to 0.14)	0.00 (-0.13 to 0.14)	-0.01 (-0.13 to 0.12)
Y-axis	±0.04	0.04 (-0.03 to 0.12)	-0.05 (-0.29 to 0.20)	-0.10 (-0.23 to 0.04)	-0.01 (-0.06 to 0.03)
Z-axis	±0.07	0.07 (-0.16 to 0.29)	-0.03 (-0.29 to 0.22)	-0.06 (-0.22 to 0.10)	-0.04 (-0.17 to 0.08)
Total	**±0.10**	**0.13* (-0.02 to 0.29)**	**0.19* (0.01 to 0.37)**	**0.15* (-0.01 to 0.31)**	**0.10 (0.01 to 0.22)**
Rotation (Degrees)[2]					
X-axis	±0.86	0.21 (-1.02 to 1.45)	-0.69 (-3.24 to 1.86)	-0.80 (-2.71 to 1.10)	-0.14 (-1.35 to 1.02)
Y-axis	±0.29	0.01 (-1.80 to 1.83)	-0.08 (-0.79 to 0.63)	0.05 (-0.85 to 0.95)	-0.13 (-1.03 to 0.73)
Z-axis	±0.44	0.13 (-0.61 to 0.86)	0.60 (-1.42 to 2.62)	0.32 (-1.28 to 1.92)	0.11 (-0.45 to 0.65)
Total	**±1.01**	**1.03* (-0.35 to 2.40)**	**1.29* (-1.58 to 4.16)**	**1.20* (-0.9 to 3.30)**	**0.77 (0.13 to 1.41)**

[1] Precision values given as the 95% confidence interval.

[2] Values are given as the mean and 95% confidence interval in parentheses, with total values calculated using the 3-D Pythagorean theorem.

* Significant measurements of total inducible that exceeded the precision threshold ($p < 0.03$).

6. DISCUSSION

6.1 MONITORING OF FRACTURE HEALING USING RSA

RSA has been used in orthopaedic implant research for over twenty years in the evaluation of micromovements at the bone-implant interface. However, only a relatively small number of studies have used RSA to evaluate the *in vivo* micromovement patterns that occur at a fracture site during the healing process. Studies utilising RSA to measure micromovements at the bone-bone interface following fractures, osteotomies, and spinal fusions have demonstrated high levels of clinical precision.

Based on RSA measurements, fracture migration during the healing period varies according to the fracture type and fixation method (**Study I**). Migration during the healing of fractures of the distal radius, spinal fusion, and tibial osteotomies varies, on average, between 0.2-3.2 mm. In femoral neck and trochanteric fractures, displacements are significantly higher ranging from 5 to 12 mm. Migration of femoral stems in THA or tibial components in TKA seems to be considerably smaller ranging from 0.05 mm to 1.3 mm (Kärrholm et al. 1994, Hansson et al. 2008, Gao et al. 2008).

It is likely that the majority of micromotion occurring in various fractures remains unrecognised on conventional plain radiographs. In rare cases, it is even possible that fracture micromotion retards fracture union without notably affecting reduction. The RSA method may serve as a predictor of compromised union. Furthermore, the RSA follow-up of a specific fracture can provide a definitive demonstration of the exact time of union, i.e. the achievement of fracture stability. The estimation of the time of fracture union using plain radiographs and clinical examination is fairly difficult. The gradual decrease of micromotion as measured by RSA can give definitive proof of early fracture union. These benefits, combined with high accuracy and precision, can enable the objective comparison of different fracture treatment modalities in small patient populations.

6.2 PHYSICAL AND COMPUTER SIMULATION PHANTOM MODELS OF RSA USE IN DISTAL RADIUS FRACTURES

The use of phantom model studies prior to the initiation of clinical trials is strongly recommended, as these validation studies will determine the achievable levels of accuracy and precision using a given experimental set-up. Additionally, these *in vitro* studies may reveal technical difficulties that can thus be addressed at an early stage. In the current study, the progress from physical modelling to computer modelling was a natural development that enabled more complex simulations to be performed.

The results for the physical phantom model (**Study II**) showed that under ideal conditions small translations could be measured with an accuracy of ± 6 µm and a

precision of 2-6 µm. The results of the study also showed that small rotations could be measured with an accuracy of ± 0.073º and a precision of 0.025º to 0.096º.

A computer simulation study (**Study III**) was performed in order to validate RSA for the measurement of complex migration in intra-articular distal radius fractures. The study showed a very high correlation between simulated movements and RSA measurements. Using a two-part fracture model, it was found that for simple movements in one axis, small translations could be measured with an accuracy of ± 2 µm. Similarly, small rotations could be measured with an accuracy of ± 0.015º. Using a three-part fracture model, the corresponding values of accuracy were found to be ± 4 µm and ± 0.031º for translation and rotation, respectively. For complex 3-D motion in a three-part fracture model the accuracy was ± 6 µm for translation and ± 0.120º for rotation.

The accuracy and precision values obtained in the physical phantom model study are higher than those reported in previous phantom RSA studies of hip arthroplasty. In the clinical setting of hip arthroplasty, precision has been shown to vary between 0.15-0.6 mm for translations and between 0.3-2° for measurements of rotation (Kärrholm et al. 1997). Önsten et al. (2001) demonstrated an accuracy of ± 45 µm to ± 139.5 µm and a precision ranging from 18 µm to 104 µm in human and canine cadaveric models. Bragdon et al. (2002) demonstrated an accuracy of 22-86 µm and a precision ranging between 5.5-16.0 µm. The main reason for these differences may be related to the different radiographic set-ups used. In the current study, the model was placed inside a cage (biplanar technique), whereas the cited studies have employed the uniplanar technique (the model placed above the cage). There are also other explanations for the improved accuracy and precision achieved in the current study, such as the use of digital measurements of the films (Börlin et al. 2002). The accuracy values obtained in the computer simulation study were somewhat higher than those obtained in the physical phantom model study. The main reason for these differences in accuracy may be due to errors associated with the use of micrometers for the measurement of translation and rotation when using a physical model.

The ME value is generally used to quantify the stability of RSA markers. In a clinical setting this value represents a sum of marker stability in the bone between different examinations and the error introduced by the film digitisation procedure or marker centre detection from consecutive radiographs. In an in vitro study, such as **Study II**, where the markers are rigidly fixed to the bone using adhesive and considered to be stable, and the bone is not exposed to significant loads, the ME value represents the digitisation error. The low ME values in **Study II** indicate a very low digitisation error, similarly low ME levels in **Study III** implied excellent marker centre detection since the radiographs did not have to be digitised. Modern-day RSA studies utilise digital radiographs and this reduces the error due to the formerly used scanning of radiographs.

In **Study II**, the number of markers and their configuration were found to have a greater impact on the accuracy and precision of rotation than on those of translation.

The results show that even with suboptimal placement of only 3 markers, it is possible to obtain a translation accuracy of ± 28 µm with a precision of 6 µm, and a rotation accuracy of ± 0.187º with a precision of 0.096º in all axes examined. In an optimal laboratory setting, such as that used in **Studies II** and **III**, markers can be placed in the exact desired locations. In a clinical setting, however, some markers may have to be placed in less than optimal locations due to fracture configuration and, on the other hand, some markers may even become loose with time. The current results favoured the use of at least four markers in each bone fragment.

6.3 RESORBABLE MARKERS FOR RSA

The results of **Study IV** showed that spherical markers made from bioactive glass with barium sulphate have sufficient bone-bonding properties for marker stability, and sufficient radio-opacity for performing RSA accurately and precisely. The *in vitro* studies demonstrated surface apatite formation, but the addition of 10% barium sulphate to the glass appeared to decrease reactivity. The *in vivo* studies confirmed that implants of bioactive glass with 10% barium sulphate do indeed incorporate with bone, although the strength of the bonding tends to be lower than that of bioactive glass implants without barium sulphate.

The fracture model RSA study indicated that a high level of accuracy and precision can be achieved using these novel markers. The high level of precision demonstrated that the RSA software was able to locate marker centres accurately from consecutive radiographs, which was further supported by low ME values. The levels of accuracy and precision obtained in this study are lower than those obtained in **Study II**. These differences in accuracy and precision between resorbable bioactive glass markers and tantalum markers were less than expected, since the original phantom study of the tantalum markers did not incorporate a soft tissue envelope.

Although tantalum markers have not resulted in any complications, one can argue for the use of non-permanent resorbable markers known to bond with bone. In a recent prospective RSA study evaluating micromotion in fractures of the distal radius in 9 patients, it was observed that 20 (38%) of the 52 tantalum markers inserted proximally and 9 (17%) of the 52 markers inserted distally to the fracture site were unstable within the bone bed during the follow-up (Downing et al. 2008). Loose markers have to be excluded from analysis since they can reduce precision and result in false calculations of migration (Biedermann et al. 2001). For most studies of fracture micromotion during healing, bioactive glass markers would have to be stable and sufficiently visible for up to one year. Technical improvements in the form of enhanced marker contrast and better spherical shape are expected to further increase accuracy and precision to approach those obtained using tantalum markers. The use of slowly reacting glass compositions can potentially make long-term (several years) follow-up studies with resorbable bioactive glass markers possible.

6.4 FRACTURE MIGRATION AND INDUCIBLE MICROMOTION IN PLATED DISTAL RADIUS FRACTURES

The results of **Study V** showed that the use of RSA in the follow-up of plated distal radius fractures is feasible yet technically challenging. The results suggest the presence of two distinct phenomena in the stability of intra-articular fractures of the radius after volar locking plating: fracture fragment migration as permanent motion (evident only during the first two weeks after surgical stabilization) and inducible interfragmentary micromotion as reversible displacement (evident up to eighteen weeks even after the radiographic evidence of fracture union).

In this study, AO type-C fractures were selected for surgical treatment with a commonly used volar titanium plate of large surface area and multiple locked screw/peg fixation capabilities. These choices were made so as to provide a worst-case scenario for RSA, i.e. if RSA could be successfully used under these conditions, then it could also be used for simpler fractures and smaller plates.

The level of precision achieved was in line with previous RSA studies of fracture healing (Matsson and Larsson 2003, Downing et al. 2008) but, as expected, the precision was somewhat lower than that measured in laboratory studies using simulated fracture models (**Studies II** and **III**). The clinical precision was enough to detect significant migration as well as inducible micromotion during the progress of fracture healing. Significant RSA migration/micro-displacement of the fracture, in the form of translation and rotation, occurred only during the first two weeks of healing. This was an expected result based on the clinical knowledge of the rapid natural healing process of cancellous bone fractures. Previous RSA studies of distal radial fractures, focusing on the degree of migration in individual patients, have reported longer periods of migration (Kopylov et al. 2001, Downing et al. 2008). It is noteworthy that early three-dimensional fracture fragment migration detected by RSA was not measurable on plain radiographs using the conventional displacement measurement techniques. The degree of early RSA migration is probably mainly dictated by the stability of the plate-screw construct, the quality of the bone and the patient's functional activity.

An unexpected finding of the study was that inducible micromotion was still detectable at eighteen weeks, when radiographic signs of union were visible in all fifteen patients. Inducible micromotion was expected to cease by the time that radiographic fracture union took place. In the study by Downing et al. (2008), inducible micromotion was present at two and six weeks, but it had ceased in all patients during the next time-point at twenty-six weeks. Their study did, however, lack observation time-points between six and twenty-six weeks. One can only speculate on the reasons for the persistence of inducible interfragmentary micromotion at eighteen weeks in our patients. Assuming that the observation is true, the result means that intra-articular fractures of the distal radius treated by volar locked plates reach high stability slower than generally believed and evident based on conventional radiographic analysis and clinical assessment. The presence of inducible interfragmentary micromotion evident

after achieving radiographic union probably represents elasticity of the uniting immature bony tissue. Interfragmentary micromotion caused by maximal voluntary grip may not be totally unexpected, since grip force is known to create high loads in the distal radius, even higher than those that plate fixation systems can withstand (Putnam et al. 2000).

One of the foremost challenges of this study was the placement of RSA markers. The large radio-opaque field created by the plate and screw/peg construct posed a challenge to targeted marker placement such that markers could be visualised in both AP and lateral RSA radiographs. The concept of the watershed line and anatomical volar plate require that the plate be placed distally, limiting the "free space" for marker placement. Marker visibility through the plate in the AP view or through the screws in the lateral view was variable and depended on the quality of the radiographs. Increasing the number of inserted markers by using an additional fracture site insertion failed to increase the number of visible markers distal to the fracture site, but increased the proportion of unstable and extra-osseous markers. This finding is in line with the findings of Downing et al. (2008). They used a fracture site insertion technique and found a relatively high proportion of unstable and extra-osseous markers. Furthermore, although the fracture site approach for marker placement may provide better access to the dorsal part of the distal radius, care must be taken when using this approach for distal marker placement since markers may have a direct path into the radiocarpal joint through intra-articular fracture cracks.

The patients in this study demonstrated good subjective and objective recovery by eighteen weeks. The range of motion as well as pinch grip and grip strength measurements presented as a percentage of the contralateral healthy side were similar to those presented in previous clinical studies of volar plating (Rozental et al. 2009, Wei et al. 2009). Pronation and supination strength measurements were performed in this study as an additional objective recovery parameter (Timm et al. 1993, Matsuoka et al. 2006). To our knowledge, this type of measurement has not been previously reported in the follow-up of patients with distal radius fractures. The measurement of pronation and supination strength may demonstrate functional deficits that are not detectable by other means. The results showed that both pronation and supination strengths reached 90-100% of the value of the contralateral healthy side by eighteen weeks, and mean values at fifty-two weeks were similar to previously published normative values (Matsuoka et al. 2006).

The high accuracy and precision of RSA made it possible to perform the current study with a relatively small number of patients. Although this number was sufficient for performing measurements of migration and inducible micromotion, it was not sufficient for examining the correlation of RSA measurements with clinical recovery parameters. Clinical outcomes of the fractured wrist at eighteen weeks were still poorer than those of the contralateral healthy side even though all of the fractures were radiologically healed. The detection of inducible micromotion at eighteen weeks may be related to these clinical observations.

Is the precision of RSA enough to enable the comparison of small patient groups in randomised clinical trials of distal radial fractures? And how many patients are needed in a prospective trial comparing two volar plates in type-C fractures? Using the paired *t* test with power set at 80% and statistical significance set at $P < 0.05$, 13 patients are needed in each group in order to detect a difference of 1 mm of total translation or 6 degrees of total rotation (corresponding to a 3.5° rotation in each axis). This patient number would also enable detecting a difference of 0.11 mm and 2° of total inducible translation and total inducible rotation, respectively. In such head-to-head comparisons, it is vital that CN and ME values are also in the same range for both treatment groups as these can confound RSA results. Taking into account the observed relatively high rate of excluded measurements due to technically inadequate RSA imaging, the total amount of patients needed in a comparative clinical trial of two plate fixation systems is expected to be about 25-30 in each group. This number corresponds to the recommended size of study groups in RSA studies.

6.5 LIMITATIONS AND STRENGTHS OF THE STUDY

The current study had several limitations. First of all, the use of a physical phantom model is only an approximation to the real clinical setting. The RSA radiographs obtained in the phantom studies are, however, expected to be close in quality to those obtained in the clinical setting, since the amount of soft tissue in the region is negligible as compared to studies of the hip region where this poses a potential problem.

One of the shortcomings of the physical phantom model used in **Study II** is the inability to mimic complex 3-D motion that may occur during a fracture of the distal radius, such as a combination of dorsal tilt with axial radial shortening. The physical phantom model was used to mimic the most significant components of this 3-D motion and examined each of them separately. Another limitation of the model is that it cannot be directly applied to more complex intra-articular fractures of the distal radius where multiple fragments are involved. Comminuted intra-articular fractures place limitations on the effective number of markers that can be inserted into fracture fragments. The limitations posed by the physical phantom model were overcome by the use of a computer simulation model.

The use of a computer simulation model in **Study III** has several advantages. There is no need for the use of micro-positioning hardware, such as micrometers, in order to simulate movements of a phantom model. In addition, this type of model may be used to simulate and examine movement in complex clinical situations, which may be difficult or impossible to simulate using physical models. The ray-tracing method is also fast and cost-effective compared to making physical radiographs; creation of images can take only minutes, depending on the speed of the processor used.

Although the results of **Study IV** showed the adequate bone bonding properties of bioactive glass with 10% barium sulphate over a two-month follow-up period, the

study did not examine how long these bioresorbable markers have sufficient radio-opacity for accurate RSA analysis. Another limitation of **Study IV** is that mechanical testing was performed using cones not spheres. *In vivo* implantation of spheres, followed by push-out testing is technically very difficult and the use of cones is an established and accepted method for testing bone bonding (Hench and Andersson 1999, Zhao et al. 2008). Furthermore, this study did not include tantalum metal cones as a control. Additionally, the current study did not examine the possible side-effects of residual barium sulphate on bone and other tissues. Barium sulphate is commonly used as an opacifier in bone cements. A study by Acarturk et al. (2008) evaluated the bone healing response to injectable calcium phosphate cement with and without barium sulphate as an opacifier. A 13 mass percent of barium sulphate was used. The cements were injected into the medullary canal of New Zealand white rabbits with a follow-up time of two years. Both cement formulations appeared to be biocompatible and osteoconductive with no evidence of inflammation or fibrous tissue around the implant materials or at the bone-material interfaces. Additionally, pathological examination of additional tissues, including regional lymph nodes, revealed no dissemination of barium sulphate (Acarturk et al. 2008). RSA markers also need to withstand high forces produced by the mechanical injector devices used for marker insertion. In this study, the manually created markers could not be inserted using an injector due to their larger size.

Due to manufacturing limitations, the glass markers used in **Study IV** had a diameter of 1.5 mm, which is larger than the conventionally-used tantalum markers with diameters of 0.5, 0.8 and 1.0 mm. Larger markers result in a larger projected X-ray image, which holds more information and can result in higher precision. However, these larger images have a less well-defined contour, since the marker image is the result of a central projection with an X-ray source of a definite size (Valstar et al. 2005). Additionally, a certain degree of error was expected in locating bioactive glass marker centres in successive radiographs, because the markers have lower radio-opacity and were not perfectly spherical because of manual manufacturing. The closer the roundness of the marker is to that of a perfect sphere the more likely the projection will approach that of a perfect circle. The precision of the RSA method relies partly on how well the RSA software locates the centres of the circular projections of the markers from radiographic images. The closer the image is to a perfect circle, the more likely the software is to identify the same point to be the centre of that circle. It should be noted that there is already available technology for manufacturing bioactive glass spheres of standard size (Välimäki et al. 2006).

Study V had several limitations. Migration and inducible micromotion could not be measured from all patients at each time point due to poor marker visibility. The image intensifier used in the study was not precise enough for visualising all the markers. The visibility of markers could be improved by intra-operatively checking marker visibility using a digital image intensifier. Another drawback of the study was that inducible micromotion measurements relied on the patient squeezing a rubber ball with maximum voluntary strength. The grip force could be verified by squeezing a dynamometer instead of a ball as performed by Downing et al. (2008). Finally, in

pronation and supination measurements, the use of a polyethylene hemisleeve to stabilize the forearm may produce more standardized measurements.

As reported previously (Ryd et al. 2000), the small bone size required the use of condition numbers higher than 150. However, as recommended in RSA standardized output guidelines **(Table 3)**, the precision of the measurements was validated by means of double examinations at each visit point. In the study of a phantom model of an extra-articular distal radius fracture (**Study II**), it was demonstrated that a high level of accuracy and precision of migration measurements could be obtained even with only three distal markers and a condition number of over 750. On the other hand, in a computer simulation model of a three-part intra-articular distal radius fracture **(Study III**) it was possible to achieve condition number levels of less than 200 with 5 optimally placed markers in the smaller of the two distal fragments.

The study by Downing et al. (2008) examined nine patients with distal radius fractures treated by a volar locked plate, and CN levels obtained were lower than those obtained in this study. There are two main reasons for this: first, in the study of Downing et al. (2008), four of the patients had type-A fractures and none of the five type-C fractures were type-C3, whereas all fractures in the current study were type-C with the majority being type-C3. Second, a very small surface area plate with only one row of distal locking screws was used in the study of Downing et al. (2008), compared with the large surface area plate with two rows of distal locking screws used in the current study. These factors together limited possibilities of achieving equally low CN values.

The main strength of **Study V** was that it was a prospective cohort study of 15 patients with a 1-year follow-up and no drop-outs. Furthermore, all patients had one type of comminuted distal radius fracture (AO type-C) and a single fixation method was used. Furthermore, the extensive repertoire of objective clinical and radiological variables examined in parallel to the RSA measurements enabled a multi-faceted evaluation of the healing process. Although the patients underwent a careful postoperative evaluation, the study was not powered to assess the value of RSA in the prediction of functional recovery.

6.6 FUTURE ASPECTS

Over the past thirty years, RSA has developed from a technique used by a few researchers to a powerful tool used by many research groups around the world (Kärrholm et al. 2006). The RSA standardization guidelines published in 2005 by Valstar and colleagues have played a critical role in enabling the comparison of RSA studies worldwide. Although RSA is a powerful tool in clinical research, it still remains unsuitable for clinical practice. RSA requires bone markers as well as investment in the technology and personnel. The minimum investment required to set-up an RSA unit is over 50,000€. Furthermore, the RSA technique is still very time consuming. The accuracy of RSA fracture studies is dependant on the placement of a sufficient number of visible, but also stable markers. The use of 3-D computer models

to simulate RSA examinations may facilitate the preoperative planning of RSA fracture studies, especially in determining optimal marker placement sites for comminuted fractures obscured by radio-opaque hardware.

One of the most important applications of RSA has been the study of prosthesis fixation. An important focus of these studies has been the relationship between short-term micromotion and long-term failure. Studies have shown that RSA data collected during the first 1-2 years can be used to identify both hip and knee replacements that are "at risk" of failure well before clinical symptoms appear (Kärrholm et al. 1994, Ryd et al. 1995). It has been suggested that an international database be developed for collecting the results of all clinical RSA studies (Kärrholm et al. 2006). This data could be used for objective comparison of fracture fixation methods, as well as prosthesis designs. Dynamic RSA and the measurement of inducible micromotion may play an important role in future studies, especially when combined with modelling methods such as finite element analysis (FE). Data provided by dynamic RSA can then be used in the estimation of stress distributions in implant components or even fracture sites (Kärrholm et al. 2006). If the phenomena of RSA migration and inducible micromotion are universal, their registration would help to create a new RSA-based staging system of fracture healing, starting from the period of early fragment migration to the appearance of radiographic union, followed by cessation of inducible interfragmentary motion. This information can provide us with more concrete and tailored guidelines for individualized fracture treatments according to the inherent stability of each fracture.

The past ten years have seen a growing use of fixed-angle plates in fracture treatment. The primary benefit of these implants is the achievement of relative stability through suitable fracture site strain levels. The knowledge of how to achieve these strain levels through appropriate locking-screw configurations relative to specific fracture patterns is still very limited. The use of RSA in the measurement of inducible micromotion may provide new insight into how to optimise the use of this treatment modality.

The use of locked plates in distal radius fractures appears to provide a more rapid recovery in the early postoperative period when compared with external fixation or closed reduction and percutaneous fixation. The load-bearing nature of these implants enables early initiation of active exercises. Early rehabilitation and return to functional activities and work may have a clear socio-economic impact. Chehade et al. (2009) introduced the concept of differentially loaded RSA (DLRSA), which is a dynamic RSA technique using standard axial loads to determine changes in fracture stiffness. The use of such standardized loads can enable more accurate comparison of dynamic RSA measurements and enable load adjustments according to specific fracture patterns. Combining clinically relevant loading patterns and RSA measurements to understand the importance of fixation stability at different stages of the fracture healing process may help in optimising rehabilitation protocols.

The RSA method may also provide some insight into the overall global three-dimensional motion of distal radius fractures before union under different fixation modalities. This data may provide the means to perform a detailed analysis of the

factors that lead to the loss of reduction during immobilization. The current enthusiasm for fixed-angle volar plates over other distal radial fracture treatment modalities has been criticised for the lack of sufficient supporting scientific evidence (Chen and Jupiter 2007). The high precision and accuracy of RSA make it an ideal candidate for the objective evaluation of fracture fixation methods, as well as for comparing the legion of different volar fixed angle plates currently available for the treatment of these fractures. Furthermore, the use of pronation and supination strength measurements is an interesting addition to the arsenal of clinical tests used in evaluating recovery after a distal radius fracture and warrants further studies.

7. CONCLUSIONS

On the basis of the present investigations, the following conclusions can be made:

1. Validation of RSA for the measurement of migration in distal radius fractures using a physical phantom model showed a high level of accuracy and precision.

2. Validation of RSA for the measurement of migration in intra-articular distal radius fractures using three-dimensional computer modelling demonstrated a high level of accuracy and precision. The method is especially useful in the simulation of complex fracture movements in comminuted fracture patterns for which physical phantom model simulations may not be feasible.

3. Investigation of the performance of novel resorbable radio-opaque bioactive glass markers demonstrated potential for use in RSA. These markers have sufficient bone-bonding properties for marker stability and sufficient radio-opacity for performing RSA accurately and precisely.

4. Application of RSA for the measurement of interfragmentary migration and inducible micromotion in plated AO type-C distal radius fractures was found to be technically demanding. The precision of RSA is sufficient for comparing fracture migration and inducible micromotion in small patient groups with the caveat that a sufficient number and configuration of stable markers must be achieved. Furthermore, cessation of fracture displacement and inducible interfragmentary micromotion are likely to be sensitive indicators of fracture union.

ACKNOWLEDGEMENTS

This study was carried out at the Orthopaedic Research Unit, Department of Orthopaedic Surgery and Traumatology, University of Turku during the years of 2004-2010.

I express my sincere and deepest gratitude to my supervisor, Professor Hannu Aro. Professor Aro has created an innovative research environment focusing on high-quality orthopaedic studies. His extensive knowledge in pre-clinical and clinical research, as well as expertise in scientific writing, has been vital to the completion of this thesis. Professor Aro's exemplary work ethic and strive for perfection have made it a privilege to be part of the Orthopaedic Research Unit.

I would like to thank Professor Juhana Leppilahti and Docent Jari Salo, the official reviewers of the dissertation, for their careful evaluation and constructive criticism.

I would like to thank all my co-authors for their contributions to this thesis. Most of all I want to thank Niko Moritz for his invaluable expertise in computer programming and biomechanics. You have been a great mentor as well as a great friend. Tatu Mäkinen, my friend and colleague, is acknowledged for introducing me to the world of RSA. Niko Strandberg, for surgical expertise related to volar plating. Professor Sune Larsson for sharing his RSA expertise. Erik Vedel, for preparation of bioactive glass compositions. Docents Erkki Svedström and Kimmo Mattila are thanked for providing excellent facilities for carrying out RSA and for technical advice related to radiography. I also wish to thank Tero Vahlberg for his assistance with the statistical analyses.

This thesis would not have been possible without the support of all the other members of the Orthopaedic Research Unit. I want to thank Satu Timlin and Katriina Halava for all the help with the logistics of the clinical trial, and Jessica Alm and Petteri Lankinen for fruitful discussions. Also, other members are thanked: Terhi Heino, Riku Alaranta, Janek Frantzén, Pauli Keränen, Eeva Hacklin, and Ville-Valtteri Välimäki. Pirjo Heino, Sanna Kolehmainen, and Eija Tuominen are acknowledged for their help in the clinical study.

I thank all my colleagues from Päijät-Häme Central Hospital, Töölö Hospital, Peijas Hospital, and the Hospital for Children and Adolescents in Helsinki. I am also thankful to all my friends and family, both in Finland and abroad, who have provided a great counterbalance to the demanding scientific work.

I would like to thank my parents, Suheil and Liisa, my sister Laura-Maria and her husband Veli-Pekka, as well as my grandmother Maija for their love and support.

Finally, I want to thank my wife, Marina and our lovely son, Mark. The past few years have not been easy. Your love, faith in me, and never-ending patience made this possible.

This work was financially supported by the National Technology Agency (TEKES), the National Graduate School of Musculoskeletal Disorders and Biomaterials (TBGS), The Finnish Research Foundation for Orthopaedics and Traumatology, The Finnish Research Foundation for Hand Surgery, the Finnish Medical Foundation, Päijät-Häme Central Hospital, Turku University Hospital, and the Turku University Foundation.

Turku, December 2010

Rami Madanat

REFERENCES

Abramo A, Kopylov P, Tagil M. Evaluation of a treatment protocol in distal radius fractures: a prospective study in 581 patients using DASH as outcome. Acta Orthop. 2008;79:376-385.

Acarturk O, Lehmicke M, Aberman H, Toms D, Hollinger JO, Fulmer M. Bone healing response to an injectable calcium phosphate cement with enhanced radiopacity. J Biomed Mater Res B Appl Biomater. 2008;86:56-62.

Adams BD. Effects of radial deformity on distal radioulnar joint mechanics. J Hand Surg [Am]. 1993;18:492-498.

Ahl T, Dalén N, Holmberg S, Selvik G. Early weight bearing of malleolar fractures. Acta Orthop Scand. 1986;57:526-529.

Ahl T, Dalén N, Holmberg S, Selvik G. Early weight bearing of displaced ankle fractures. Acta Orthop Scand. 1987;58:535-538.

Ahl T. Ankle fractures with special reference to early postoperative weight bearing. Thesis, Karolinska Institutet, Stockholm, Sweden 1988.

Ahl T, Dalén N, Lundberg A, Wykman A. Biodegradable fixation of ankle fractures. A roentgen stereophotogrammetric study of 32 cases. Acta Orthop Scand. 1994;65:166-170.

Alberius P. Bone reactions to tantalum markers. A scanning electron microscopy study. Acta Anat (Basel). 1983;115:310-318.

Albrekstsson BE, Ryd L, Carlsson LV, Freeman MA, Herberts P, Regnér L, Selvik G. The effect of a stem on the tibial component of knee arthroplasty. A roentgen stereophotogrammetric study of uncemented tibial components of the Freeman-Samuelson knee arthroplasty. J Bone Joint Surg [Br]. 1990;72:252-258.

Alfaro-Adrián J, Gill HS, Murray DW. Cement migration after THR. A comparison of charnley elite and Exeter femoral stems using RSA. J Bone Joint Surg [Br]. 1999;81:130-134.

Alffram PA, Bauer GC. Epidemiology of fractures of the forearm. A biomechanical investigation of bone strength. J Bone Joint Surg [Am]. 1962;44:105-114.

Allen MJ, Hartman SM, Sacks JM, Calabrese J, Brown PR: Technical feasibility and precision of radiostereometric analysis as an outcome measure in canine cemented total hip replacement. J Orthop Sci. 2004;9:66-75.

Amadio PC, Silverstein MD, Ilstrup DM, Schleck CD, Jensen LM. Outcome after Colles fracture: the relative responsiveness of three questionnaires and physical examination measures. J Hand Surg [Am]. 1996;21:781-787.

Aro HT, Koivunen T. Minor axial shortening of the radius affects outcome of Colles' fracture treatment. J Hand Surg [Am]. 1991;16:392-398.

Aro HT, Chao EY. Bone-healing patterns affected by loading, fracture fragment stability, fracture type, and fracture site compression. Clin Orthop Relat Res. 1993;(293):8-17.

Aronson AS, Holst L, Selvik G. An instrument for insertion of radiopaque bone markers. Radiology. 1974;113:733-734.

ASTM. Annual book of ASTM standards. Standard practice for use of the terms precision and bias in ASTM test methods. Designation: E 177-90a (reapproved 1996), 1990.

Augat P, Merk J, Ignatius A, Margevicius K, Bauer G, Rosenbaum D, Claes L. Early, full weightbearing with flexible fixation delays fracture healing. Clin Orthop Relat Res. 1996;328:194-202.

Augat P, Simon U, Liedert A, Claes L. Mechanics and mechano-biology of fracture healing in normal and osteoporotic bone. Osteoporosis Int. 2005;16(Suppl 2):S36-S43.

Augé WK 2nd, Velazquez PA. The application of indirect reduction techniques in the distal radius: the role of adjuvant arthroscopy. Arthroscopy. 2000;16:830-835.

Axelrod TS, McMurtry RY. Open reduction and internal fixation of comminuted, intraarticular fractures of the distal radius. J Hand Surg [Am]. 1990;15:1-11.

Benoist LA, Freeland AE. Buttress pinning in the unstable distal radial fracture. A modification of the Kapandji technique. J Hand Surg [Br]. 1995;20:82-96.

Bey MJ, Zauel R, Brock SK, Tashman S. Validation of a new model-based tracking technique for measuring three-dimensional, in vivo glenohumeral joint kinematics. J Biomech Eng. 2006;128:604-609

Bhandari M, Guyatt GH, Swiontkowski MF, Tornetta III P, Sprague S, Schemitsch EH. A lack of consensus in the assessment of fracture healing among orthopaedic surgeons. J Orthop Trauma. 2002;16:562-566.

Biedermann R, Stöckl B, Krismer M, Mayrhofer P, Ornstein E, Franzén H. Evaluation of accuracy and precision of bone markers for the measurement of migration of hip prostheses. A comparison of conventional measurements. J Bone Joint Surg [Br] 2001;83:767-771.

Björk A. The use of metallic implants in the study of facial growth in children: method and application. Am J Phys Anthropol. 1968;29:243-254.

Boyer MI, Korcek KJ, Gelberman RH, Gilula LA, Ditsios K, Evanoff B. Anatomical tilt views of the distal radius: an ex-vivo analysis of operative fixation. J Hand Surg [Am]. 2004;29:116-122.

Boyer MI. Distal radius fractures: what's in and what's out. Instr Course Lect. 2007;56:61-64.

Bragdon CR, Malchau H, Yuan X, Perinchief R, Kärrholm J, Börlin N, Estok DM, Harris WH. Experimental assessment of precision and accuracy of radiostereometric analysis for the determination of polyethylene wear in a total hip replacement model. J Orthop Res. 2002;20:688-695.

Bragdon CR, Estok DM, Malchau H, Kärrholm J, Yuan X, Bourne R, Veldhoven J, Harris WH: Comparison of two digital radiostereometric analysis methods in the determination of femoral head penetration in a total hip replacement phantom. J Orthop Res. 2004;22:659-664.

Bragonzoni L, Russo A, Loreti I, Montagna L, Visani A, Marcacci M. The stress-inducible displacement detected through RSA in non-migrating UKR. Knee. 2005;12:301-306.

Brandsson S, Karlsson J, Sward L, Kartus J, Eriksson BI, Kärrholm J. Kinematics and laxity of the knee joint after anterior cruciate ligament reconstruction: pre- and postoperative radiostereometric studies. Am J Sports Med. 2002;30:361-367.

Burke GL. The corrosion of metals in tissues; and an introduction to tantalum. Can Med Ass J. 1940;43:125-128.

Börlin N, Thien T, Kärrholm J. The precision of radiostereometric measurements. Manual vs. digital measurements. J Biomech. 2002;35:69-79.

Catalano LW 3rd, Cole RJ, Gelberman RH, Evanoff BA, Gilula LA, Borrelli J Jr. Displaced intra-articular fractures of the distal aspect of the radius. Long-term results in young adults after open reduction and internal fixation. J Bone Joint Surg [Am]. 1997;79:1290-1302.

Changulani M, Okonkwo U, Keswani T, Kalairajah Y. Outcome evaluation measures for wrist and hand: which one to choose? Int Orthop. 2008;32:1-6.

Chao EY, Aro HT, Lewallen DG, Kelly PJ. The effect of rigidity on fracture healing in external fixation. Clin Orthop Relat Res. 1989;241:24-35.

Chehade MJ, Solomon LB, Callary SA, Benveniste SH, Pohl AP, Howie DW. Differentially loaded radiostereometric analysis to monitor fracture stiffness: a feasibility study. Clin Orthop Relat Res. 2009;467:1839-1847.

Chung KC, Pillsbury MS, Walters MR, Hayward RA. Reliability and validity testing of the Michigan Hand Outcomes Questionnaire. J Hand Surg [Am]. 1998;23:575-587.

Chung KC, Watt AJ, Kotsis SV, Margaliot Z, Haase SC, Kim HM. Treatment of unstable distal radial fractures with the volar locking plating system. J Bone Joint Surg [Am]. 2006;88:2687-2694.

Chung KC, Squitieri L, Kim HM. Comparative outcomes study using the volar locking plating system for distal radius fractures in both young adults and adults older than 60 years. J Hand Surg [Am]. 2008;33:809-819.

Claes LE, Wilke HJ, Augat P, Rübenacker S, Margevicius KJ. Effect of dynamization on gap healing of diaphyseal fractures under external fixation. Clin Biomech (Bristol, Avon). 1995;10:227-234.

Cole RJ, Bindra RR, Evanoff BA, Gilula LA, Yamaguchi K, Gelberman RH. Radiographic evaluation of osseous displacement following intra-articular fractures of the distal radius: reliability of plain radiography versus computed tomography. J Hand Surg [Am]. 1997;5:792-800.

Colles A. On the fracture of the carpal extremity of the radius. Edinburgh Medical Surgical Journal. 1814;10:182-186.

Cooney WP. Fracture of the distal radius: a modern treatment-based classification. Orthop Clin North Am. 1993;24:211-216.

Court-Brown C, McQueen M, Tornetta P. Fractures of the distal radius and ulna. In: Orthopaedic surgery essentials, trauma. (Eds. Tornetta P, Einhorn TA). Lippincott Williams & Wilkins, Philadelphia 2006:153-169.

Cummings SR, Black DM, Rubin SM. Lifetime risks of hip, Colles', or vertebral fracture and coronary heart disease among white postmenopausal women. Arch Intern Med. 1989;149:2445-2448.

de Lange A, Kauer JM, Huiskes R. Kinematic behavior of the human wrist joint: a roentgen-stereophotogrammetric analysis. J Orthop Res. 1985;3:56-64.

Dodds SD, Cornelissen S, Jossan S, Wolfe SW. A biomechanical comparison of fragment-specific fixation and augmented external fixation for intra-articular distal radius fractures. J Hand Surg [Am]. 2002;27:953-964.

Downing MR, Ashcroft PB, Johnstone AJ, Bach O, Mackenzie S, Ashcroft GP. Assessment of inducible fracture micromotion in distal radial fractures using radiostereometry. J Orthop Trauma. 2008;22:S96-105.

Downing ND, Karantana A. A revolution in the management of fractures of the distal radius? J Bone Joint Surg [Br]. 2008;90:1271-1275.

Drobetz H, Bryant AL, Pokorny T, Spitaler R, Leixnering M, Jupiter JB. Volar fixed-angle plating of distal radius extension fractures: influence of plate position on secondary loss of reduction—a biomechanic study in a cadaveric model. J Hand Surg [Am]. 2006;31:615-622.

Duffy P, Trask K, Hennigar A, Barron L, Leighton RK, Dunbar MJ. Assessment of fragment micromotion in distal femur fracture fixation with RSA. Clin Orthop Relat Res. 2006;448:105-113.

Edwards CC 2nd, Haraszti CJ, McGillvary GR, Gutow AP. Intra-articular distal radius fractures: arthroscopic assessment of radiographically assisted reduction. J Hand Surg [Am]. 2001;26:1036-1041.

Egol KA, Kubiak EN, Fulkerson E, Kummer FJ, Koval KJ. Biomechanics of locked plates and screws. J Orthop Trauma. 2004;18:488-493.

Egol K, Walsh M, Tejwani N, McLaurin T, Wynn C, Paksima N. Bridging external fixation and supplementary Kirschner-wire fixation versus volar locked plating for unstable fractures of the distal radius: a randomised, prospective trial. J Bone Joint Surg [Br]. 2008;90:1214-1221.

Engelberg R, Martin DP, Agel J, Obremsky W, Coronado G, Swiontkowski MF. Muskuloskeletal Function Assessment instrument: criterion and construct validity. J Orthop Res. 1996;14:182-192.

Euler L. Novi commentarii academiae scientiarum Petropolitanae (1775) 1776;20:189-207. Reprint in: Leonhardi Euleri Opera Omnia, Formulae generales pro translatione quacunque corporum rigidorum. Series Secunda. (Ed. Blanc C). Orell Füssli Turici, Basel. 1968;9:84-98.

Fernandez DL. Fractures of the distal radius. Operative treatment. Instr Course Lect. 1993;42:73-88.

Frykman GK. Fracture of the distal radius including sequelae-shoulder hand finger syndrome. Disturbance in the distal radioulnar joint and impairment of nerve function. A clinical and experimental study. Acta Orthop Scand (Suppl). 1967;108:1-155.

Frykman GK, Peckham RH, Willard K, Saha S. External fixators for treatment of unstable wrist fractures. A biomechanical, design feature, and cost comparison. Hand Clin 1993;9:555-565.

Gao F, Henricson A, Nilsson KG. Cemented versus uncemented fixation of the femoral component of the NexGen CR total knee replacement in patients younger than 60 years: a prospective randomized controlled RSA study. Knee. 2009;16:200-206.

Gardner TN, Mishra S. The biomechanical environment of a bone fracture and its influence upon the morphology of healing. Med Eng Phys. 2003;25:455-464.

Gartland JJ Jr., Werley CW. Evaluation of healed Colles' fractures. J Bone Joint Surg [Am]. 1951;33:895-907.

Geissler WB, Fernandez DL. Percutaneous and limited open reduction of the articular surface of the distal radius. J Orthop Trauma. 1991;5:255-264.

Gesensway D, Putnam MD, Mente PL, Lewis JL. Design and biomechanics of a plate for the distal radius. J Hand Surg [Am]. 1995;20:1021-1027.

Glyn-Jones S, Polgár K, Hicks J, Murray DW, Gill HS. RSA-measured inducible micromotion and interface modeling with finite element methods. Clin Orthop Relat Res. 2006;448:98-104.

Gofton W, Liew A. Distal radius fractures: nonoperative and percutaneous pinning treatment options. Orthop Clin North Am. 2007;38:175-185.

Goldhahn J, Scheele WH, Mitlak BH, Abadie E, Aspenberg P, Augat P, Brandi ML, Burlet N, Chines A, Delmas PD, Dupin-Roger I, Ethgen D, Hanson B, Hartl F, Kanis JA, Kewalramani R, Laslop A, Marsh D, Ormarsdottir S, Rizzoli R, Santora A, Schmidmaler G, Wagener M, Reginster JY. Clinical evaluation of medicinal products for acceleration of fracture healing in patients with osteoporosis. Bone. 2008;43:343-347.

Goodship AE, Kenwright J. The influence of induced micromovement upon the healing of experimental tibial fractures. J Bone Joint Surg [Br]. 1985:67:650-655.

Goodship AE, Watkins PE, Rigby HS, Kenwright J. The role of fixator frame stiffness in the control of fracture healing. An experimental study. J Biomech. 1993;26:1027-1035.

Goodship AE, Lawes TJ, Rubin CT. Low-magnitude high-frequency mechanical signals accelerate and augment endochondral bone repair: preliminary evidence of efficacy. J Orthop Res. 2009;27:922-930.

Gradl G, Wendt M, Gierer P, Beck M, Mittlmeier T. Fixation of distal radial fractures with the Targon DR nail. Oper Orthop Traumatol. 2009;21:472-483.

Graham TJ. Surgical correction of malunited fractures of the distal radius. J Am Acad Orthop Surg. 1997;5:270-281.

Greatting MD, Bishop AT. Intrafocal (Kapandji) pinning of unstable fractures of the distal radius. Orthop Clin North Am. 1993;24:301-307.

Grewal R, Perey B, Wilmink M, Stothers K. A randomized prospective study on the treatment of intra-articular distal radius fractures: open reduction and internal fixation with dorsal plating versus mini open reduction, percutaneous fixation, and external fixation. J Hand Surg [Am]. 2005;30:764-772.

Grewal R, MacDermid JC, Pope J, Chesworth BM. Baseline predictors of pain and disability one year following extra-articular distal radius fractures. Hand (NY). 2007;2:104-111.

Grundschober FM, Kellner G, Eschberger J, Plenck H. Long-term osseous anchorage of endosseous dental implants made of titanium and tantalum. In: Biomaterials 1980, First World Biomaterials Congress. (Eds. Winter GD, Gibbons DF, Plenk H). Wiley, Chichester 1982:365-370.

Haddad M, Jacoby B, Snerum L, Hede J, Overgaard S. External fixation of distal radius fractures: 3 or 5 weeks of external fixation. Int Orthop. 2000;24:224-226.

Hallert B. X-ray photogrammetry. Basic geometry and quality. Elsevier, Amsterdam 1970.

Hallström E, Kärrholm J. Shoulder rhythm in patients with impingement and in controls: dynamic RSA during active and passive abduction. Acta Orthop. 2009;80:456-464.

Handoll HH, Madhok R. Conservative interventions for treating distal radial fractures in adults. Cochrane Database Syst Rev. 2003;(2):CD000314.

Handoll HH, Madhok R. Surgical interventions for treating distal radial fractures in adults. Cochrane Database Syst Rev. 2003;(3):CD003209.

Hansson LI, Olsson TH, Selvik G, Sundén G. A roentgen stereophotogrammetric investigation of

innominate osteotomy (Salter). Acta Orthop Scand. 1978;49:68-72.

Hansson U, Ryd L, Toksvig-Larsen S. A randomized RSA study of Peri-Apatite HA coating of a total knee prosthesis. Knee. 2008;15:211-216.

Haus BM, Jupiter JB. Intra-articular fractures of the distal end of the radius in young adults: reexamined as evidence-based and outcomes medicine. J Bone Joint Surg [Am]. 2009;91:2984-2991.

Hegeman JH, Oskam J, Vierhout PA, Ten Duis HJ. External fixation for unstable intra-articular distal radial fractures in women older than 55 years. Acceptable functional end results in the majority of the patients despite significant secondary displacement. Injury. 2005;36:339-344.

Hench LL, Andersson Ö. Bioactive glasses. In: Hench LL, Wilson J, eds. An Introduction to Bioceramics. Singapore: World Scientific, 1999. p. 41-62.

Henry MH, Griggs SM, Levaro F, Clifton J, Masson MV. Volar approach to dorsal displaced fractures of the distal radius. Tech Hand Up Extrem Surg. 2001;5:31-41.

Hove LM, Nilsen PT, Furnes O, Oulie HE, Solheim E, Mölster AO. Open reduction and internal fixation of displaced intraarticular fractures of the distal radius. 31 patients followed for 3-7 years. Acta Orthop Scand. 1997;68:59-63.

Hurschler C, Seehaus F, Emmerich J, Kaptein BL, Windhagen H. Comparison of the modell-based and marker-based roentgen stereophotogrammetry methods in a typical clinical setting. J Arthroplasty. 2009;24:594-606.

Hägglund G, Bylander B, Hansson LI, Kärrholm J, Selvik G, Svensson K. Longitudinal growth of the distal fibula in children with slipped capital femoral epiphysis. J pediatr Orthop. 1986;6:274-277.

Ilyas AM, Jupiter JB. Distal radius fractures—classification of treatment and indications for surgery. Orthop Clin North Am. 2007;38:167-173.

Ilyas AM, Thoder JJ. Intramedullary fixation of displaced distal radius fractures: a preliminary report. J Hand Surg [Am]. 2008;33:1706-1715.

Jebsen RH, Taylor N, Trieschmann RB, Trotter MJ, Howard LA. An objective and standardized test of hand function. Arch Phys Med Rehabil. 1969;50:311-319.

Jenkins NH. The unstable Colles' fracture. J Hand Surg [Br]. 1989;14:149-154.

Johnsson R, Selvik G, Strömqvist B, Sundén G. MMobility of the lower lumbar spine after posterolateral fusion determined by roentgen stereophotogrammetric analysis. Spine. 1990;15:347-350.

Johnsson R, Axelsson P, Strömqvist B. Posterolateral lumbar fusion using facet joint fixation with biodegradable rods: a pilot study. Eur Spine J. 1997;6:144-148.

Johnsson R, Strömqvist B, Aspenberg P. Randomized radiostereometric study comparing osteogenic protein-1 (BMP-7) and autograft bone in human noninstrumented posterolateral lumbar fusion: 2002 Volvo Award in clinical studies. Spine. 2002;27:2654-2661.

Jupiter JB. Commentary: the effect of ulnar styloid fractures on patient-related outcomes after volar locking plating of distal radius fractures. J Hand Surg [Am]. 2009;34:1603-1604.

Kamath AF, Zurakowski D, Day CS. Low-profile dorsal plating for dorsally angulated distal radius fractures: an outcomes study. J Hand Surg [Am]. 2006;31:1061-1067.

Kapandji A. [Internal fixation by double intrafocal plate. Functional treatment of non articular fractures of the lower end of the radius (author's tranls)]. Ann Chir. 1976;30:855-857.

Kaptein BL, Valstar ER, Stoel BC, Rozing PM, Reiber JH. A new model-based RSA method validated using CAD models and models from reverse engineering. J Biomech. 2003;36:873-882.

Kaptein BL, Valstar ER, Spoor CW, Stoel BC, Rozing PM. Model-based RSA of a femoral hip stem using surface and geometrical shape models. Clin Orthop Relat Res. 2006;448:92-97.

Kaptein BL, Valstar ER, Stoel BC, Reiber HC, Nelissen RG. Clinical validation of model-based RSA for a total knee prosthesis. Clin Orthop Relat Res. 2007;464:205-209.

Katz MA, Beredjiklian PK, Bozentka DJ, Steinberg DR. Computed tomography scanning of intra-articular distal radius fractures: does it influence treatment? J Hand Surg [Am]. 2001;26:244-251.

Kaukonen JP. Fractures of the distal forearm in the Helsinki district. Ann Chir Gynaecol. 1985;74:19-21.

Kaukonen JP, Karaharju E, Lüthje P, Porras M. External fixation of Colles' fracture. Acta Orthop Scand. 1989;60:54-56.

Kenwright J, Richardson JB, Cunningham JL, White SH, Goodship AE, Adams MA, Magnussen PA, Newman JH. Axial movement and tibial fractures. A controlled randomised trial of treatment. J Bone Joint Surg [Br]. 1991;73:654-659.

Knirk JL, Jupiter JB. Intra-articular fractures of the distal end of the radius in young adults. J Bone Joint Surg [Am]. 1986;68:647-659.

Konrath GA, Bahler S. Open reduction and internal fixation of unstable distal radius fractures: results using the trimed fixation system. J Orthop Trauma. 2002;16:578-585.

Kopylov P, Johnell O, Redlund-Johnell I, Bengner U. Fractures of the distal end of the radius in young adults: a 30-year follow-up. J Hand Surg [Br]. 1993;18:45-49.

Kopylov P, Aspenberg P, Yuan X, Ryd L. Radiostereometric analysis of distal radial fracture displacement during treatment: a randomized study comparing norian SRS and external fixation in 23 patients. Acta Orthop Scand. 2001;72:57-61.

Kärrholm J, Hansson LI, Selvik G. Roentgen stereophotogrammetric analysis of growth pattern after supination adduction ankle injuries in children. J Pediatr Orthop. 1982;2:271-279.

Kärrholm J, Selvik G, Elmqvist LG, Hansson LI. Active knee motion after cruciate ligament rupture. Stereoradiography. Acta Orthop Scand. 1988;59:158-164.

Kärrholm J. Roentgen stereophotogrammetry. Review of orthopaedic applications. Acta Orthop Scand. 1989;60:491-503.

Kärrholm J, Borssén B, Löwenhielm G, Snorrason F. Does erly micromotion of femoral stem prosthese matter? 4-7-year stereoradiographic follow-up of 84 cemented prostheses. J Bone Joint Surg [Br]. 1994;76:912-917.

Kärrholm J, Jonsson H, Nilsson KG, Söderqvist I. Kinematics of successful knee prostheses during weight-bearing: three-dimensional movements and positions of screw axes in the Tricon-M and Miller-Galante designs. Knee Surg Sports Traumatol Arthrosc. 1994;2:50-59.

Kärrholm J, Malchau H, Snorrason F, Herberts P. Micromotion of femoral stems in total hip arthroplasty. A randomized study of cemented, hydroxyapatite-coated and porous-coated stems with roentgen stereophotogrammetric analysis. J Bone Joint Surg [Am]. 1994;76:1692-1705.

Kärrholm J, Herberts P, Hultmark P, Malchau H, Nivbrant B, Thanner J: Radiostereometry of hip prostheses. Review of methodology and clinical results. Clin Orthop Relat Res. 1997;344:94-110.

Kärrholm J, Gill RH, Valstar ER. The history and future of radiostereometric analysis. Clin Orthop Relat Res. 2006;448:10-21.

Ladd AL, Pliam NB. The role of bone graft and alternatives in unstable distal radius fracture treatment. Orthop Clin North Am. 2001;32:337-351.

Laende EK, Deluzio KJ, Hennigar AW, Dunbar MJ. Implementation and validation of an implant-based coordinate system for RSA migration calculation. J Biomech. 2009;42:2387-2393.

Lafontaine M, Delince P, Hardy D, Simons M. Instabiliry of fractures of the lowe end of the radius: apropos of a series of 167 cases. Acta Orthop Belg. 1989;55:203-216.

Lafontaine M, Hardy D, Delince P. Stability assessment of distal radius fractures. Injury. 1989;20:208-210.

Larsson S, Berg P, Sagerfors M. Augmentation of tibial plateau fractures with calcium phosphate cement. A randomized study using radiostereometry. Orthopaedic Trauma Association, 2004 Annual Meeting, October 8-10, Florida.

Lenoble E, Dumontier C, Goutallier D, Apoil A. Fracture of the distal radius. A prospective comparison between trans-styloid and Kapandji fixations. J Bone Joint Surg [Br]. 1995;77:562-567.

Li MG, Yao F, Joss B, Ioppolo J, Nivbrant B, Wood D. Mobile vs. fixed bearing unicondylar knee arthroplasty: A randomized study on short term clinical outcomes and knee kinematics. Knee. 2006;13:365-370.

Lichtman DM, Bindra RR, Boyer MI, Putnam MD, Ring D, Slutsky DJ, Taras JS, Watters WC3rd, Goldberg MJ, Keith M, Turkelson CM, Wies JL, Haralson RH 3rd, Boyer KM, Hitchcock K, Raymond L. Treatment of distal radius fractures. J Am Acad Orthop Surg. 2010;18:180-189.

Lidstrom A. Fractures of the distal end of the radius. A clnical and statistical study of end results. Acta Orthop Scand Suppl. 1959;41:1-118.

Lindau T, Arner M, Hagberg L. Intraarticular lesions in distal fractures of the radius in young adults. A descriptive arthroscopic study in 50 patients. J Hand Surg [Br]. 1997;22:638-643.

Lindau T, Hagberg L, Adlercreutz C, Jonsson K, Aspenberg P. Distal radioulnar instability is an independent worsening factor in distal radial fractures. Clin Orthop Relat Res. 2000;(376):229-235.

Liporace FA, Kubiak EN, Jeong GK, Iesaka K, Egol KA, Koval KJ. A biomechanical comparison of two volar locked plates in a dorsally unstable distal radius fracture model. J Trauma. 2006;61:668-672.

Liporace FA, Adams MR, Capo JT, Koval KJ. Distal radius fractures. J Orthop Trauma. 2009;23:739-748.

Lundberg A. Patterns of motion of the ankle/foot complex. Thesis, Karolinska Institutet, Stockholm, Sweden 1988.

Lundberg A, Svensson OK, Németh G, Selvik G. The axis of rotation of the ankle joint. J Bone Joint Surg [Br]. 1989;71:94-99.

MacDermid JC, Richards RS, Donner A, Bellamy N, Roth JH. Responsiveness of the short form-36, disability of the arm, shoulder, and hand questionnaire, patient-rated wrist evaluation, and physical impairment measurements in evaluating recovery after a distal radius fracture. J Hand Surg [Am]. 2000;25:330-340.

MacDermid JC, Donner A, Richards RS, Roth JH. Patient versus injury factors as predictors of pain and disability six months after a distal radius fracture. J Clin Epidemiol. 2002;55:849-854.

Mackenney PJ, McQueen MM, Elton R. Prediction of instability in distal radial fractures. J Bone Joint Surg [Am]. 2006;88:1944-1951.

Magyar G, Toksvig-Larsen S, Lindstrand A. Changes in osseous correction after proximal tibial osteotomy: radiostereometry of closed- and open-wedge osteotomy in 33 patients. Acta Orthop Scand. 1999;70:473-477.

Martineau PA, Waitayawinyu T, Malone KJ, Hanel DP, Trumble TE. Volar plating of AO CS distal radius fractures: biomechanical evaluation of locking screw and locking smooth peg configurations. J Hand Surg [Am]. 2008;33:827-834.

Martinez AA, Canales V, Cuenca J, Herrera A. Minifragment plating for fractures of the distal radius. Acta Orthop Belg. 2004;70:311-314.

Mathiowetz V, Kashman N, Volland G, Weber K, Dowe M, Rogers S. Grip and pinch strength: normative data for adults. Arch Phys Med Rehabil. 1985;66:69-74.

Matsuoka J, Berger RA, Berglund LJ, An KN. An analysis of symmetry of torque strength of the forearm under resisted forearm rotation in normal subjects. J Hand Surg [Am]. 2006;31:801-805.

Mattsson P, Larsson S. Stability of internally fixed femoral neck fractures augmented with resorbable cement. A prospective randomized study using radiostereometry. Scand J Surg. 2003;92:215-219.

Mattsson P, Larsson S. Unstable trochanteric fractures augmented with calcium phosphate cement. A prospective randomized study using radiostereometry to measure fracture stability. Scand J Surg. 2004;93:223-228.

McKay SD, MacDermid JC, Roth JH, Richards RS. Assessment of complications of distal radius fractures and development of a complication checklist. J Hand Surg [Am]. 2001;26:916-922.

McMurtry RY, Jupiter JB. Fractures of the distal radius. In: Browner BD, Jupiter JB, Levine AM et

al, editors. Skeletal trauma. Philadelphia: Saunders; 1991. P. 1063-1094.
McQueen MM. Redisplaced unstable fractures of the distal radius. Arandomised, prospective study of bridging versus non-bridging external fixation. J Bone Joint Surg [Br]. 1998;80:665-669.

Medoff RJ. Essential radiographic evaluation for distal radius fractures. Hand Clin. 2005;21:279-288.

Melone CP. Articular fractures of the distal radius. Orthop Clin North Am. 1984;15:217-236.

Missakian ML, Cooney WP, Amadio PC, Glidewell HL. Open reduction and internal fixation for distal radius fractures. J Hand Surg [Am]. 1992;17:745-755.

Morgan EF, Gleason RE, Hayward LN, Leong PL, Palomares KT. Mechanotransduction and fracture repair. J Bone Joint Surg [Am]. 2008;90 (Suppl 1):25-30.

Mudgal CS, Jupiter JB. Plate fixation of osteoporotic fractures of the distal radius. J Orthop Trauma. 2008;22:S106-115.

Munson GO, Gainor BJ. Percutaneous pinning of distal radius fractures. J Trauma. 1981;21:1032-1035.

Müller ME. Distal Radius. In: Müller ME, Nazarian S, Koch P, Schatzker J, eds. AO classification of fractures. Berlin: Springer Verlag,1987:106-115.

Mäkinen TJ, Koort JK, Mattila KT, Aro HT: Precision measurements of the RSA method using a phantom model of hip prosthesis. J Biomech. 2004;37:487-493.

Nabhan A, Pape D, Pitzen T, Steudel WI, Bachelier F, Ahlhelm F. Radiographic analysis of fusion progression following one-level cervical fusion with or without plate fixation. Zentralbl Neurochir. 2007;68:133-138.

Nana AD, Joshi A, Lichtman DM. Plating of the distal radius. J Am Acad Orthop Surg. 2005;13:159-171.

Older TM, Stabler EU, Cassebaum WH. Colles' fracture: evaluation of selection of therapy. J Trauma. 1965;5:469-476.

Olsson TH, Selvik G, Willner S. Kinematic analysis of posterolateral fusion in the lumbosacral spine. Acta Radiol Diagn (Stockh). 1976;17:519-530.

Olsson TH, Selvik G, Willner S. Postoperative kinematics in structural scoliosis. Acta Radiol Diagn (Stockh). 1977;18:75-86.

Olsson TH, Selvik G, Willner S. Mobility in the lumbosacral spine after fusion studied with the aid of roentgen stereophotogrammetry. Clin Orthop Relat Res. 1977;129:181-190.

Orbay JL, Fernandez DL. Volar fixation for dorsally displaced fractures of the distal radius: a preliminary report. J Hand Surg [Am]. 2002;27:205-215.

Orbay JL, Fernandez DL. Volar fixed-angle plate fixation for unstable distal radius fractures in the elderly patient. J Hand Surg [Am]. 2004;29:96-102.

Orbay J. Volar plate fixation of distal radius fractures. Hand Clin. 2005;21:347-354.

Orbay JL, Touhami A. Current concepts in volar fixed-angle fixation of unstable distal radius fractures. Clin Orthop Relat Res. 2006;445:58-67.

Overgaard S, Solgaard S. Osteoarthritis after Colles' fracture. Orthopaedics. 1989;12:413-416.

Önsten I, Berzins A, Shott S, Sumner DR. Accuracy and precision of radiostereometric analysis in the measurement of THR femoral component translations: human and canine in vitro models. J Orthop Res. 2001;19:1162-1167.

Palmer AK, Werner FW. Biomechanics of the distal radioulnar joint. Clin Orthop Relat Res. 1984;187:26-35.

Pape D, Adam F, Seil R, Georg T, Kohn D. Fixation stability following high tibial osteotomy: a radiostereometric analysis. J Knee Surg. 2005;18:108-115.

Park MJ, Cooney WP 3rd, Hahn ME, Lool KP, An KN. The effects of dorsally angulated distal radius fractures on carpal kinematics. J Hand Surg [Am]. 2002;27:223-232.

Park SA, Fayyazi AH, Ordway NR, Sun MH, Fredrickson BE, Yuan HA. Correlation of

radiostereometric measured cervical range of motion with clinical radiographic findings after anterior cervical discectomy and fusion. Spine. 2009;34:680-686.

Pearcy MJ. Stereo radiography of lumbar spine motion. Acta Orthop Scand Suppl. 1985;212:1-45.

Petersen P, Petrick M, Connor H, Conklin D. Grip strength and hand dominance: challenging the 10% rule. Am J Occup Ther. 1989;43:444-447.

Pogue DJ, Viegas SF, Patterson RM, Peterson PD, Jenkins DK, Sweo TD, Hokanson JA. Effects of distal radius fracture malunoin on wrist joint mechanics. J Hand Surg [Am]. 1990;15:721-727.

Putnam MD, Meyer NJ, Nelson EW, Gesensway D, Lewis JL. Distal radial metaphyseal forces in an extrinsic grip model: implications for postfracture rehabilitation. J Hand Surg [Am]. 2000;25:469-475.

Ranstam J, Ryd L, Önsten I. Accurate accuracy assessment: review of basic principles. Acta Orthop Scand. 2000;71:106-108.

Ragnarsson JI, Hansson LI, Kärrholm J. Stablity od femoral neck fractures. A postoperative roentgen stereophotogrammetric analysis. Acta Orthop Scand. 1989;60:283-287.

Ragnarsson JI, Eliasson P, Kärrholm J, Lundström B. The accuracy of measurements of femoral neck fractures. Conventional radiography versus roentgen stereophotogrammetric analysis. Acta Orthop Scand. 1992;63:152-156.

Ragnarsson JI, Kärrholm J. Factors influencing postoperative movement in displaced femoral neck fractures: evaluation by conventional radiography and stereoradiography. J Orthop Trauma. 1992;6:152-158.

Ragnarsson JI, Boquist L, Ekelund L, Kärrholm J. Instability and femoral neck vitality in fractures of the femoral neck. Clin Orthop Relat Res. 1993;287:30-40.

Rahme H, Mattsson P, Wikblad L, Nowak J, Larsson S. Stability of cemented in-line pegged glenoid compared with keeled glenoid components in total shoulder arthroplasty. J Bone Joint Surg [Am]. 2009;91:1965-1972.

Regnér L, Carlsson L, Kärrholm J, Herberts P. Tibial component fixation in porous- and hydroxyapatte-coated total knee arthroplasty: a radiostereometric evaluation of migration and inducible displacement after 5 years. J Arthroplasty. 2000; 15:681-689.

Rikli DA, Regazzoni P. Fractures of the distal end of the radius treated by internal fixation and early function. A preliminary report of 20 cases. J Bone Joint Surg [Br]. 1996;78:588-592.

Roysam GS. The distal radio-ulnar joint in Colles' fractures. J Bone Joint Surg [Br]. 1993;75:58-60.

Rozental TD, Blazar PE. Functional outcome and complications after volar plating for dorsally displaced, unstable fractures of the distal radius. J Hand Surg [Am]. 2006;31:359-365.

Rozental TD, Blazar PE, Franko OI, Chacko AT, Earp BE, Day CS. Functional outcomes for unstable distal radial fractures treated with open reduction and internal fixation or closed reduction and percutaneous fixation. A prospective randomized trial. J Bone Joint Surg [Am]. 2009;91:1837-1846.

Russo A, Montagna L, Bragonzoni L, Visani A, Marcacci M. Changes in knee motion over the first 3 years with a mobile-bearing prosthesis. Knee. 2006;13:301-306.

Ryd L. Micromotion in knee arthroplasty. A roentgen stereophotogrammetric analysis of tibial component fixation. Acta Orthop Scand Suppl. 1986;220:1-80.

Ryd L. Roentgen stereophotogrammetric analysis of prosthetic fixation in the hip and knee joint. Clin Orthop Relat Res. 1992;(276):56-65.

Ryd L, Carlsson L, Herberts P. Micromotion of a noncemented tibial component with screw fixation. An in vivo roentgen stereophotogrammetric study of the Miller-Galante prosthesis. Clin Orthop Relat Res. 1993;295:218-225.

Ryd L, Toksvig-Larsen S. Early postoperative fixation of tibial components: an in vivo roentgen stereophotogrammetric analysis, J Orthop Res. 1993;11:142-148.

Ryd L, Albrektsson BE, Carlsson L, Dansgård F, Herberts P, Lindstrand A, Régner L, Toksvig-Larsen S. Roentgen stereophotogrammetric analysis as a predictor of mechanical loosening of

knee prostheses. J Bone Joint Surg [Br]. 1995;77:377-383.

Ryd L, Yuan X, Löfgren H. Methods for determining the accuracy of radiostereometric analysis (RSA). Acta Orthop Scand. 2000;71:403-408.

Saari T, Carlsson L, Karlsson J, Kärrholm J. Knee kniematics in medial arthrosis. Dynamic radiostereometry during active extension and weight-bearing. J Biomech. 2005;38:285-292.

Sammer DM, Shah HM, Shauver MJ, Chung KC. The effect of ulnar styloid fractures on patient-rated outcomes after volar locking plating of distal radius fractures. J Hand Surg [Am]. 2009;34:1595-1602.

Schnall SB, Kim BJ, Abramo A, Kopylov P. Fixation of distal radius fractures using a fragment-specific system. Clin Orthop Relat Res. 2006;445:51-57.

Sears ED, Chung KC. Validity and responsiveness of the Jebsen-Taylor Hand Function Test. J Hand Surg [Am]. 2010;35:30-37.

Selvik G, Alberius P, Aronson AS. A roentgen stereophotogrammetric system. Construction, calibration and technical accuracy. Acta Radiol Diagn (Stockh). 1983;24:343-352.

Selvik G. A roentgen-stereophotogrammetric method for the study of the kinematics of the skeletal system. Thesis, University of Lund, Lund, Sweden 1974. (Reprinted Acta Orthop Scand (Suppl 232). 1989;60:1-51).

Shih JT, Lee HM, Hou YT, Tan CM. Arthroscopically-assisted reduction of intra-articular fractures and soft tissue management of distal radius. Hand Surg. 2001;6:127-135.

Short WH, Palmer AK, Werner FW, Murphy DJ. A biomechanical study of distal radial fractures. J Hand Surg [Am]. 1987;12:529-534.

Slutsky DJ, Herman M. Rehabilitation of distal radius fractures: a biomechanical guide. Hand Clin. 2005;21:455-468.

Slutsky DJ. External fixation of distal radius fractures. J Hand Surg [Am]. 2007;32:1624-1637.

Solomon LB, Stevenson AW, Callary SA, Sullivan TR, Howie DW, Chehade MJ. The accuracy and precision of radiostereometric analysis in monitoring tibial plateau fractures. Acta Orthop. 2010;81:487-494.

Söderkvist I, Wedin PÅ. Determining the movements of the skeleton using well-configured markers. J Biomech. 1993;26:1473-1477.

Thomas FB. Reduction of Smith's fracture. J Bone Joint Surg [Br]. 1957;39:463-470.

Timm WN, O'Driscoll SW, Johnson ME, An KN. Functional comparison of pronation and supination strengths. J Hand Ther. 1993;6:190-193.

Tjörnstrand B, Selvik G, Egund N, Lindstrand A. Roentgen stereophotogrammetry in high tibial osteotomy for gonarthrosis. Arch Orthop Trauma Surg. 1981;99:73-81.

Toksvig-Larsen S, Ryd L, Lindstrand A. Effect of a cooled saw blade on prosthesis fixation. Randomized radiostereometry of 33 knee cases. Acta Orthop Scand. 1994;65:533-537.

Toksvig-Larsen S, Ryd L, Lindstrand A. Early inducible displacement of tibial components in total knee prostheses inserted with and without cement: a randomized study with roentgen stereophotogrammetric analysis. J Bone Joint Surg [Am]. 1998;80:83-89.

Uvehammer J, Kärrholm J, Brandsson S. In vivo kinematics of total knee arthroplasty. Concave versus posterior-stabilised tibial joint surface. J Bone Joint Surg [Br]. 2000;82:499-505.

Uvehammer J, Kärrholm J. Inducible displacements of cemented tibial components during weight-bearing and knee extension observations during dynamic radiostereometry related to joint posistions and 2 years history of migration in 16 TKR. J Orthop Res. 2001;19:1168-1177.

Valstar ER, de Jong FW, Vrooman HA, Rozing PM, Reiber JH. Model-based roentgen stereophotogrammetry of orthopaedic implants. J Biomech. 2001;34:715-722.

Valstar ER, Gill R, Ryd L, Flivik G, Börlin N, Kärrholm J. Guidelines for standardization of radiostereometry (RSA) of implants. Acta Orthop. 2005;76:563-572.

van der Linden W, Ericson R. Colles' fracture. How should its displacement be measured and how should it be immobilized? J Bone Joint Surg [Am]. 1981;63:1285-1288.

Varitimidis SE, Basdekis GK, Dailiana ZH, Hantes ME, Bargiotas K, Malizos K. Treatment of intra-articular fractures of the distal radius: fluoroscopic or arthroscopic reduction? J Bone Joint Surg [Br]. 2008;90:778-785.

Vasenius J. Operative treatment of distal radius fractures. Scand J Surg. 2008;97:290-296.

Vedel E. Predicting the properties of Bioactive Glasses. Academic dissertation. Åbo Akademi University. Faculty of technology. Process chemistry centre. Laboratory of inorganic chemistry. 2008. p. 73.

Vrooman HA, Valstar ER, Brand GJ, Admiraal DR, Rozing PM, Reiber JH. Fast and accurate automated measurements in digitized stereophotogrammetric radiographs. J Biomech. 1998;31:491-498.

von Schewelov T, Sanzén L, Börlin N, Markusson P, Onsten I. Accuracy of radiographic and radiostereometric wear measurement of different hip prostheses: an experimental study. Acta Orthop Scand. 2004;75:691-700.

Välimäki VV, Moritz N, Yrjäns JJ, Vuorio E, Aro HT, Effect of zoledronic acid on incorporation of a bioceramic bone graft substitute. Bone 2006;38:432-443.

Warwick D, Field J, Prothero D, Gibson A, Bannister GC. Function ten years after Colles' fracture. Clin Orthop Relat Res. 1993;(295):270-274.

Wei DH, Raizman NM, Bottino CJ, Jobin CM, Strauch RJ, Rosenwasser MP. Unstable distal radial fractures treated with external fixation, a radial column plate, or a volar plate. A prospective randomized trial. J Bone Joint Surg [Am]. 2009;91:1568-1577.

Werman BS, Rietschel RL. Chronic urticaria from tantalum staples. Arch Dermatol. 1981;117:438-439.

Willis AA, Kutsumi K, Zobitz ME, Cooney WP 3rd. Internal fixation of dorsally displaced fractures of the distal part of the radius. A biomechanical analysis of volar plate fracture stability. J Bone Joint Surg [Am]. 2006;88:2411-2417.

Wilson DA, Astephen JL, Hennigar AW, Dunbar MJ. Inducible displacement of a trabecular metal monoblock component. J Arthroplasty. 2010;25:893-900.

Wood GW II. General principles of fracture treatment. In Beaty JH and Canale ST (eds). Campbell's Operative Orthopaedics 11th ed. Philadelphia, Mosby 2008: 3039-3041.

Wulf CA, Ackerman DB, Rizzo M. Contemporary evaluation and treatment of distal radius fractures. Hand Clin. 2007;23:209-226.

Zhao D, Moritz N, Vedel E, Hupa L, Aro HT. Mechanical verification of soft-tissue attachment on bioactive glasses and titanium implants. Acta Biomater 2008;4:1118-1122.

Zoëga B, Kärrholm J, Lind B. One-level cervical spine fusion. A randomized study, with or without plate fixation, using radiostereometry in 27 patients. Acta Orthop Scand. 1998;69:363-368.

Zoëga B, Kärrholm J, Lind B. Plate fixation adds stability to two-level anterior fusion in the cervical spine: a randomized study using radiostereometry. Eur Spine J. 1998;7:302-307.

Zoëga B, Kärrholm J, Lind B. Mobility provocation radiostereometry in anterior cervical spine fusions. Eur Spine J. 2003;12:631-636.

Zollinger PE, Tuinebreijer WE, Breederveld RS, Kreis RW. Can vitamin C prevent complex regional pain syndrome in patients with wrist fracture? A randomized, controlled, multicenter dose-response study. J Bone Joint Surg [Am]. 2007;89:1424-1431.

Zollinger PE, Tuinebreijer WE, Kreis RW, Breederveld RS. Effect of vitamin C on frequency of reflex sympathetic dystrophy in wrist fractures: a randomised trial. Lancet. 1999;354:2025-2028.